

SEARCHING FOR THE QCD SIGMA RESONANCE ON GPU ARCHITECTURE.

By

Dean Howarth

A Dissertation Submitted to the Graduate
Faculty of Rensselaer Polytechnic Institute

in Partial Fulfillment of the
Requirements for the Degree of
DOCTOR OF PHILOSOPHY

Major Subject: PHYSICS

Examining Committee:

Prof. Joel Giedt, Dissertation Adviser

Prof. Ethan Brown, Member

Prof. Simon Catterall, Member

Prof. Peter Kramer, Member

Prof. Vincent Meunier, Member

Rensselaer Polytechnic Institute
Troy, New York

April 2016
(For Graduation May 2016)

© Copyright 2016
by
Dean Howarth
All Rights Reserved

CONTENTS

LIST OF TABLES	vi
LIST OF FIGURES	vii
ACKNOWLEDGMENT	ix
ABSTRACT	xiv
1. Introduction	1
2. The Path Integral	2
2.1 (1+1)D Quantum Mechanics	3
2.2 (3+1)D Quantum Scalar Field	8
2.3 Euclidean Scalar Field Correlation Functions	14
3. Quantum Chromodynamics	16
3.1 Quarks	16
3.2 $SU(3)$ Gauge Invariance	17
3.3 Gluons	24
3.4 QCD equations of motion	29
3.5 The Wilson Loop.	31
4. Lattice Gauge Theory for QCD	35
4.1 Naïve Discretisation of the QCD Action	35
4.2 The Doubling Problem and its Solution	39
4.3 Wilson Fermions	41
4.4 Wilson Gauge Action	45
4.5 Clover Improved Fermions	50
5. Numerical Simulation	55
5.1 Simulation of a Pure Gauge Field	56
5.1.1 Metropolis Algorithm for $SU(3)$	58
5.1.2 Heatbath Algorithm	61
5.2 Fermions on the Lattice.	64
5.2.1 Hopping Parameter	65

5.2.2	Pseudo-Fermions	66
5.3	Hybrid Monte-Carlo Algorithm	69
5.4	<i>Caveat Emptor</i> : A Note on Exceptional Configurations	73
6.	Correlation Functions and Propagators	76
6.1	A Pseudo-scalar Correlation Function	76
6.2	Signal to Noise Improvement Strategies	83
6.2.1	Isospin Projection	83
6.2.2	Vacuum Expectation Value Removal	84
6.2.3	Fierz Rearrangement	85
6.3	Propagator Construction and Approximation	85
6.3.1	Point Sources	86
6.3.2	Stochastic Sources	88
6.3.3	Momentum Sources	90
6.3.4	Truncated Singular Value Decomposition	91
6.3.5	Correlation Functions Using S.V.D Propagators	94
7.	High Frequency Decoupling and Gauge Fixing	95
7.1	Smearing	95
7.1.1	Source Smearing	95
7.1.2	Sink Smearing	100
7.1.3	Link Smearing	100
7.2	Gauge Fixing	102
7.2.1	Gribov Density	104
8.	Extracting Physics and the σ Meson	112
8.1	Theoretical Background	112
8.2	Experimental Evidence of the σ Meson	114
8.3	Effective Mass Plateaux	116
8.3.1	Conventional method	116
8.3.2	Log-Normal Method	119
8.4	Lattice and physical scales: the Sommer parameter	121
8.5	Lüscher's Method	125
9.	Computational Setup	127
9.1	Software	127
9.2	Hardware and Benchmarks	127

10. Conclusions and Outlook	130
10.1 Preliminary Calculations	130
10.2 Future Work	135
APPENDICES	
A. Details on $SU(N)$	138
A.1 Generators and Algebra	138
B. Fermionic Path Intergrals	142
B.1 Grassmann Algebra	142
B.2 Berezin Calculus	144
B.3 Gaussian Integration of Fermion Fields	145
C. Error Calculations	150
C.1 Error on correlation functions	150
C.2 Autocorrelation and Jack-Knife Error Estimates	150
C.3 Error on the Sommer parameter	151
C.4 Error on effective mass extrapolation	152
C.5 Error on $\Delta E(L_1)/\Delta E(L_2)$	153
ACKNOWLEDGMENT	154

LIST OF TABLES

3.1	The six known quarks.	16
9.1	Benchmarks for $12^3 \times 24, \beta = 5.60(a = 0.22fm)$ quenched lattices on Tesla K20	128
9.2	Benchmarks for $16^3 \times 32, \beta = 5.60(a = 0.22fm)$ quenched lattices on Tesla K20	128
9.3	Benchmarks for $24^3 \times 48, \beta = 5.30(a = 0.16fm)$ dynamical lattices on Kepler C2075	129
10.1	Preliminary simulation data	130

LIST OF FIGURES

2.1	Running coupling of the strong coupling constant	3
3.1	Cross sections for hadron ($q\bar{q}$) production via e^-e^+	18
3.2	Triple and quadruple vertices of interacting gluons.	28
4.1	E-p relations for doubler modes	45
4.2	Wilson loop diagram	47
4.3	Clover diagram	52
6.1	Quark propagator diagram for the $C_0(t)$ correlation function.	82
6.2	Quark propagator diagram for the $C_1(t)$ correlation function.	82
6.3	Quark propagator diagram for the $C_2(t)$ correlation function.	82
6.4	Quark propagator diagram for the $C_4(t)$ correlation function.	83
7.1	Gaussian profile of a covariantly smeared point source.	96
7.2	A covariantly smeared $\mathbf{p} = (0, 0, 0)$ momentum source.	97
7.3	Gaussian profile of a the distribution of absolute link traces.	105
7.4	Attenuation parameter $ \alpha $	106
7.5	Evolution of Gribov density with β for L=10.	107
7.6	Evolution of Gribov density with β for L=12.	107
7.7	Evolution of Gribov density with β for L=14.	108
7.8	Evolution of Gribov density with β for L=18.	108
7.9	Probability of finding the FMR at L=10	109
7.10	Probability of finding the FMR at L=12	110
7.11	Probability of finding the FMR at L=14	110
7.12	Probability of finding the FMR at L=18	111
8.1	Pseudoscalar nonet	113
8.2	Scalar nonet	114

8.3	BESII sigma resonance data	115
8.4	Effective mass for point source	118
8.5	Effective mass for momentum source	118
8.6	Evolution of μ (left) and σ (right) with t for smeared point and momentum sources for heavy mass pion from an $16^3 32$ quenched $\beta = 5.45$ ensemble.	120
8.7	Effective mass plateaux for a heavy pion with from an $16^3 32$ quenched $\beta = 5.45$ ensemble.	120
8.8	Static Quark Potential calculation	122
8.9	Static Quark Potential for Quenched $\beta = 5.60$ at $L = 18$	124
10.1	m_σ extrapolation, quenched, Coulomb gauge, $L = 12$	131
10.2	m_σ extrapolation, quenched, unfixed gauge, $L = 10$	132
10.3	m_σ extrapolation, quenched, unfixed gauge, $L = 12$	133
10.4	Two effective mass plateaux for dynamical $L = 16, \beta = 445\text{MeV}$ lattices	134

ACKNOWLEDGMENT

Many thanks go to my supervisor Joel Giedt who, like all other supervisors, took a risk in employing me as a researcher. I will be eternally grateful for the opportunity that choice afforded me. I would also like to give particular thanks to Joel for exhibiting the patience of a saint when it came to my education in quantum field theory, lattice gauge theory, and need for 3rd, 4th, and 5th explanations of concepts in this project. On more than one occasion, these conversations would diverge to string theory, chirality, advanced mathematics, and computer science, which often had nothing to with the project! The fact that his office door was more open than closed to me, whether or not it was relevant to this work, will always be appreciated .

I have also been lucky enough to have made some very firm friends during my time here, each of whom I am indebted to for their continued support. The people with whom I have lived, Adam Simbeck, Jonathan Owens, Nicholas Lanzillo¹, and David Elsaesser, have each played the role of confidant, sounding board, chauffeur, and never has a cross word been exchanged between us. Albert Owens, who is unaware of the complexity of the universe in which he lives (like many of us) has never failed to bring happiness to my life and wanted nothing in return but company... and the odd bacon flavoured treat.

I would not have even been able to reach this point in my life and education were it not for my family and their support. My mother, Carol, and sister, Nicola, have been incredible figures of admiration in my life, both of whom have dealt with great adversity, an adversity that I as a male have never had to deal with, and I will always look to them for guidance. My nieces, Hannah and Leah, have always been on my mind. I often wonder what kind of women you'll both be when you're all grown up, and I think you will be very good ones. When you're old enough, I'll take you both on a tour of NYC :)

¹I never actually lived with Nick, but his patriotic fervour is so intense that living ANYWHERE in the USA means you can say you lived with Nick.

A Note In The Road

Part I: The Quantum State

What goes up must come down.
The ancient laws from those renown
Would governed all, until we peer,
Into a world of inner fear.
We seek it here, we seek it there,
But Heisenberg has hid it! Where
Exactly is it? I need to know!
It's here! It's here!... But where did it go?

And so, in keeping with scholarly tradition,
An example to explain; take 'superposition.'
It's a word, nothing more, that perfectly contains,
The quantum laws and the human pains.
It describes how a single electron can be,
In two different places at once. Don't you see?
You don't see. Who would at first cognition?
The quantum world holds no recognition,
To anything you might have seen before.
Relinquish tradition and Newton's Law,
And allow these lines to meet you afresh,
As if you've been freed from a tightening mesh,
Of indoctrinated, classic tradition,
Where entities have but a single position.

So imagine now please a quantum state,
In superposition, awaiting its fate.
The classic experiment in many books told,

Has an electron's future confined, two-fold.
It starts in a well-defined region, we trust,
And we let it evolve and do, as it must.
At some later time we observe it to be,
An inch to the left. It's gone A to B!
No mystery here! It started at A,
Then moved to the left, it traveled one way.
But the mind is curious and wracked with pain:
If it is to be truth, it must do it again.
The equipment is set exactly the same,
The white coats fixed still, dreaming of fame,
'The electron's at A, let it go, run to B!'
When they switch on the light, they find it at C!
'An inch to the right! Something went wrong,'
The classical mind's predictable throng,
Attributes this manifestation of terror,
To some unforeseen, experimental error.
A million times over we can re-administer,
Half will be dexter and half will be sinister.
And no law of man is able to tell,
Which way it will go. Are these rules from hell?
Or heaven? Are we simply not privy?
Has He made us all His collective skivvy?

Now those who pay exquisite attention,
Will have on their lips a burning question.
'Maybe there's something that we overlook,
A variable, hidden, not known in the book.'
Kudos to you! A fine conjecture!
We just don't know the full architecture!
Precisely the thoughts, some eight decades ago,

Of Einstein, Podolsky, and Rosen. They'd show,
That quantum systems belie hidden truths,
And we must persevere and become like sleuths,
But Bell, with a marvelous and simple theory,
Showed that these truths, if true, must be eerie.
If nothing is true, we know this as right:
Nothing moves faster than the speed of light.
And if you choose to believe in the hidden,
Then this block of stone must be gotten ridden.
Whence causality would be turned on its head,
And the heart of all logic shall become, at once, dead.
From this rabbit hole there is no escape,
So let the philosophers undress and undrape.
The physicist's tools are the truths we know,
They will guide us, and we shall thus go.
So fie this folly of determinism,
I shall construct a formalism,
And scaffold around the elusive blue,
A system of controlling you!
A solid base of integrations,
Support our slippery interpretations,
And the iron clasps of Hilbert spaces,
Confine infinities to manageable places.
The math will predict with perfect precision,
The chance that comes from God's die's decision,
So Schrödinger's rule may coldly assign,
How much of the real each chance may divine.
Then the concrete logic of the Dirac equation,
Splits and spins and this fine creation,
Into left- and right-hand, distinct parts,
Numbing our minds and beating our hearts,

And to find the path we traverse the field,
And hope that Nature will her secrets, yield.

ABSTRACT

In chapters 2, 3, and 4, the salient properties of continuum QCD will be outlined, as will those of path integral formalism and lattice gauge theory. In chapter 5, the numerical algorithms necessary to perform lattice calculations on a computer will be explained. In chapters 6 and 7 the lattice gauge theory techniques used to simulate the $\pi^+\pi^- \rightarrow \pi^+\pi^-$ scattering process and in chapter 8, the significance $f_0(500)$ or σ will be given, as will the process of matching numerical results with observable physics. In chapter 9 we explain the process of software design that was required to utilise GPU architecture and in chapter 10 we present our results and give outlook for further research.

CHAPTER 1

Introduction

The aim of this work is to investigate the low-lying energy spectrum of the $\pi^+\pi^-$ system by investigating the properties of $\pi^+\pi^- \rightarrow \pi^+\pi^-$ scattering, and thereby investigate the nature of the lowest lying scalar state in QCD, the $f_0(500)$ or σ meson. The $\pi^+\pi^-$ system is a desirable one to study as it already has all the properties of the σ state. For example, the total charge and spin of the two pions is zero, and also the total isospin of the system is zero, conducive with the (so far) observed quantum numbers of the σ meson (1).

CHAPTER 2

The Path Integral

A standard technique in physics is to take the solution of some simple system and change (perturb) the parameters in the system by a small amount. A simple example is to take the infinite square well of 1d quantum mechanics and ‘perturb’ the bottom of the well by a small constant α . The resulting energy levels of that system can be found using perturbation theory and will be dependent on α . In quantum electrodynamics, a similar (but more complex) procedure allows us to write down the solution to the free-field, and then perturb that free-field by allowing interactions. These interactions are characterised by a small number known as the **fine structure constant** whose value is indeed a small number, $\alpha \approx \frac{1}{137}$. All scattering cross-sections (probabilities) in QED can be computed using this perturbation theory. Each successive term in the perturbation series carries an increasing power of α so that (very schematically) the cross section of some process such as $e^+e^- \rightarrow e^+e^-$ may be expressed as²,

$$\sigma(e^+e^- \rightarrow e^+e^-) \propto c_0\alpha^0 + c_1\alpha^1 + c_2\alpha^2 + \dots + c_n\alpha^n. \quad (2.0.1)$$

The coupling constant g characterising the interactions in QCD is seen to increase as the quarks become more separated, and perturbation theory can only be applied when the expansion parameter is small. Figure 2.1 shows this behaviour. At high Q momentum transfer (small separation) perturbation theory gives good results, but it doesn’t give a full description of the dynamics of the theory as the energy in the system at these scales is not enough to cause pair production of new quarks. To investigate the dynamics of pair production, one must also consider low momentum transfer (large separation); this scale is referred to as the **low energy sector**. In order to investigate the low energy sector of QCD, one must use a non perturbative tool, such as lattice gauge theory, which is built on the path integral formalism.

²Notice that this series is truncated due to the Landau Pole.

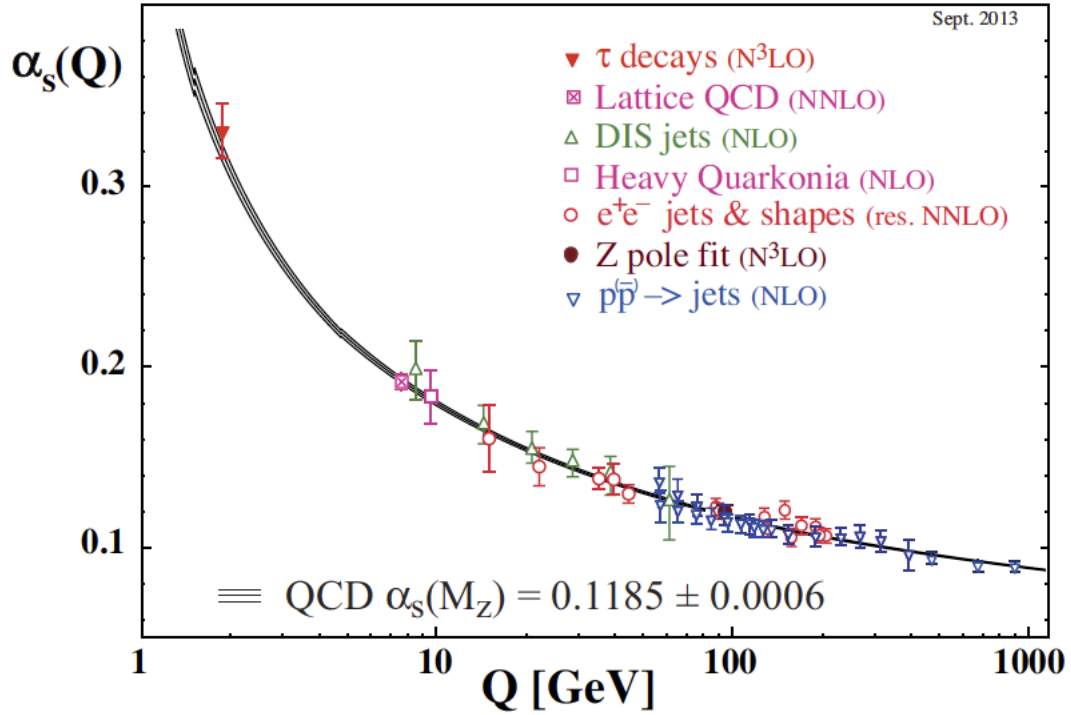


Figure 2.1: Running coupling of the strong coupling constant $\alpha_s(Q)$ as a function of momentum transfer, given in natural units on the x -axis. The renormalisation scale is the mass of the Z boson $M_Z = 91.2\text{GeV}$. (Figure from Olive et al.(2))

2.1 (1+1)D Quantum Mechanics

Consider the time dependent Schrödinger equation in one space dimension and its formal solution in terms of the time evolution operator,

$$\begin{aligned}
 i\partial_t|\psi(x, t)\rangle &= \hat{H}|\psi(x, t)\rangle \\
 \Rightarrow |\psi(x, t)\rangle &= U(t, t_0)|\psi(x, t_0)\rangle
 \end{aligned}
 \tag{2.1.1}$$

We define the time evolution operator $U(t, t_0)$ as,

$$U(t, t_0) \equiv e^{-i\hat{H}(t-t_0)}.
 \tag{2.1.2}$$

If we can identify this operator, it will tell us how some initial eigenstate $|q_i\rangle$ evolves into some final eigenstate $\langle q_f|$ during a time $t - t_0$. In the following, we will work in 1+1 dimensions of spacetime using a non-relativistic Hamiltonian, and then move on to a 3+1 spacetime field theory.

We split the time interval $t - t_0$ into N finitely small, equal steps Δt and insert a complete set of basis states between each time step,

$$\langle q_f | e^{-i\hat{H}(t-t_0)} | q_i \rangle = \int dq_{N-1} \dots \int dq_1 \underbrace{\langle q_f | e^{-i\hat{H}\Delta t} | q_{N-1} \rangle \dots \langle q_1 | e^{-i\hat{H}\Delta t} | q_i \rangle}_{N \text{ factors}}. \quad (2.1.3)$$

The final step will be to take the simultaneous limits $N \rightarrow \infty$ and $\Delta t \rightarrow 0$. At this point it is convenient to define the *transfer matrix*,

$$T_{q',q} := \langle q' | e^{-i\hat{H}\Delta t} | q \rangle, \quad (2.1.4)$$

so that,

$$\langle q_f | e^{-i\hat{H}(t-t_0)} | q_i \rangle = \int dq_{N-1} \dots \int dq_1 T_{q_f, q_{N-1}} T_{q_{N-1}, q_{N-2}} \dots T_{q_1, q_i}. \quad (2.1.5)$$

To proceed, we will define the Hamiltonian for a non-relativistic quantum system and evaluate the integral over the N products of transfer matrices. Let

$$\hat{H} = \frac{\hat{p}^2}{2m} + V(\hat{q}), \quad (2.1.6)$$

and recall the procedure for multiplying the exponentiation of two non-commuting matrices,

$$e^{A+B} = e^A e^B \left(1 - \frac{1}{2}[A, B] + \dots \right). \quad (2.1.7)$$

This relationship allows us to rewrite the time evolution operator with the defined Hamiltonian as,

$$e^{-i\hat{H}\Delta t} = e^{-i\Delta t \hat{p}^2 / (2m)} e^{-i\Delta t V(\hat{q})} (1 + \mathcal{O}(\Delta t^2)). \quad (2.1.8)$$

By neglecting terms of order $(\Delta t)^2$, we can insert a complete set of momentum

eigenstates between the exponentials and evaluate the integral over position-space eigenstates using the Fourier transform relation,

$$\langle p|q\rangle = \frac{1}{(2\pi)^{1/2}} e^{-ipq}, \quad (2.1.9)$$

giving,

$$\begin{aligned} T_{q',q} &= \int dp \langle q'|e^{-i\Delta t \hat{p}^2/(2m)}|p\rangle \langle p|e^{-i\Delta t V(\hat{q})}|q\rangle \\ &= \int dp \langle q'|p\rangle \langle p|q\rangle e^{-iH(p,q)\Delta t} \\ &= \int \frac{dp}{2\pi} e^{-ip(q'-q)} e^{-iH(p,q)\Delta t}. \end{aligned} \quad (2.1.10)$$

Inserting this definition of the transfer matrix into (2.1.5) we arrive at the following,

$$\begin{aligned} \langle q_f|e^{-i\hat{H}\Delta t}|q_i\rangle &= \int dq_{N-1} \int \frac{dp_{N-1}}{2\pi} \int dq_{N-2} \frac{dp_{N-2}}{2\pi} \dots \int dq_1 \int \frac{dp_1}{2\pi} \int \frac{dp_0}{2\pi} \\ &\times \exp \left\{ i \sum_{n=0}^{N-1} \Delta t \left[p_n \frac{q_{n+1} - q_n}{\Delta t} - H(p_n, q_n) \right] \right\}. \end{aligned} \quad (2.1.11)$$

We can now take the continuum limits of $N \rightarrow \infty$ and $\Delta t \rightarrow 0$ and make the following identifications,

$$\frac{q_{n+1} - q_n}{\Delta t} \rightarrow \dot{q}(t), \quad \sum_{n=0}^{N-1} \Delta t \rightarrow \int_{t_i}^{t_f} dt. \quad (2.1.12)$$

By using the abbreviated notation,

$$d[p] = \prod_{n=0}^{N-1} \frac{dp_n}{2\pi}, \quad d[q] = \prod_{n=0}^{N-1} dq_n, \quad S[p, q] = \int_{t_i}^{t_f} dt [p(t)\dot{q}(t) - H(p(t), \dot{q}(t))], \quad (2.1.13)$$

we can write can write down a compact expression for the amplitude of an initial position eigenstate $|q_i\rangle$ to evolve into a final eigenstate $\langle q_f|$ over a finite time $t - t_0$,

$$\langle q_f|e^{-i\hat{H}(t-t_0)}|q_i\rangle = \int_{q_i}^{q_f} d[p]d[q] e^{iS[p,q]}. \quad (2.1.14)$$

Some points to note:

- The limits of the integration $q_i = q(t_i)$ and $q_f = q(t_f)$ are fixed boundary conditions associated with the two fixed eigenstates. The integration sums over all possible paths and all possible momenta. These paths and momenta are not necessarily physical in that they need not obey classical laws of motion.
- The notation $A[\dots]$ implies that A is a function of a function, or a **functional**.
- The integration measures $d[p]$ and $d[q]$ are infinite dimensional in the limit $N \rightarrow \infty$.

From here, we may perform the integration over $d[p]$ analytically. There are two ways in which this can be done, which are equivalent. One is to add a small, imaginary component to the initial and final times which has the effect of suppressing the integrand as $p \rightarrow \pm\infty$. Another method, more pertinent to lattice gauge theory, is to perform a Wick rotation on the time temporal coordinate from $t \rightarrow -i\tau$. This is known as the *Euclidean time* approach and is useful when calculating ground state energies from correlation functions, as will be shown schematically in subsection 2.3 and in more detail in chapter 4. Consider the transfer matrix $T_{q',q}$ after Wick rotation to Euclidean time, which we shall denote as $T_{q',q}^E$

$$\begin{aligned} T_{q',q}^E &= \int \frac{dp}{2\pi} \exp \left\{ i(q' - q)p - \Delta\tau \left[\frac{p^2}{2m} + V(q) \right] \right\} \\ &= e^{-\Delta\tau V(q)} \int \frac{dp}{2\pi} e^{-Ap^2 + iBp}, \quad \text{for} \quad A = \frac{\Delta\tau}{2m}, \quad B = (q' - q). \end{aligned} \quad (2.1.15)$$

By completing the square in the exponent and shifting integration variables, we are

able to perform the integration over p ,

$$\begin{aligned}
-Ap^2 + iBp &= -A \left(p - \frac{iB}{2A} \right)^2 - \frac{B^2}{4A}, \quad \text{let} \quad p' = \left(p - \frac{iB}{2A} \right) \\
\Rightarrow T_{q',q}^E &= e^{-\Delta t V(q)} e^{-\frac{B^2}{4A}} \int_{-\infty}^{\infty} \frac{dp'}{2\pi} e^{-Ap'^2} \\
&= e^{-\Delta t V(q)} e^{-\frac{B^2}{4A}} \left(\frac{1}{4\pi A} \right)^{\frac{1}{2}} \\
&= \left(\frac{m}{2\pi\Delta\tau} \right)^{\frac{1}{2}} \exp \left\{ -\Delta\tau \left[\frac{m}{2} \left(\frac{q' - q}{\Delta\tau} \right)^2 + V(q) \right] \right\}. \quad (2.1.16)
\end{aligned}$$

We may now define the Euclidean path integral as,

$$\begin{aligned}
\langle q_f | e^{\hat{H}^E(\tau-\tau_0)} | q_i \rangle &= \left(\frac{m}{2\pi\Delta\tau} \right)^{\frac{N}{2}} \int dq_{N-1} \dots \int dq_1 \\
&\quad \times \exp \left\{ -\Delta\tau \sum_{n=0}^{N-1} \left[\frac{m}{2} \left(\frac{q'_{n+1} - q_n}{\Delta\tau} \right)^2 + V(q_n) \right] \right\}, \quad (2.1.17)
\end{aligned}$$

whereupon in the limit of $N \rightarrow \infty$ and $\Delta\tau \rightarrow 0$, and using further abbreviated notation,

$$C = \left(\frac{m}{2\pi\Delta\tau} \right)^{\frac{1}{2}}, \quad d[q] = \prod_{n=0}^{N-1} C dq, \quad S^E[q] = \int_{\tau_i}^{\tau_f} d\tau \left[\frac{1}{2} m \dot{q}^2 + V(q) \right], \quad (2.1.18)$$

we arrive at an expression for the amplitude of a Euclidean path integral,

$$\langle q_f | e^{\hat{H}^E(\tau-\tau_0)} | q_i \rangle = C \int_{q_i}^{q_f} d[q] e^{-S^E[q]}. \quad (2.1.19)$$

Some points to note:

- By performing the integration over p , the Hamiltonian action in (2.1.14) has been replaced by the *Lagrangian action*. This is very useful as the Lagrangian is a manifestly covariant object and remains invariant under Lorentz transformations.
- By Wick rotating to Euclidean time, the imaginary phase of the exponent in

(2.1.14) is now replaced with a purely real number. This will prove to be a highly desirable property of the path integral when we try to calculate the energy eigenvalues.

- The constant factor C is highly divergent in the limit $\Delta\tau \rightarrow 0$. However, when we actually calculate physical quantities, this constant factor will cancel out.

2.2 (3+1)D Quantum Scalar Field

We will now show that (2.1.19) generalises to field theory. The calculation is very similar, though we will need to consider more degrees of freedom. The Lagrangian of a classical scalar field $\phi(x)$ is,

$$\begin{aligned} L &= \int d^3\vec{x} \left[\frac{1}{2} \partial^\mu \phi(x) \partial_\mu \phi(x) - V(\phi(x)) \right] \\ &= \int d^3\vec{x} \left[\frac{1}{2} \dot{\phi}(x) - (\vec{\nabla} \phi(x))^2 - V(\phi(x)) \right]. \end{aligned} \quad (2.2.1)$$

By using the canonical momentum,

$$\pi(x) = \frac{\partial}{\partial \dot{\phi}(x)} L = \dot{\phi}(x), \quad (2.2.2)$$

and performing a Legendre transform on the Lagrangian,

$$H = \int d^3x \left[\pi(x) \dot{\phi}(x) - L \right], \quad (2.2.3)$$

we arrive at the scalar field Hamiltonian,

$$H = \int d^3x \left[\frac{1}{2} \hat{\pi}^2(x) + \frac{1}{2} (\vec{\nabla} \hat{\phi}(x))^2 + V(\hat{\phi}(x)) \right]. \quad (2.2.4)$$

Further, by imposing the canonical equal time commutation relations,

$$[\hat{\phi}(\vec{x}), \hat{\pi}(\vec{y})] = i\delta(\vec{x} - \vec{y}), \quad [\hat{\phi}(\vec{x}), \hat{\phi}(\vec{y})] = 0, \quad [\hat{\pi}(\vec{x}), \hat{\pi}(\vec{y})] = 0, \quad (2.2.5)$$

and quantising the classical Hamiltonian, we can express (2.2.4) as a time-independent Schrödinger operator,

$$\hat{H} = \int d^3x \left[\frac{1}{2} \hat{\pi}^2(\vec{x}) + \frac{1}{2} (\vec{\nabla} \hat{\phi}(\vec{x}))^2 + V(\hat{\phi}(\vec{x})) \right]. \quad (2.2.6)$$

At this point, in continuum theory, one would need to introduce a ultra-violet regulator in order to be able to renormalise the theory and extract physical results. This is where lattice gauge theory differs in that a discrete lattice spacing is introduced and remains as a natural ultra-violet cut-off for the theory. We discretise the lattice by replacing the continuous variable \vec{x} with lattice points, and by replacing the integral with a discrete sum,

$$\vec{x} \rightarrow \vec{x} = a(n_x, n_y, n_z), \quad \text{for } a \in \mathbb{R}^+, n \in \mathbb{Z}, \quad \int d^3x \rightarrow \sum_{\vec{x}} a^3, \quad (2.2.7)$$

and by replacing the continuum derivative $\vec{\nabla}$ with a central difference operator,

$$\vec{\nabla}_i \hat{\phi}(\vec{x}) = \frac{\hat{\phi}(\vec{x} + i) - \hat{\phi}(\vec{x} - i)}{2a}, \quad \text{for } i = (a, 0, 0), (0, a, 0), (0, 0, a). \quad (2.2.8)$$

The value of a is the lattice spacing in physical units. At this point, it is useful to introduce a more compact notation. We shall now express the argument of field operator as a subscript,

$$\hat{\phi}(\vec{x}) \equiv \hat{\phi}_{\vec{x}}. \quad (2.2.9)$$

which allows us to express the lattice Hamiltonian as,

$$\hat{H} = \sum_{\vec{x}} a^3 \left[\frac{1}{2} (\hat{\pi}_{\vec{x}})^2 + \frac{1}{2} \sum_i \left(\frac{\hat{\phi}_{\vec{x}+i} - \hat{\phi}_{\vec{x}-i}}{2a} \right)^2 + \frac{m^2}{2} (\hat{\phi}_{\vec{x}})^2 + V(\hat{\phi}_{\vec{x}}) \right]. \quad (2.2.10)$$

We will also switch to a more common notation for the functional integration measure,

$$\mathcal{D}\phi = \prod_{\vec{x}} d\phi_{\vec{x}}, \quad \mathcal{D}\pi = \prod_{\vec{x}} d\pi_{\vec{x}}. \quad (2.2.11)$$

Now, the time evolution operator we wish to evaluate is from an initial field configuration ϕ^i to a final field configuration ϕ^f of field operator eigenstates,

$$\widehat{\phi}_{\vec{x}}|\phi\rangle = \phi_{\vec{x}}|\phi\rangle. \quad (2.2.12)$$

To proceed, we must split the Hamiltonian (2.2.10) into free (\widehat{H}_0) and interacting (\widehat{U}) parts,

$$\widehat{H} = \widehat{H}_0 + \widehat{U} \quad (2.2.13)$$

$$= \sum_{\vec{x}} a^3 \left[\frac{1}{2} \left(-\frac{i}{a^3} \frac{\partial}{\partial \phi_{\vec{x}}} \right)^2 + \left(\frac{1}{2} \sum_i \left[\frac{\widehat{\phi}_{\vec{x}+i} - \widehat{\phi}_{\vec{x}-i}}{2a} \right]^2 + \frac{m^2}{2} (\widehat{\phi}_{\vec{x}})^2 + V(\widehat{\phi}_{\vec{x}}) \right) \right]. \quad (2.2.14)$$

The free Hamiltonian eigenstate is a product over all the plane waves on the lattice. For simplicity, let us consider lattices where n_i runs from $0 \dots N-1$ for $i = x, y, z$, which gives N^3 lattice sites. The field representation of the eigenstate is then,

$$\langle \phi | \pi \rangle = \prod_{\vec{x}} \left(\frac{a^3}{2\pi} \right)^{\frac{1}{2}} e^{ia^3 \pi_{\vec{x}} \phi_{\vec{x}}}, \quad (2.2.15)$$

hence the eigenstate and eigenvalues of \widehat{H}_0 are,

$$\begin{aligned} \langle \phi | \widehat{H}_0 | \pi \rangle &= -\frac{1}{2a^3} \sum_{\vec{x}} \frac{\partial^2}{\partial \phi_{\vec{x}}^2} \langle \phi | \pi \rangle \\ &= \frac{a^3}{2} \sum_{\vec{x}} \pi_{\vec{x}}^2 \langle \phi | \pi \rangle. \end{aligned} \quad (2.2.16)$$

We can use this result to write down an expression for the transfer matrix for the free Hamiltonian by inserting a complete set of field momentum eigenstates,

$$\begin{aligned}
\langle \phi^f | e^{-i\hat{H}_0(t-t_0)} | \phi^i \rangle &= \int \mathcal{D}\pi \langle \phi_f | e^{-i\hat{H}_0(t-t_0)} | \pi \rangle \langle \pi | \phi^i \rangle \\
&= \int \mathcal{D}\pi \langle \phi_f | \pi \rangle \langle \pi | \phi^i \rangle e^{-i\frac{a^3}{2}(t-t_0)\sum_{\vec{x}} \pi_{\vec{x}}^2} \\
&= \prod_{\vec{x}} \frac{a^3}{2\pi} \int_{-\infty}^{\infty} d\pi_{\vec{x}} \exp \left[ia^3 \pi_{\vec{x}} \left(\phi_{\vec{x}}^f - \phi_{\vec{x}}^i \right) \right] \exp \left[-i\frac{a^3}{2}(t-t_0)\pi_{\vec{x}}^2 \right].
\end{aligned} \tag{2.2.17}$$

The above has the form of a Gaussian integral with $\pi_{\vec{x}}$ as the quadratic variable. Using the same technique of completing the square and shifting integration variable, as was performed in the 1D quantum mechanical treatment, we arrive at an expression for the matrix elements of the Euclidean time transporter of the free Hamiltonian,

$$\langle \phi^f | e^{-i\hat{H}_0(t-t_0)} | \phi^i \rangle = \left(\frac{a^3}{2i\pi(t-t_0)} \right)^{\frac{N^3}{2}} \exp \left[-\frac{a^3}{2(t-t_0)} \sum_{\vec{x}} \left(\phi_{\vec{x}}^f - \phi_{\vec{x}}^i \right)^2 \right]. \tag{2.2.18}$$

To calculate the corresponding time transporter for the interacting part of the Hamiltonian, we will be required perform a Wick rotation to Euclidean time $t \rightarrow -i\tau$ and to break the time interval $(\tau - \tau_0)$ into N_t small, equal steps and insert a complete set of basis states at each step. The procedure is very similar to the 1D quantum mechanical case. To begin, we define a new operator \widehat{W} that is equivalent to \widehat{H} to leading order when we expand in powers of $\Delta\tau$,

$$\begin{aligned}
\widehat{W} &= e^{-\frac{\Delta\tau}{2}\widehat{U}} e^{-\Delta\tau\widehat{H}_0} e^{-\frac{\Delta\tau}{2}\widehat{U}} \\
&= \left(1 - \frac{\Delta\tau}{2}\widehat{U} + \mathcal{O}(\Delta\tau)^2 \right) \left(1 - \Delta\tau\widehat{H}_0 + \mathcal{O}(\Delta\tau)^2 \right) \left(1 - \frac{\Delta\tau}{2}\widehat{U} + \mathcal{O}(\Delta\tau)^2 \right) \\
&= 1 - \Delta\tau(\widehat{H}_0 + \widehat{U}) + \mathcal{O}(\Delta\tau)^2.
\end{aligned} \tag{2.2.19}$$

We apply this operator $N_\tau = \frac{(\tau - \tau_0)}{\Delta\tau}$ times, inserting a complete set of field states, totalling $N_\tau - 1$, between each application,

$$\begin{aligned} \langle \phi^f | e^{\widehat{H}(\tau - \tau_0)} | \phi^i \rangle &= \lim_{N_t \rightarrow \infty} \langle \phi^f | \widehat{W}^{N_\tau} | \phi^i \rangle \\ &= \lim_{N_\tau \rightarrow \infty} \int \mathcal{D}\phi^{N_\tau-1} \dots \int \mathcal{D}\phi^1 \langle \phi^f | \widehat{W} | \phi^{N_\tau-1} \rangle \dots \langle \phi^1 | \widehat{W} | \phi^i \rangle. \end{aligned} \quad (2.2.20)$$

The *exact* time evolution operator is obtained in the simultaneous limit $N_\tau \rightarrow \infty$ and $\Delta\tau \rightarrow d\tau$, however, we will not be taking this limit and our results will remain as a discretised approximation. Now, each matrix element will be composed of eigenvalues of \widehat{H}_0 and eigenvalues of \widehat{U} . We have already calculated the former, and we shall use the notation,

$$\widehat{U}|\phi\rangle \equiv U[\phi]|\phi\rangle,$$

to denote the eigenvalues of the interaction term,

$$U[\phi] = a^3 \sum_{\vec{x}} \left(\frac{1}{2} \sum_i \left[\frac{\phi_{\vec{x}+i} - \phi_{\vec{x}-i}}{2a} \right]^2 + \frac{m^2}{2} (\phi_{\vec{x}})^2 + V(\phi_{\vec{x}}) \right). \quad (2.2.21)$$

The Euclidean time transporter between two temporally adjacent complete field basis states j and $j + 1$ is then given by,

$$\begin{aligned} \langle \phi^{j+1} | \widehat{W} | \phi^j \rangle &= \langle \phi^{j+1} | e^{-\frac{\Delta\tau}{2} \widehat{U}} e^{-\Delta\tau \widehat{H}_0} e^{-\frac{\Delta\tau}{2} \widehat{U}} | \phi^j \rangle \\ &= \langle \phi^{j+1} | e^{-\frac{\Delta\tau}{2} \widehat{U}} e^{-\Delta\tau \widehat{H}_0} | \phi^j \rangle e^{-\frac{\Delta\tau}{2} U[\phi^j]} \\ &= \langle \phi^{j+1} | e^{-\frac{\Delta\tau}{2} \widehat{U}} | \phi^j \rangle e^{-\Delta\tau H_0} e^{-\frac{\Delta\tau}{2} U[\phi^j]} \\ &= \left(\frac{a^3}{2\pi\Delta\tau} \right)^{\frac{N^3}{2}} \exp \left[-\frac{\Delta\tau}{2} U[\phi^j] - \frac{a^3}{2\Delta\tau} \sum_{\vec{x}} (\phi_{\vec{x}}^{j+1} - \phi_{\vec{x}}^j)^2 - \frac{\Delta\tau}{2} U[\phi^j] \right] \\ &= \left(\frac{a^3}{2\pi\Delta\tau} \right)^{\frac{N^3}{2}} \exp \left[-\Delta\tau \left\{ \frac{U[\phi^j]}{2} + \frac{a^3}{2} \sum_{\vec{x}} \left(\frac{\phi_{\vec{x}}^{j+1} - \phi_{\vec{x}}^j}{\Delta\tau} \right)^2 + \frac{U[\phi^j]}{2} \right\} \right] \\ &= \left(\frac{a^3}{2\pi\Delta\tau} \right)^{\frac{N^3}{2}} \exp \left[-\Delta\tau \frac{a^3}{2} \sum_{\vec{x}} \left\{ \left(\frac{\phi_{\vec{x}}^{j+1} - \phi_{\vec{x}}^j}{\Delta\tau} \right)^2 + \sum_i \frac{(\phi_{\vec{x}+i}^j - \phi_{\vec{x}-i}^j)^2}{4a^2} \right. \right. \\ &\quad \left. \left. + m^2 (\phi_{\vec{x}}^j)^2 + V(\phi_{\vec{x}}^j) \right\} \right]. \end{aligned} \quad (2.2.22)$$

We now make the assertion that the finite spatial lattice spacing a and the Euclidean temporal spacing $\Delta\tau$ be of the same magnitude (in natural units) which allows us to express the above as a sum over all the 4D lattice points, and we recognise the expression in the exponential as the discretised Euclidean action,

$$\begin{aligned} \langle \phi^f | e^{\hat{H}(\tau-\tau_0)} | \phi^i \rangle &= C^{N^3 N_\tau} \int \mathcal{D}\phi^1 \dots \mathcal{D}\phi^{N_\tau-1} \\ &\times \exp \left[-a^4 \sum_x \left\{ \frac{1}{2} \sum_\mu \left(\frac{\phi_{\vec{x}+\mu} - \phi_{\vec{x}-\mu}}{2a} \right)^2 + \frac{m^2}{2} (\phi_{\vec{x}})^2 + V(\phi_{\vec{x}}) \right\} \right], \\ &= C^{N^3 N_\tau} \int_{\phi^i}^{\phi^f} \mathcal{D}[\phi] e^{-S_E[\phi]}, \end{aligned} \quad (2.2.23)$$

where,

$$\begin{aligned} C &= \left(\frac{a^2}{2\pi} \right)^{\frac{1}{2}}, \quad \mathcal{D}[\phi] = \prod_{j=0}^{N_\tau-1} \int \mathcal{D}\phi^j, \quad S_E[\phi] = a^4 \sum_x \mathcal{L}_E, \\ \mathcal{L}_E &= \frac{1}{2} (\partial_\mu \phi_{\vec{x}})^2 + \frac{m^2}{2} \phi_{\vec{x}}^2 + V(\phi_{\vec{x}}), \quad \partial_\mu = \sum_\mu \left(\frac{\delta_{\vec{x}+\mu} - \delta_{\vec{x}-\mu}}{2a} \right). \end{aligned}$$

Some points to note:

- The forward temporal difference operator in (2.2.22) was replaced, with no loss of generality, by a central difference operator in (2.2.23).
- The sum over temporally separated field eigenstates was incorporated into the sum over lattice points by replacing the 3D \vec{x} with the 4D x . Further, the temporal difference operator was incorporated into the sum over adjacent lattice sites by extending the spatial index $i = x, y, z$ to a Euclidean spacetime index $\mu = x, y, z, \tau$.
- The constant factor C , which was highly divergent in the continuum limit of $\Delta t \rightarrow 0$ in the quantum mechanical treatment, has now been tamed to be of order a^2 . Of course, if one were to construct an anisotropic lattice where $\frac{\Delta\tau}{a^3} \rightarrow 0$, the divergence of this factor would reappear, but given that we are restricting ourselves to finite lattice spacing, this will not be a problem. As mentioned in the previous section, this constant factor is irrelevant when

extracting physical quantities and we will see in the next section that it cancels out in such calculations.

2.3 Euclidean Scalar Field Correlation Functions

The partition function of a quantum system is formally given by the trace over the state space,

$$Z = \text{Tr}[e^{-\hat{H}T}]. \quad (2.3.1)$$

For our discrete, Euclidean scalar field, this means that we should impose periodic temporal boundary conditions on our functional integral, i.e., assert that the initial and final field configurations are the same,

$$\begin{aligned} Z_E &= \langle \phi^i | e^{\hat{H}(\tau-\tau_0)} | \phi^i \rangle, \\ &= \int \mathcal{D}\phi^{N_{\tau-1}} \dots \int \mathcal{D}\phi^0 \langle \phi^0 | \widehat{W} | \phi^{N_{\tau-1}} \rangle \dots \langle \phi^1 | \widehat{W} | \phi^0 \rangle, \\ &= C^{N^3 N_{\tau}} \oint_{\tau} \mathcal{D}[\phi] e^{-S_E[\phi]}. \end{aligned} \quad (2.3.2)$$

Now, in perfect analogy with statistical mechanics, we can extract probabilities from our Euclidean scalar field by inserting operators into our path integral, which play the rôle of microstates weighted by an ensemble average. For a two-point correlation function with one operator inserted at $\tau = 0$ and another at some $\tau \geq 0$, we find that,

$$\begin{aligned} \langle \mathcal{O}_2(\tau) \mathcal{O}_1(0) \rangle &= \frac{1}{Z_E} \text{Tr}[\widehat{W}^{N_{\tau}-\tau} \widehat{\mathcal{O}}_2(\tau) \widehat{W}^{\tau} \widehat{\mathcal{O}}_1(0)] \\ &= \frac{1}{Z_E} \int \mathcal{D}\phi^0 \dots \mathcal{D}\phi^{N_{\tau}-1} \mathcal{D}\tilde{\phi}^0 \mathcal{D}\tilde{\phi}^{\tau} \langle \phi^0 | \widehat{W} | \phi^{N_{\tau}-1} \rangle \langle \phi^{N_{\tau}-1} | \widehat{W} | \phi^{N_{\tau}-2} \rangle \dots \\ &\quad \langle \phi^{\tau+1} | \widehat{W} | \tilde{\phi}^{\tau} \rangle \langle \tilde{\phi}^{\tau} | \widehat{\mathcal{O}}_2(\tau) | \phi^{\tau-1} \rangle \dots \langle \phi^1 | \widehat{W} | \tilde{\phi}^0 \rangle \langle \tilde{\phi}^0 | \widehat{\mathcal{O}}_1(0) | \phi^0 \rangle. \end{aligned} \quad (2.3.3)$$

Notice the extra insertions of the tilded field basis states $|\tilde{\phi}\rangle\langle\tilde{\phi}|$. This allows us to replace the operators $\widehat{\mathcal{O}}_1$ and $\widehat{\mathcal{O}}_2$ with their eigenvalues, which are Green functions

in field configuration space,

$$\langle \tilde{\phi} | \hat{\mathcal{O}} | \phi \rangle = \mathcal{O}[\phi] \delta(\tilde{\phi} - \phi). \quad (2.3.4)$$

Using the above eigenvalues and integrating out the tilded fields, the normalisation factors C will cancel out and we have a finite expression for the correlation two-point correlation function,

$$\langle \mathcal{O}_2(\tau) \mathcal{O}_1(0) \rangle = \frac{\int \mathcal{D}[\phi] \mathcal{O}_2(\tau) \mathcal{O}_1(0) e^{-S_E[\phi]}}{\int \mathcal{D}[\phi] e^{-S_E[\phi]}}. \quad (2.3.5)$$

This is a crucial result. If we now recast the $\mathcal{O}_2(t)$ operator into the Schrödinger picture,

$$\mathcal{O}_2(t) = e^{\hat{H}t} \mathcal{O}_2(0) e^{-\hat{H}t}, \quad (2.3.6)$$

insert a complete set of momentum eigenstates labeled by k between the operators, and allow the temporal extent of our lattice to become sufficiently large, we are able to extract the ground-state energy of the system,

$$\begin{aligned} \lim_{N_\tau \rightarrow \infty} \langle \mathcal{O}_2(\tau) \mathcal{O}_1(0) \rangle &= \sum_k \langle \Omega | e^{\hat{H}\tau} \mathcal{O}_2(0) e^{-\hat{H}\tau} | k \rangle \langle k | \mathcal{O}_1(0) | \Omega \rangle \\ &= \sum_k \langle \Omega | \mathcal{O}_2(0) | k \rangle \langle k | \mathcal{O}_1(0) | \Omega \rangle \\ &= \langle \Omega | \mathcal{O}_2(0) | 0 \rangle \langle 0 | \mathcal{O}_1(0) | \Omega \rangle + \text{Excited States}, \end{aligned} \quad (2.3.7)$$

where we label the vacuum state as $|\Omega\rangle$. By taking repeated measurements of this two-point correlation function at different τ , we can measure the exponential decay of the correlation function values and fit the data to obtain a value for E_0 . This rather general argument will form the basis for extracting ground state energies of n -point correlation functions in QCD using lattice gauge theory in the next section.

CHAPTER 3

Quantum Chromodynamics

The accepted theory of strong dynamics in the Standard Model is Quantum Chromodynamics (QCD). In this model, hadrons and baryons are composed of spin- $\frac{1}{2}$ fundamental fermions, called quarks, of which there are six flavours. There is an inter-quark potential mediated by gauge bosons known as gluons, which carry no flavour structure. All objects in QCD carry an unobservable quantum number known as colour. The properties of quarks will be briefly described and, in more detail, the properties of gluons as the gauge bosons of QCD. This more detailed description will serve to justify the discrete lattice gauge theory used to study continuum QCD.

3.1 Quarks

Each quark in QCD is a massive, spin- $\frac{1}{2}$ Dirac fermion. As well as spin quantum numbers (and spacetime dependence) quarks carry an additional quantum number called colour. Quarks carry fractional charges of $Q|e|$ where e is the charge of the positron. The six quark flavours are listed, with their respective electromagnetic charges in table 3.1. Quarks are usually denoted as q and anti-quarks as \bar{q} .

Table 3.1: The six known quarks. Each box shows the name (flavour), symbol, and electromagnetic charge of each quark.

up u $+\frac{2}{3}e$	charm c $+\frac{2}{3}e$	top t $+\frac{2}{3}e$
down d $-\frac{1}{3}e$	strange s $-\frac{1}{3}e$	bottom b $-\frac{1}{3}e$

The number of different colour states that a quark can have can be determined

by studying the cross section of the well understood quantum electrodynamics process of $e^+e^- \rightarrow \mu^+\mu^-$. In the high energy limit, the cross section for this process is,

$$\sigma(e^+e^- \rightarrow \mu^+\mu^-) = \frac{4\pi\alpha^2}{3E_{cm}^2}, \quad \text{for } E_{cm} \gg m_\mu, \quad (3.1.1)$$

where $\alpha = \frac{1}{4\pi\epsilon_0} \frac{e^2}{\hbar c}$ is the fine structure constant in SI units and E_{cm} is the centre of mass energy of the system. For the analogous process of $e^+e^- \rightarrow q\bar{q}$, (3.1.1) must be modified to account for the different charges of the quarks by replacement of the value of the lepton electric charge e by $Q|e|$. The colour phase space of the $q\bar{q}$ system is included by multiplying the cross section by a factor of n , the number of possible final colour states. This gives a cross section for $q\bar{q}$ production of,

$$\sigma(e^+e^- \rightarrow q\bar{q}) = n \cdot Q^2 \cdot \frac{4\pi\alpha^2}{3E_{cm}^2} = n \cdot Q^2 \cdot \sigma(e^+e^- \rightarrow \mu^+\mu^-), \quad (3.1.2)$$

where again the limit of high E_{cm} is taken. The experimental evidence supporting this claim, with the electromagnetic charge values of Q shown in table 3.1 and a colour factor of $n = 3$ is very good. Figure 3.1 shows the ratio of the cross section for quark production to muon production as a function of centre of mass energy. The dots, with their respective error bars, are experimental measurements for the given $q\bar{q}$ pairs and the solid line is the prediction given by (3.1.2) with $n = 3$. This places the quark model, and the properties of the quarks as given in table 3.1, each with three possible colour states, in a firm position as a theory of hadronic structure.

3.2 $SU(3)$ Gauge Invariance

Although the quarks carry electric charge, the principal force experienced by quarks is due to the colour charges they carry. This force is mediated by a gauge boson called a gluon. The gluon itself is a massless spin-1 vector boson. Consequently, a gluon has only two longitudinal spin states, and no third transverse state, as would be the case for a massive spin-1 vector boson. In Nature, the hadrons do not carry colour quantum numbers. The hadrons are said to be colour singlets. This means that colour is a gauge degree of freedom and hence all observable properties of

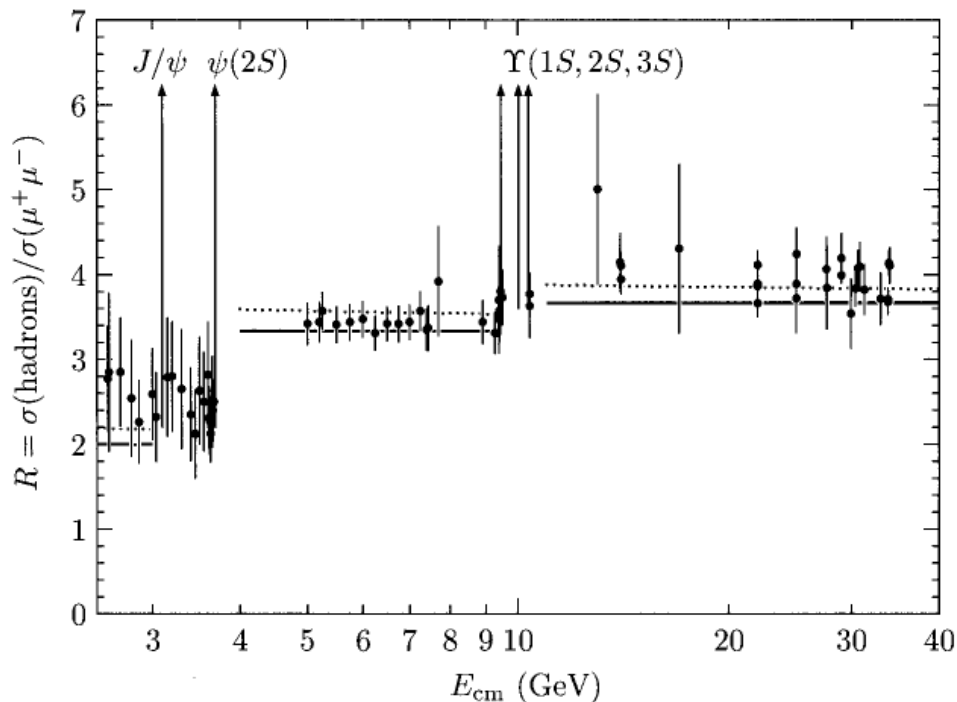


Figure 3.1: Cross sections for hadron ($q\bar{q}$) production via e^-e^+ . (Figure from Peskin and Schroeder (3))

hadrons must be colour gauge invariant. Any gauge transformation on, say, a $\langle q|\bar{q}\rangle$ system must leave the inner product invariant. Important properties of the colour gauge can be deduced from this constraint. Consider a quark, with spin quantum numbers suppressed, in some colour state,

$$|q\rangle = q_a = \begin{bmatrix} g \\ r \\ b \end{bmatrix}, \quad \text{for } a = 1, 2, 3. \quad (3.2.1)$$

The convention here is to name the three colour states as red, blue, and green. However, given that these quantum numbers are not observable, the order in which the r , g , and b states are placed is immaterial, provided one is consistent. Also note that there is no difference between a raised or lowered colour index. By applying

some colour gauge transformation V_{ab} on the $|q\rangle = q_b$ quark state,

$$q'_a = V_{ab}q_b, \quad (3.2.2)$$

and then conjugating this result to get the transformed $\langle q'| = \bar{q}'_a$ state,

$$\bar{q}'_b = \bar{q}_a V_{ab}^\dagger, \quad (3.2.3)$$

it is clear that in order to preserve the relationship $\langle q|q\rangle = \langle q'|q'\rangle$, the condition,

$$V_{ab}^\dagger = V_{ab}^{-1}, \quad (3.2.4)$$

must be imposed. Therefore, all colour gauge transformations must be, at the very least, part of the $U(3)$ unitary group.

The above transformation was strictly speaking a global transformation, i.e., the transformation had no explicit spacetime dependence, but there is no reason to believe that Nature would be so kind that only global transformations on the colour field need be considered. A local gauge transformation that has explicit spacetime dependence,

$$V_{ab} \rightarrow V_{ab}(x), \quad (3.2.5)$$

ought to be considered, where x is understood to represent the four-vector x^μ . It is useful at this point to recognise that an element of the $U(N)$ group where N is any positive integer value, can be decomposed into a complex constant, and a corresponding element of a subgroup of $U(N)$, that of $SU(N)$,

$$U(N) = U(1) \times SU(N). \quad (3.2.6)$$

$U(N)$ has the properties,

$$\det[U(N)U^\dagger(N)] = 1 \quad \text{and} \quad \det[U(N)] = z, \quad z \in \mathbb{C}. \quad (3.2.7)$$

By contrast, $SU(N)$ has the properties,

$$\det[SU(N)SU^\dagger(N)] = 1 \quad \text{and} \quad \det[SU(N)] = +1. \quad (3.2.8)$$

The effect of promoting the colour gauge transformation from global to local can be understood in terms of the effect it has on the action. Consider the Lagrangian of a some quark field $\psi(x)$,

$$\mathcal{L}_q = \bar{\psi}(x) [i\gamma^\mu \partial_\mu - m] \psi(x), \quad (3.2.9)$$

where colour indices have been suppressed for clarity. At this point, it is convenient to introduce the Feynman Slash notation $\gamma^\mu A_\mu \equiv \not{A}$ for any four-vector operator A_μ . If a colour gauge transformation is applied to \mathcal{L}_q ,

$$\begin{aligned} \mathcal{L}_q \rightarrow \mathcal{L}'_q &= \bar{\psi}(x)V^\dagger(x) [i\partial - m] V(x)\psi(x) \\ &= \bar{\psi}(x)V^\dagger(x) [i\partial(V(x)\psi(x)) - mV(x)\psi(x)] \\ &= \bar{\psi}(x)[i\partial - m]\psi(x) + \bar{\psi}(x)V^\dagger(x)[i\partial V(x)]\psi(x) \\ &= \mathcal{L}_q + \bar{\psi}(x)V^\dagger(x)[i\partial V(x)]\psi(x), \end{aligned} \quad (3.2.10)$$

it is clear that the Lagrangian does not change by a total derivative. Therefore, the transformation $V(x)$ is patently not gauge invariant as, by definition, gauge transformations do not affect the action. This is because the partial differential operator ∂ is acting on quark fields at two infinitesimally separated points in spacetime, so the gauge transformations of these two points will also differ infinitesimally. A gauge covariant derivative must be formed. This new derivative, \not{D} must, under a gauge transformation, take the form,

$$\not{D}\psi(x) \rightarrow V(x)\not{D}\psi(x), \quad (3.2.11)$$

so that,

$$\begin{aligned}
\mathcal{L}_q &= \bar{\psi}(x) [i\mathcal{D} - m] \psi(x) \rightarrow \mathcal{L}'_q = \bar{\psi}(x)V^\dagger(x)V(x)i\mathcal{D}\psi(x) - \bar{\psi}(x)V^\dagger(x)mV(x)\psi(x) \\
&= \bar{\psi}(x)[i\mathcal{D} - m]\psi(x) \\
&= \mathcal{L}_q.
\end{aligned} \tag{3.2.12}$$

Consider, then, some operator $U(y, x)$ which is an element of $SU(3)$, has spacetime dependence on two points, x and y , transforms as,

$$U(y, x) \rightarrow V(y)U(y, x)V^\dagger(x), \tag{3.2.13}$$

and acts on some quark field located at x . If a colour gauge transformation is applied,

$$\begin{aligned}
U(y, x)\psi(x) &\rightarrow V(y)U(y, x)V^\dagger(x)V(x)\psi(x) \\
&= V(y)U(y, x)\psi(x),
\end{aligned} \tag{3.2.14}$$

one can see that the object $U(y, x)\psi(x)$ transforms in exactly as $\psi(y)$. The object $U(y, x)$ is a parallel transport from x to y . $U(y, x)$ can be constructed by considering y to be infinitesimally close to x ,

$$y^\mu \rightarrow x^\mu + \epsilon n^\mu, \tag{3.2.15}$$

where ϵ is an infinitesimal constant and n^μ is the unit four-vector, and then Taylor expanding about x . Given that $U(y, x)$ is an element of $SU(3)$, it is convenient to use the exponential representation,

$$U(y, x) \in SU(3) = \exp(i\lambda^a(y, x)\tau^a) \quad \text{for } a = 1, \dots, 8, \tag{3.2.16}$$

where τ^a are the generators of $SU(3)$ and $\lambda^a(y, x)$ are infinitesimal parameters defin-

ing the element. Expanding just $U(x + \epsilon n, x)$ first,

$$\begin{aligned} U(x + \epsilon n, x) &= 1 + i\lambda^a(x + \epsilon n, x)\tau^a + \mathcal{O}(\lambda^2), \\ &\cong 1 + ig\epsilon n^\mu A_\mu(x) \quad \text{for} \quad A_\mu(x) = \sum_a A_\mu^a(x)\tau^a, \end{aligned} \quad (3.2.17)$$

where $A_\mu(x)$ is a traceless, hermitian operator, defined at x only. It is called the gauge connection. The dimensionless constant factor g has been inserted for later convenience [see (3.3.13) and (3.3.14).]

Aside: Even though the parameter $\lambda^a(x + \epsilon n, x)$ is defined at two different points in spacetime, $A_\mu(x)$ is defined at x only because it is directed towards $x + \epsilon n$ and the infinitesimal change in $\lambda^a(x + \epsilon n, x)$ is defined to be linear. Further, $A_\mu(x)$ must be traceless and hermitian so that $U(x + \epsilon n, x)$ remains unitary³.

Recall from (3.2.14) how the quark fields with a gauge connection are expected to transform. Using this, and an exponential representation $e^{i\alpha(x)} = \exp(i\alpha^a(x)\tau^a)$ for the $SU(3)$ elements, the gauge transformation for the gauge transport can be inferred by computing the necessary transformation for the gauge connection $A_\mu(x)$,

$$\begin{aligned} U(x + \epsilon n, x) &\rightarrow V(x + \epsilon n)U(x + \epsilon n, x)V^\dagger(x) \\ &= e^{i\alpha(x+\epsilon n)}(1 + ig\epsilon n^\mu A_\mu^a(x)\tau^a)e^{-i\alpha(x)} \\ &= e^{i\alpha(x)}(1 + i\epsilon n^\mu[\partial_\mu\alpha(x)] + \mathcal{O}(\epsilon^2))(1 + ig\epsilon n^\mu A_\mu^a(x)\tau^a)e^{-i\alpha(x)} \\ &= e^{i\alpha(x)}(1 + ig\epsilon n^\mu A_\mu^a(x)\tau^a + i\epsilon n^\mu[\partial_\mu\alpha(x)] + \mathcal{O}(\epsilon^2))e^{-i\alpha(x)} \\ &= e^{i\alpha(x)}(1 + ig\epsilon n^\mu A_\mu^a(x)\tau^a - \epsilon n^\mu\partial_\mu)e^{-i\alpha(x)}. \end{aligned} \quad (3.2.18)$$

In the third line, $e^{i\alpha(x+\epsilon n)}$ is expanded about x . Evidently, the gauge transformation

³see appendix A.

of $A_\mu(x)$ contains a derivative term,

$$\begin{aligned} A_\mu^a(x)\tau^a &\rightarrow e^{i\alpha(x)} \left[A_\mu^a(x)\tau^a + \frac{i}{g}\partial_\mu \right] e^{-i\alpha(x)} \\ &= e^{i\alpha(x)} \left[A_\mu^a(x)\tau^a + \frac{1}{g}\partial_\mu\alpha(x) \right] e^{-i\alpha(x)}. \end{aligned} \quad (3.2.19)$$

Putting all this together, one concludes that the gauge covariant differential operator must take the form,

$$\mathcal{D} = [\not{\partial} - ig\not{A}(x)] \rightarrow \mathcal{D}' = [\not{\partial} - ig(\not{A}(x) + \frac{1}{g}[\not{\partial}\alpha(x)])]. \quad (3.2.20)$$

Putting (3.2.20) to the test by substituting into (3.2.12) will confirm it is the desired form of \mathcal{D} we required from (3.2.11). However, one must be careful to account for the non-commutativity of $A_\mu^a(x)\tau^a$ and $e^{-i\alpha(x)}$. By considering infinitesimal gauge transformations,

$$e^{i\alpha(x)} = 1 + i\alpha^a(x)\tau^a + \mathcal{O}(\alpha^2) \quad (3.2.21)$$

so that,

$$\begin{aligned} A_\mu^a(x)\tau^a &\rightarrow (1 + i\alpha^b(x)\tau^b)(A_\mu^a(x)\tau^a + \frac{i}{g}\partial_\mu)(1 - i\alpha^c(x)\tau^c) \\ &= (1 + i\alpha^b(x)\tau^b)(A_\mu^a(x)\tau^a - iA_\mu^a(x)\tau^a\alpha^c(x)\tau^c + \frac{1}{g}\partial_\mu\alpha^c(x)\tau^c) \\ &= A_\mu^a(x)\tau^a + \frac{1}{g}[\partial_\mu\alpha^a(x)]\tau^a + i\alpha^b(x)\tau^b A_\mu^c(x)\tau^c - iA_\mu^b(x)\tau^b\alpha^c(x)\tau^c + \mathcal{O}(\alpha^2) \\ &= A_\mu^a(x)\tau^a + \frac{1}{g}[\partial_\mu\alpha^a(x)]\tau^a - [\tau^b, \tau^c]\alpha^b(x)A_\mu^c(x) \\ &= \left[A_\mu^a(x) + \frac{1}{g}[\partial_\mu\alpha^a(x)] - f^{abc}\alpha^b(x)A_\mu^c(x) \right] \tau^a, \end{aligned} \quad (3.2.22)$$

where in the above calculation, relabelling over summed indices was employed and in the commutator we used the relationship,

$$[\tau^b, \tau^c] = if^{abc}\tau^a, \quad (3.2.23)$$

where a, b, c represent the 8 generators of $SU(3)$ and f^{abc} are the structure constants

of the algebra,⁴ (3.2.11) is shown to hold. Dependence on x will be suppressed in the following,

$$\begin{aligned}
\mathcal{D}\psi &\rightarrow \mathcal{D}'(1 + i\alpha^a\tau^a)\psi \\
&= i\gamma^\mu(\partial_\mu - igA_\mu^a\tau^a - i[\partial_\mu\alpha^a]\tau^a + g[\alpha^a\tau^a, A_\mu^b\tau^b])(1 + i\alpha^c\tau^c)\psi \\
&= i\gamma^\mu(\partial_\mu\psi + \cancel{i[\partial_\mu\alpha^c]\tau^c\psi} + i\alpha^c\tau^c[\partial_\mu\psi] - igA_\mu^a\tau^a\psi + \cancel{gA_\mu^a\tau^a\alpha^c\tau^c\psi} \\
&\quad \cancel{-i[\partial_\mu\alpha^a]\tau^a\psi} + g\alpha^a\tau^a A_\mu^b\tau^b\psi - \cancel{gA_\mu^b\tau^b\alpha^a\tau^a} + \mathcal{O}(\alpha^2)) \\
&= (1 + i\alpha^b\tau^b)i\gamma^\mu(\partial_\mu - igA_\mu^a\tau^a)\psi \\
&= (1 + i\alpha^a\tau^a)\mathcal{D}'\psi.
\end{aligned} \tag{3.2.24}$$

The γ^μ matrices commute with the $SU(3)$ colour matrices as they act on different spaces. Finite colour gauge transformations are built up of infinite products of infinitesimal transformations and hence a full gauge covariant Lagrangian for the quark colour interaction has been constructed and it is simple to check using (3.2.24),

$$\begin{aligned}
\mathcal{L}_q &= \bar{\psi}(x) [i\mathcal{D} - m] \psi(x) \rightarrow \bar{\psi}(x)e^{-i\alpha(x)}[i\mathcal{D}' - m]e^{i\alpha(x)}\psi(x) \\
&= \bar{\psi}(x)e^{-i\alpha(x)}e^{i\alpha(x)}[i\mathcal{D} - m]\psi(x) \\
&= \mathcal{L}_q.
\end{aligned} \tag{3.2.25}$$

The part of the QCD colour gauge invariant Lagrangian governing quarks of flavour f may now be written down, with latin indices for colour,

$$\mathcal{L}_q = \bar{\psi}_f^i(x) [i(\mathcal{D})^{ij} - m\delta^{ij}] \psi_f^j(x). \tag{3.2.26}$$

3.3 Gluons

As can be seen from the previous section, the gauge connection,

$$A_\mu(x) = \sum_a A_\mu^a(x)\tau^a \quad \text{for } a = 1, \dots, 8, \tag{3.3.1}$$

⁴see appendix A.

plays a crucial role in gauge invariance. The τ^a are a set of 8 matrices known as the generators of $SU(3)$. They are constant matrices, but can take on various forms depending on which representation of $SU(3)$ in which one wishes to work. The $A_\mu^a(x)$ are gauge fields and are dynamical. As such, a kinetic term for these fields must be formed that is independent of the quark fields and contains terms dependent on $A_\mu^a(x)$ and its derivatives only. Furthermore, any such kinetic term must be gauge invariant. These restrictions are enough to deduce the properties of the gauge kinetic term.

In analogy with electrodynamics, a field strength tensor $G_{\mu\nu}^a$ can be formed by computing the commutator of the covariant derivative. However, in contrast to the electromagnetic field strength tensor $F_{\mu\nu}$, $G_{\mu\nu}^a$ will contain products of gauge fields. These arise due to the non-commutative property of the $SU(3)$ generators present in $A_\mu^a(x)\tau^a$. The spacetime dependence of $A_\mu^a(x)\tau^a$ will be assumed and suppressed in the following.

$$\begin{aligned}
[D_\mu, D_\nu] &= (\partial_\mu - igA_\mu^a\tau^a)(\partial_\nu - igA_\nu^b\tau^b) - (\partial_\nu - igA_\nu^b\tau^b)(\partial_\mu - igA_\mu^a\tau^a) \\
&= \cancel{\partial_\mu\partial_\nu} - ig(\partial_\mu A_\nu^b\tau^b + \cancel{A_\mu^a\tau^a\partial_\nu}) - g^2 A_\mu^a\tau^a A_\nu^b\tau^b \\
&\quad - \cancel{\partial_\nu\partial_\mu} + ig(\partial_\nu A_\mu^a\tau^a + \cancel{A_\nu^b\tau^b\partial_\mu}) + g^2 A_\nu^b\tau^b A_\mu^a\tau^a.
\end{aligned} \tag{3.3.2}$$

The partial derivatives cancel due to their commutative property, and the terms with the derivatives on the right may be relabelled so that they cancel each other. This freedom to relabel is because the derivatives act on spinors colour space only, i.e., $\psi^i(x)$. The partial derivatives acting on the gauge fields do not have such freedom and their indices must be preserved. Continuing from above,

$$\begin{aligned}
[D_\mu, D_\nu] &= ig(\partial_\nu A_\mu^a\tau^a - \partial_\mu A_\nu^b\tau^b - ig[A_\nu^b\tau^b, A_\mu^a\tau^a]) \\
&= ig(\partial_\nu A_\mu^a\tau^a - \partial_\mu A_\nu^a\tau^a - ig[\tau^b, \tau^a]A_\nu^b A_\mu^a).
\end{aligned} \tag{3.3.3}$$

In (3.3.3), the A_μ^a gauge fields are simply four-vector coefficients of the generators,

and hence commute among themselves and with τ^a . (3.3.3) can be rewritten as,

$$\begin{aligned}
[D_\mu, D_\nu] &= ig(\partial_\nu A_\mu^a \tau^a - \partial_\mu A_\nu^a \tau^a - ig[\tau^b, \tau^c] A_\nu^b A_\mu^c) \\
&= ig(\partial_\nu A_\mu^a - \partial_\mu A_\nu^a + gf^{abc} A_\nu^b A_\mu^c) \tau^a \\
&\equiv igG_{\nu\mu}^a \tau^a \tag{3.3.4}
\end{aligned}$$

$$\begin{aligned}
&\equiv -igG_{\mu\nu} \quad (G_{\mu\nu}^a \tau^a \equiv G_{\mu\nu}) \\
\Rightarrow G_{\mu\nu}^a &= \partial_\mu A_\nu^a - \partial_\nu A_\mu^a + gf^{abc} A_\mu^b A_\nu^c. \tag{3.3.5}
\end{aligned}$$

In order to ascertain if this field strength tensor (or functions thereof) is a candidate object for a gauge invariant term in the Lagrangian, its gauge transformation properties must be computed. For a finite gauge transformation, one can use the transformation properties of the gauge covariant derivative to ascertain how the finite gauge field transformation,

$$\begin{aligned}
D_\mu \psi &\rightarrow D'_\mu V(x) \psi, \\
&= V(x) D_\mu \psi, \\
\Rightarrow \bar{\psi} D_\mu \psi &\rightarrow \bar{\psi} V^\dagger(x) D_\mu V(x) \psi, \\
\Rightarrow D_\mu &\rightarrow V^\dagger(x) D_\mu V(x), \tag{3.3.6}
\end{aligned}$$

and hence,

$$\begin{aligned}
-igG_{\mu\nu} &= [D_\mu, D_\nu] \rightarrow [D'_\mu, D'_\nu] \\
&= V^\dagger(x) D_\mu \overbrace{[V(x) V^\dagger(x)]}^{=1} D_\nu V(x) - V^\dagger(x) D_\nu \overbrace{[V(x) V^\dagger(x)]}^{=1} D_\mu V(x) \\
&= V^\dagger(x) [D_\mu, D_\nu] V(x) \\
&= -igV^\dagger(x) G_{\mu\nu} V(x) \tag{3.3.7}
\end{aligned}$$

Using an infinitesimal gauge transformation (3.2.21) and the $SU(3)$ algebra (3.2.23),

$$\begin{aligned}
G_{\mu\nu} &\rightarrow (1 - i\alpha^b \tau^b) G_{\mu\nu}^a \tau^a (1 + i\alpha^c \tau^c) \\
&= G_{\mu\nu}^a \tau^a + \underbrace{i G_{\mu\nu}^a \tau^a \alpha^c \tau^c}_{\text{let } a \rightarrow b} - \underbrace{i\alpha^b \tau^b G_{\mu\nu}^a \tau^a}_{\text{let } a \rightarrow c} + \mathcal{O}(\alpha^2) \\
&= G_{\mu\nu}^a \tau^a + i G_{\mu\nu}^b \tau^b \alpha^c \tau^c - i\alpha^b \tau^b G_{\mu\nu}^c \tau^c + \mathcal{O}(\alpha^2) \\
&= G_{\mu\nu}^a \tau^a + i[\tau^b, \tau^c] G_{\mu\nu}^b \alpha^c \\
&= (G_{\mu\nu}^a - f^{bca} G_{\mu\nu}^b \alpha^c) \tau^a \\
&= (G_{\mu\nu}^a - f^{abc} G_{\mu\nu}^b \alpha^c) \tau^a \quad \text{using } f^{bca} = f^{abc}. \tag{3.3.8}
\end{aligned}$$

Evidently, the field strength tensor is not a gauge invariant quantity. However, the product $\text{Tr}(G^2)$ is indeed gauge invariant,

$$\begin{aligned}
\text{Tr}[G^2] &= \text{Tr}[G_{\mu\nu} G^{\mu\nu}] \rightarrow \text{Tr}[G'_{\mu\nu} G'^{\mu\nu}] \\
&= \text{Tr}[V^\dagger(x) G_{\mu\nu} V(x) V^\dagger(x) G^{\mu\nu} V(x)] \\
&= \text{Tr}[V(x) V^\dagger(x) G_{\mu\nu} G^{\mu\nu}] \tag{3.3.9a}
\end{aligned}$$

$$\begin{aligned}
&= \text{Tr}[G_{\mu\nu} G^{\mu\nu}] \\
&= \text{Tr}[G^2], \tag{3.3.9b}
\end{aligned}$$

where in (3.3.9a), the cyclic property of traces was employed. This pure gauge term is often written as,

$$\frac{1}{4} (G_{\mu\nu})^a (G^{\mu\nu})^a = \frac{1}{2} \text{Tr}[G^2], \tag{3.3.10}$$

so that the subsequent equation of motions of the gluons has no overall coefficient. The factor of $\frac{1}{2}$ in the trace is due to the trace over the generators⁵ present in G^2 ,

$$\text{Tr}[\tau^a \tau^b] = \frac{1}{2} \delta^{ab}. \tag{3.3.11}$$

There is now enough information to write down a gauge invariant, interacting

⁵See appendix A

Lagrangian⁶ for both quark fields $\psi(x)$, and gluon fields $A_\mu^a(x)$,

$$\mathcal{L}_{QCD} = \bar{\psi}_f^i(x)(i\not{D})^{ij}\psi_f^j(x) - \frac{1}{2}\text{Tr}[G^2] - \bar{\psi}_f^i(x)m\delta^{ij}\psi_f^j(x) \quad (3.3.12)$$

This new gauge invariant term of the gluon fields has some interesting properties. Primarily, the non-abelian nature of the gauge fields (3.3.5) gives rise to a product of gauge fields in the Lagrangian. In the full quantum theory, this translates to triple vertex and quartic vertex gluon interactions; a phenomenon not seen in the strictly abelian case for quantum electrodynamics where photons do not interact with each other. This can be seen by multiplying out the trace term in (3.3.12).

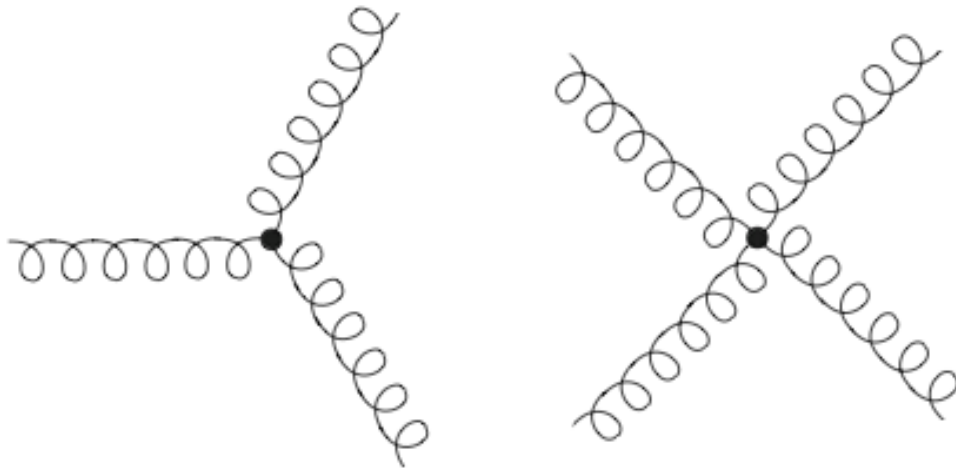


Figure 3.2: Triple and quadruple vertices of interacting gluons.

The triple vertex part of the Lagrangian is,

$$\mathcal{L}_{triple} \propto -g(\partial_\mu A_\nu^a - \partial_\nu A_\mu^a)f^{abc}A_\mu^b A_\nu^c, \quad (3.3.13)$$

which clearly involves the interaction of three terms at a single spacetime point. Further, the dimensionless coupling constant introduced in (3.2.17) is justified as g now appears naturally as a coupling constant of the gauge fields. The quadruple

⁶Another gauge invariant quantity of significant importance to beyond standard model physics is the term $-\frac{1}{2}\theta_{ab}\epsilon^{\mu\nu\rho\sigma}G_{\mu\nu}^a G_{\rho\sigma}^b$. However, this term does not respect CP symmetry and we do not see CP violation in QCD, therefore it is omitted from the standard model.

vertex part is,

$$\mathcal{L}_{quartic} \propto -g^2 f^{abc} f^{ade} A_\mu^b A_\nu^c A^{\mu d} A^{\nu e}. \quad (3.3.14)$$

In the quantum theory, these gauge interactions correspond to the Feynman diagrams in figure 3.2.

3.4 QCD equations of motion

Following Lagrangian formalism, the equations of motion can be deduced from the Euler-Lagrange equation,

$$\frac{\partial \mathcal{L}}{\partial q_i} - \partial_\mu \left(\frac{\partial \mathcal{L}}{\partial (\partial_\mu q_i)} \right) = 0, \quad (3.4.1)$$

for any generalised coordinate q_i . The QCD Lagrangian contains two dynamic fields, ψ and A and their derivatives. The equation of motion for ψ is obtained by varying with respect to $\bar{\psi}$,

$$\begin{aligned} \frac{\partial \mathcal{L}}{\partial \bar{\psi}} &= (i\not{D} - m)\psi, \quad \partial_\mu \left(\frac{\partial \mathcal{L}}{\partial (\partial_\mu \bar{\psi})} \right) = 0 \\ &\Rightarrow (i\not{D} - m)\psi = 0, \\ \text{or} \quad (i\overleftarrow{\not{D}} - m)\psi &= -g\gamma^\mu \frac{\lambda^a}{2}\psi, \end{aligned} \quad (3.4.2)$$

which is just the Dirac equation for the spinor ψ (λ here denote the Gell-Mann matrices (A.1.4)). Notice that there are no derivative terms in $\bar{\psi}$ in the Lagrangian. One can also vary the Lagrangian with respect to ψ to get the equation of motion for $\bar{\psi}$, which will result in the Dirac equation for $\bar{\psi}$, but with a subtlety in notation,

$$\begin{aligned} \bar{\psi}(i\overleftarrow{\not{D}} - m) &= 0, \\ \text{or} \quad \bar{\psi}(i\overleftarrow{\not{D}} - m) &= -g\bar{\psi}\gamma^\mu \frac{\lambda^a}{2}. \end{aligned} \quad (3.4.3)$$

The arrow over the derivative simply instructs us to operate to the left so that the left-right ordering of $\bar{\psi}$ and ψ is preserved.

For the gauge fields, variation with respect to A_μ will yield two non-zero terms.

Using the relation,

$$\frac{\partial A_\mu^a}{\partial A_\nu^b} = \eta_\mu^\nu \delta^{ab} = \delta_\mu^\nu \delta^{ab} \quad \text{from} \quad \eta_{\mu\rho} \eta^{\rho\nu} = \eta_\mu^\nu = \delta_\mu^\nu, \quad (3.4.4)$$

the first term in the Euler-Lagrange equation is found to be,

$$\begin{aligned} \frac{\partial \mathcal{L}}{\partial A_\rho^j} &= -g \bar{\psi} \gamma^\rho \frac{\lambda^j}{2} \psi - \frac{1}{4} \left(\frac{\partial G_{\mu\nu}^a}{\partial A_\rho^j} G^{\mu\nu a} + G_{\mu\nu}^a \frac{\partial G^{\mu\nu a}}{\partial A_\rho^j} \right) \\ &= -g \bar{\psi} \gamma^\rho \frac{\lambda^j}{2} \psi - \frac{1}{4} g f^{abc} \left(\left[\frac{\partial A_\mu^b}{\partial A_\rho^j} A_\nu^c + A_\mu^b \frac{\partial A_\nu^c}{\partial A_\rho^j} \right] G^{\mu\nu a} \right. \\ &\quad \left. + G_{\mu\nu}^a \left[\frac{\partial A^{\mu b}}{\partial A_\rho^j} A^{\nu c} + A^{\mu b} \frac{\partial A^{\nu c}}{\partial A_\rho^j} \right] \right) \\ &= -g \bar{\psi} \gamma^\rho \frac{\lambda^j}{2} \psi - \frac{1}{4} g (f^{ajc} A_\nu^c G^{\rho\nu a} + f^{abj} A_\mu^b G^{\mu\rho a} + f^{ajc} A^{\nu c} G_{\nu}^{\rho a} + f^{abj} A^{\mu b} G_{\mu}^{\rho a}), \end{aligned} \quad (3.4.5)$$

where in the second line,

$$\frac{\partial(\partial_\mu A_\nu)}{\partial A_\rho} = 0,$$

was employed. In the next steps, summed indices are relabelled and repositioned, and the cyclic and totally antisymmetric properties of the structure constants are invoked,

$$\begin{aligned} \frac{\partial \mathcal{L}}{\partial A_\rho^j} &= -g \bar{\psi} \gamma^\rho \frac{\lambda^j}{2} \psi \\ &\quad - \frac{1}{4} g (-f^{abj} A^{\mu b} G_{\mu}^{\rho a} + f^{abj} A^{\mu b} G_{\mu}^{\rho a} - f^{abj} A^{\mu b} G_{\mu}^{\rho a} + f^{abj} A^{\mu b} G_{\mu}^{\rho a}), \\ &= -g \bar{\psi} \gamma^\rho \frac{\lambda^j}{2} \psi - \frac{1}{4} g (4 f^{abj} A^{\mu b} G_{\mu}^{\rho a}), \\ \frac{\partial \mathcal{L}}{\partial A^{\nu a}} &= -g \bar{\psi} \gamma_\nu \frac{\lambda^a}{2} \psi + g f^{abc} A^{\mu b} G_{\mu\nu}^c. \end{aligned} \quad (3.4.6)$$

In the last two steps, the antisymmetry property of $G_{\mu\nu}$ was used and indices were relabelled and rearranged for later clarity. The second term in the Lagrangian will

yield,

$$\begin{aligned}
\partial_\sigma \left(\frac{\partial \mathcal{L}}{\partial(\partial_\sigma A_\rho^j)} \right) &= -\frac{1}{4} \partial_\sigma \left(\frac{\partial G_{\mu\nu}^a}{\partial(\partial_\sigma A_\rho)} G^{\mu\nu a} + G_{\mu\nu}^a \frac{\partial G_{\mu\nu}^a}{\partial(\partial_\sigma A_\rho)} \right) \\
&= -\frac{1}{4} \partial_\sigma \left(\left[\frac{\partial(\partial_\mu A_\nu^a)}{\partial(\partial_\sigma A_\rho^j)} - \frac{\partial(\partial_\nu A_\mu^a)}{\partial(\partial_\sigma A_\rho^j)} \right] G^{\mu\nu a} \right. \\
&\quad \left. + G_{\mu\nu}^a \left[\frac{\partial(\partial^\mu A^{\nu a})}{\partial(\partial_\sigma A_\rho^j)} - \frac{\partial(\partial^\nu A^{\mu a})}{\partial(\partial_\sigma A_\rho^j)} \right] \right) \\
&= -\frac{1}{4} \partial_\sigma \left([\delta_\mu^\sigma \delta_\nu^\rho \delta^{aj} - \delta_\nu^\sigma \delta_\mu^\rho \delta^{aj}] G^{\mu\nu a} + G_{\mu\nu}^a [\delta^{\sigma\mu} \delta^{\nu\rho} \delta^{aj} - \delta^{\sigma\nu} \delta^{\mu\rho} \delta^{aj}] \right) \\
&= -\frac{1}{4} \partial_\sigma (G^{\sigma\rho j} - G^{\rho\sigma j} + G^{\sigma\rho j} - G^{\rho\sigma j}) \\
\partial^\mu \left(\frac{\partial \mathcal{L}}{\partial(\partial^\mu A^{\nu a})} \right) &= -\partial^\mu G_{\mu\nu}^a, \tag{3.4.7}
\end{aligned}$$

where again, antisymmetry properties, relabelling and,

$$\frac{\partial A_\mu}{\partial(\partial_\sigma A_\rho)} = 0,$$

were employed. One can now see why the factor of $\frac{1}{4}$ appears in the Lagrangian.

The QCD equations of motion are therefore,

$$\partial^\mu G_{\mu\nu}^a + g f^{abc} A^{\mu b} G_{\mu\nu}^c = g \bar{\psi} \gamma_\nu \frac{\lambda^a}{2} \psi \tag{3.4.8}$$

$$(i\cancel{\partial} - m)\psi = -g \gamma_\nu \frac{\lambda^a}{2} \psi \tag{3.4.9}$$

$$\bar{\psi}(i\overleftarrow{\cancel{\partial}} - m) = -g \bar{\psi} \gamma_\nu \frac{\lambda^a}{2} \tag{3.4.10}$$

From these equations, one can employ the canonical quantisation procedure by imposing (anti-) commutation relations, or use the path integral formalism to quantise the classical theory.

3.5 The Wilson Loop.

Another important object in gauge theories is the Wilson Loop. In section 3.2, the parallel transport $U(y, x)$ was introduced as a way of computing the infinitesimal form of the gauge transformation of the gauge connection $A_\mu(x)$. However, in that

computation, only infinitesimally separated points in spacetime were considered. One can also define the parallel transport between two finitely separated points x and y by splitting some path between them into n finitely small parallel transports and then allowing n to go to infinity. Consider, therefore, the parallel transport between finitely separated points x and y , composed of finitely small, path-ordered intervals over the curve γ ,

$$\begin{aligned}
U_\gamma(y, x) &= \overbrace{U(y, x_n)U(x_n, x_{n-1})\dots U(x_2, x_1)U(x_1, x)}^{n \text{ steps}} \\
&\approx [1 + igA_\mu^a(x_n)(y - x_n)^\mu \tau^a][1 + igA_\nu^b(x_{n-1})(x_n - x_{n-1})^\nu \tau^b] \\
&\quad \dots [1 + igA_\rho^c(x)(x_1 - x)^\rho \tau^c] \\
&= \prod_{i=0}^n (1 + igA_\mu^a(x_i)\Delta x_i^\mu \tau^a) \quad \text{where} \quad \Delta x_i \equiv x_{i+1} - x_i, \quad x_0 = x, \quad x_{n+1} = y \\
&= 1 + ig \sum_{i=0}^n A_\mu^a(x_i)\Delta x_i^\mu \tau^a + (ig)^2 \sum_{i=0}^n \sum_{j=0}^{i-1} A_\mu^a(x_i)\Delta x_i^\mu \tau^a A_\nu^b(x_j)\Delta x_j^\nu \tau^b + \dots
\end{aligned} \tag{3.5.1}$$

Notice how the non-commutative nature of the gauge connections imposes path-ordering. Further, notice that the second line is only an approximation to the finite differences Δx_i . Later, a limit will be taken so that these differences become infinitesimal. Now, one can parameterise the curve γ via the variable s and the function $x^\mu(s)$ such that,

$$x^\mu(0) = x^\mu, \quad x^\mu(1) = y^\mu \quad s \in [0, 1] \tag{3.5.2}$$

Using this parameterisation in (3.5.1) and taking the limit $n \rightarrow \infty \Rightarrow \Delta x \rightarrow dx$,

$$\begin{aligned}
U_\gamma(y, x) &= 1 + (ig) \int_0^1 ds_1 A_\mu^a(x(s_1)) \tau^a \frac{dx^\mu}{ds_1} \\
&\quad + (ig)^2 \int_0^1 ds_1 \int_0^{s_1} ds_2 A_\mu^a(x(s_1)) \tau^a \frac{dx^\mu}{ds_1} A_\nu^b(x(s_2)) \tau^b \frac{dx^\nu}{ds_2} + \dots \\
&= \sum_{n=0}^{\infty} (ig)^n \int_0^1 ds_1 \int_0^{s_1} ds_2 \dots \int_0^{s_{n-1}} ds_n A_\mu^a(x(s_1)) \tau^a \frac{dx^\mu}{ds_1} \dots A_\nu^b(x(s_n)) \tau^b \frac{dx^\nu}{ds_n} \\
&\equiv \exp \left[P \left\{ ig \int_0^1 A_\mu^a(x(s)) \tau^a \frac{dx^\mu}{ds} \right\} \right] \\
&= P \exp \left[ig \int_\gamma A_\mu(x) dx^\mu \right] \tag{3.5.3}
\end{aligned}$$

The operator P here simply imposes path-ordering of the infinitesimal segments along γ . Under a gauge transformation, this *Wilson Line* will transform as,

$$U_\gamma(y, x) \rightarrow V(y) U_\gamma(y, x) V^\dagger(x), \tag{3.5.4}$$

which can be proved using the gauge transformation property of $A_\mu(x)$ given in (3.2.19). The most important property of (3.5.3) becomes apparent when the end points are chosen to coincide. Consider a closed loop Γ , starting and ending at x . The gauge transformation of such a loop would, according to (3.5.4) take the form,

$$U_\Gamma(x, x) \rightarrow V(x) U_\Gamma(x, x) V^\dagger(x), \tag{3.5.5}$$

therefore the trace of such an object will remain gauge invariant,

$$\begin{aligned}
\text{Tr}[U_\Gamma(x, x)] &\rightarrow \text{Tr}[\overbrace{V^\dagger(x) V(x)}{=1} U_\Gamma(x, x)] \\
&= \text{Tr} \left(P \exp \left[ig \oint_\Gamma A_\mu(x) dx^\mu \right] \right). \tag{3.5.6}
\end{aligned}$$

This object is the *Wilson Loop* and it is of enormous significance in lattice gauge theory and hence standard model physics and beyond.

For an Abelian gauge theory, such as the $U(1)$ gauge invariance of electromagnetism, one need not be concerned with the commutativity of the gauge connections

and (3.5.6) may be expressed using Stokes's theorem. Consider the integral of the gauge connection over some loop denoted by $\partial\Omega$,

$$\begin{aligned}
ie \oint_{\partial\Omega} A_\mu(x) dx^\mu &= ie \int_{\Omega} \partial_\mu A_\nu(x) dx^\mu \wedge dx^\nu. \\
&= \frac{ie}{2} \int_{\Omega} [\partial_\mu A_\nu(x) - \partial_\nu A_\mu(x)] dx^\mu \wedge dx^\nu \\
&= \frac{ie}{2} \int_{\Omega} F_{\mu\nu}(x) d\sigma^{\mu\nu} \\
\Rightarrow \text{Tr}[U_{\partial\Omega}(x, x)] &= \text{Tr} \left[\exp \left(ie \oint_{\partial\Omega} A_\mu(x) dx^\mu \right) \right] \\
&= \text{Tr} \left[\exp \left(\frac{ie}{2} \int_{\Omega} F_{\mu\nu}(x) d\sigma^{\mu\nu} \right) \right], \tag{3.5.7}
\end{aligned}$$

where $d\sigma^{\mu\nu} = dx^\mu \wedge dx^\nu$ is an infinitesimal area element and Ω is the closed surface enclosed by the curve $\partial\Omega$. This result also applies to non-Abelian gauges, though the proof is more involved due to the strict path ordering. It will be of paramount importance in the Wilson formulation of lattice gauge theory.

CHAPTER 4

Lattice Gauge Theory for QCD

In chapter 2 we laid out the generalities of the path integral formulation of a quantum field theory and in chapter 3 we investigated the classical equations of motion for QCD. These two ingredients will together allow us to formulate the non-perturbative tool of lattice gauge theory and measure physical quantities in QCD. Our task is to discretise (and quantise) the classical continuum QCD Lagrangian (3.3.12) presented in section 3.3.

4.1 Naïve Discretisation of the QCD Action

As the title of the subsection suggests, this first attempt at discretisation will not prove successful. However, it is illuminating to see why this first ‘common sense’ approach fails as it paves the way for the freedom associated with generating lattice QCD actions. For the moment, simply to ease notation, we will work in a single flavour. We begin by separating the continuum Lagrangian into fermion and gauge parts, and thence into free and interacting parts. The free part of the fermion action (with no gauge terms) is,

$$\begin{aligned} S_F^0[\psi, \bar{\psi}] &= \int d^4x \mathcal{L}[\psi, \bar{\psi}] \\ &= \int d^4x \bar{\psi}(x) (\gamma^\mu \partial_\mu + m) \psi(x). \end{aligned} \tag{4.1.1}$$

Before we discretise, we will first set some conventions. Colour indices will be raised and Latin, spin indices will be lowered and Greek. We will make use of a Kronecker delta function that serves to pick out field values from adjacent lattice points a distance a away (one lattice unit) in the μ direction,

$$\delta_{x+\hat{\mu}, y} \psi(y) = \psi(x + \hat{\mu}). \tag{4.1.2}$$

We will Wick rotate to Euclidean time, and hence the Clifford algebra of the gamma matrices will obey the Euclidean anti-commutation relation,

$$\{\gamma_\mu, \gamma_\nu\} = 2\delta_{\mu,\nu}, \quad (4.1.3)$$

and we will replace the continuum differential operator with a finite difference central operator,

$$\begin{aligned} \Delta_{x,y}^\mu &= \sum_\mu \left(\frac{\delta_{x+\hat{\mu},y} - \delta_{x-\hat{\mu},y}}{2a} \right), \\ \text{so that } \Delta_{x,y}^\mu \psi(y) &= \sum_\mu \left(\frac{\psi(x + \hat{\mu}) - \psi(x - \hat{\mu})}{2a} \right), \end{aligned} \quad (4.1.4)$$

giving,

$$S_F^0[\psi, \bar{\psi}] = a^4 \sum_x \bar{\psi}_\alpha^a(x) [(\gamma^\mu)_{\alpha\beta} \Delta_{x,y}^\mu + m\delta^{a,b} \delta_{\alpha,\beta} \delta_{x,y}] \psi_\beta^b(y). \quad (4.1.5)$$

From here we introduce the gauge field. Discretisation of the derivative operator posed no problem in the free fermion action, but $SU(3)$ gauge invariance will require us to add additional artefacts to our theory. Consider the fermion bilinear created by the central difference operator under a gauge transformation $V(x)$,

$$\begin{aligned} \bar{\psi}(x)\psi(x + \hat{\mu}) &\rightarrow \bar{\psi}(x)V^\dagger(x)V(x + \hat{\mu})\psi(x + \hat{\mu}) \\ &\neq \bar{\psi}(x)\psi(x + \hat{\mu}). \end{aligned} \quad (4.1.6)$$

It is patently not gauge invariant. In order to solve this problem, we introduce an object known as a *link* that resides on the links between lattice sites. It is a directed object, such that if we were to consider the link between lattice site x and $x + \hat{\mu}$, the corresponding link variable would be $U_\mu(x)$. Further, the link variable from lattice site $x + \hat{\mu}$ to x is simply the complex conjugate of $U_\mu(x)$,

$$U_{-\mu}(x + \hat{\mu}) = U_\mu^\dagger(x). \quad (4.1.7)$$

We define the link variables such that, when inserted into the bilinear created by the central difference operator, the whole object undergoes a gauge transformation that enforces gauge invariance of the bilinear,

$$\begin{aligned}
 U_\mu(x) &\rightarrow U'_\mu(x) = V(x)U_\mu(x)V^\dagger(x + \hat{\mu}) \\
 \Rightarrow \bar{\psi}(x)U_\mu(x)\psi(x + \hat{\mu}) &\rightarrow \bar{\psi}(x)V^\dagger(x)V(x)U_\mu(x)V^\dagger(x + \hat{\mu})V(x + \hat{\mu})\psi(x + \hat{\mu}) \\
 &= \bar{\psi}(x)U_\mu(x)\psi(x + \hat{\mu})
 \end{aligned} \tag{4.1.8}$$

These link variables are not simply hacks to make our lattice field theory gauge invariant, in fact, we have encountered them before in section 3.5; they are Wilson lines, as given by (3.5.3),

$$\begin{aligned}
 U_\mu(x) &= \exp[igaA_\mu(x)], \\
 &= 1 + igaA_\mu(x) + \mathcal{O}(a^2).
 \end{aligned} \tag{4.1.9}$$

Notice that the integral in (3.5.3) has been replaced by the linear approximation $aA_\mu(x)$. Expanding the above to $\mathcal{O}(a^2)$, we can write down a fermion action over the fermion fields $\psi, \bar{\psi}$ and the link variables U , and show that it is equivalent, up to $\mathcal{O}(a)$, of a free fermion action and an interacting fermion action over gauge fields,

$$\begin{aligned}
& S_F^I[\psi, \bar{\psi}, U] \\
&= a^4 \sum_x \bar{\psi}_\alpha^a(x) \left[\frac{1}{2a} \sum_\mu (\gamma_\mu)_{\alpha\beta} (U_\mu^{ab}(x) \psi_\beta^b(x + \hat{\mu}) - U_{-\mu}^{ab}(x) \psi_\beta^b(x - \hat{\mu})) \right. \\
&\quad \left. + m \delta^{a,b} \delta_{\alpha,\beta} \psi_\beta^b(x) \right], \\
&= a^4 \sum_x \bar{\psi}_\alpha^a(x) \left[\frac{1}{2a} \sum_\mu (\gamma_\mu)_{\alpha\beta} \left((1 + i g a A_\mu^{ab}(x)) \psi_\beta^b(x + \hat{\mu}) \right. \right. \\
&\quad \left. \left. - (1 - i g a A_\mu^{ab}(x - \hat{\mu})) \psi_\beta^b(x - \hat{\mu}) \right) \right. \\
&\quad \left. + m \delta^{a,b} \delta_{\alpha,\beta} \psi_\beta^b(x) \right] + \mathcal{O}(a^2) \\
&= a^4 \sum_x \bar{\psi}_\alpha^a(x) \left[\frac{1}{2a} \sum_\mu (\gamma^\mu)_{\alpha\beta} (\psi_\beta^b(x + \hat{\mu}) - \psi_\beta^b(x - \hat{\mu})) + m \delta^{a,b} \delta_{\alpha,\beta} \psi_\beta^b(x) \right] \\
&\tag{4.1.10a}
\end{aligned}$$

$$\begin{aligned}
& + i g a^4 \sum_x \bar{\psi}_\alpha^a(x) \left[\frac{1}{2} \sum_\mu (\gamma^\mu)_{\alpha\beta} (A_\mu^{ab}(x) \psi_\beta^b(x + \hat{\mu}) + A_\mu^{ab}(x - \hat{\mu}) \psi_\beta^b(x - \hat{\mu})) \right] \\
&\tag{4.1.10b}
\end{aligned}$$

$$+ \mathcal{O}(a^2)$$

One can instantly recognise (4.1.10a) as the free fermion action $S_F^0[\psi, \bar{\psi}]$ given in equation (4.1.5). In the second term, (4.1.10b), we must Taylor expand both the gauge field and the fermion field about x to deduce that it is indeed an interacting fermion field,

$$\psi(x \pm \mu) = \psi(x) + \mathcal{O}(a), \quad A(x \pm \mu) = A(x) + \mathcal{O}(a), \tag{4.1.11}$$

whereupon (4.1.10b) becomes,

$$S_F^I[\psi, \bar{\psi}, A] = i g a^4 \sum_x \sum_\mu \bar{\psi}_\alpha^a(x) (\gamma_\mu)_{\alpha\beta} A_\mu^{ab}(x) \psi_\beta^b(x) + \mathcal{O}(a), \tag{4.1.12}$$

which is clearly the two fermion fields interacting via the gauge field. It would appear, therefore, that we have developed an action for interacting fermions in QCD, but this fermion action belies a subtle problem that we will explore in the next section. After that, we will go on to describe the gauge action and arrive at a working model for lattice gauge theory.

4.2 The Doubling Problem and its Solution

As we will see when we compute correlation functions in lattice gauge theory, the most important object we will encounter is the quark propagator, which is the position-space inverse of the Dirac operator in the lattice QCD action. This propagator is the source of a ‘doubling problem’ in that unwanted poles in the propagator are present due to the discrete nature of the lattice. We will see that there are 2^D poles, where D is the spacetime dimension of the lattice (hence the name ‘doubling problem.’) In order to see where these ‘doubblers’ come from, we must compute the quark propagator. We will use the free fermion action (4.1.5) which is equivalent to working with unit valued links, $U_\mu(x) = \delta^{ab} \forall x, \mu$ and does not lead to any loss of generality as the problem is independent of colour gauge.

We first identify and isolate the Dirac operator M in the free fermion action,

$$\begin{aligned}
S_F^0[\psi, \bar{\psi}] &= a^4 \sum_x \bar{\psi}_\alpha^a(x) [(\gamma^\mu)_{\alpha\beta} \Delta_{x,y}^\mu + m \delta^{a,b} \delta_{\alpha,\beta} \delta_{x,y}] \psi_\beta^b(y) \\
&= a^4 \sum_x \bar{\psi}_\alpha^a(x) M_{\alpha\beta}^{ab}(x, y) \psi_\beta^b(y) \\
\Rightarrow M_{\alpha\beta}^{ab}(x, y) &= \sum_\mu \frac{1}{2a} (\gamma^\mu)_{\alpha\beta} (\delta_{x+\hat{\mu},y} - \delta_{x-\hat{\mu},y}) + m \delta^{a,b} \delta_{\alpha,\beta} \delta_{x,y}. \tag{4.2.1}
\end{aligned}$$

To simplify the inversion of M , we will Fourier transform M to momentum space using the discrete Fourier transforms,

$$\tilde{F}(p) = \frac{1}{\sqrt{N^3 N_T}} \sum_x F(x) e^{-iapx}, \tag{4.2.2}$$

$$F(x) = \frac{1}{\sqrt{N^3 N_T}} \sum_p \tilde{F}(p) e^{iapx}, \tag{4.2.3}$$

where p represents all possible (discrete) momenta on the lattice. From here, we will drop the spin and colour indices. The Fourier transforms on x and y give,

$$\begin{aligned}
\widetilde{M}(p, q) &= \frac{1}{N^3 N_T} \sum_{x, y} e^{-iapx} M(x, y) e^{iaqy} \\
&= \frac{1}{N^3 N_T} \sum_{x, y} e^{-iapx} \left[\sum_{\mu} \frac{1}{2a} (\gamma^{\mu}) (\delta_{x+\hat{\mu}, y} - \delta_{x-\hat{\mu}, y}) + m\delta_{xy} \right] e^{iaqy} \\
&= \frac{1}{\sqrt{N^3 N_T}} \sum_x e^{-iapx} \left[\sum_{\mu} \frac{1}{2a} (\gamma^{\mu}) (e^{iaqx} e^{iaq_{\mu}} - e^{iaqx} e^{-iaq_{\mu}}) + m\mathbb{I} e^{iaqx} \right] \\
&= \frac{1}{\sqrt{N^3 N_T}} \sum_x e^{-iax(p-q)} \left[\sum_{\mu} \frac{1}{2a} (\gamma^{\mu}) (e^{iaq_{\mu}} - e^{-iaq_{\mu}}) + m\mathbb{I} \right] \\
&= \delta_{p, q} \left[m\mathbb{I} + \frac{i}{a} \sum_{\mu} \gamma^{\mu} \sin(q_{\mu} a) \right] \\
&= \delta_{p, q} \widetilde{M}(q)
\end{aligned} \tag{4.2.4}$$

We now use the formula general formula for the inverse of a linear series of gamma matrices,

$$\left(a\mathbb{I} + i \sum_{\mu} \gamma_{\mu} b_{\mu} \right)^{-1} = \frac{a\mathbb{I} - i \sum_{\mu} \gamma_{\mu} b_{\mu}}{a^2 + \sum_{\mu} b_{\mu}^2} \tag{4.2.5}$$

to express the momentum-space inverse of M as,

$$\widetilde{M}^{-1}(q) = \frac{m\mathbb{I} - ia^{-1} \sum_{\mu} \gamma_{\mu} \sin(q_{\mu} a)}{m^2 + a^{-2} \sum_{\mu} \sin^2(q_{\mu} a)}. \tag{4.2.6}$$

Consider now the relativistic limit of a fermion on the lattice, i.e., $m \ll E$, in the continuum limit $a \rightarrow 0$,

$$\widetilde{M}^{-1}(q) \Big|_{m \ll E} \rightarrow \frac{-ia^{-1} \sum_{\mu} \gamma_{\mu} \sin(q_{\mu} a)}{a^{-2} \sum_{\mu} \sin^2(q_{\mu} a)} \Big|_{a \rightarrow 0} \rightarrow \frac{-i \sum_{\mu} \gamma_{\mu} q_{\mu}}{q^2}. \tag{4.2.7}$$

This is an encouraging result: it tells us that in the massless, continuum limit, there is a single pole in the momentum propagator and it takes the correct form. However, on the lattice, we may not explicitly take the continuum limit and, as such, the denominator of the momentum propagator will permit 15 more poles. Consider

a fermion momentum where the components are populated exclusively with values of 0 or $\frac{\pi}{a}$. In that case, one can clearly see there are 2^D permutations of the momentum components that will give rise to poles. One of these permutations, namely $(0, 0, 0, 0)$, is the one we associate with the physical fermion we are simulating. The others are the doublers of the theory. This problem was identified by Wilson (4) and, in a *tour de force*, immediately solved in the same paper.

4.3 Wilson Fermions

Throughout our investigation of lattice gauge theory, we have been very careful to ensure that in the continuum limit, all of the objects we construct are asymptotic to their continuum field theory counterparts. This obvious precaution, which seems to be more of a constriction than anything else, actually affords us a great deal of freedom as we are at liberty to add *any* terms we want to any object, provided that they disappear in the continuum. With this in mind, Wilson proposed the following solution to the doubling problem: to simply add to the momentum-space Dirac operator a term which removes the doublers in a systematic fashion, while at the same time having no effect on the $(0, 0, 0, 0)$ mode and disappearing in the continuum limit. His proposed operator is,

$$\begin{aligned}\widetilde{M}_W(q) &= m\mathbb{I} + \frac{i}{a} \sum_{\mu} \gamma^{\mu} \sin(q_{\mu}a) + \mathbb{I} \frac{1}{a} \sum_{\mu} (1 - \cos(q_{\mu}a)), \\ &= \left(m + \frac{1}{a} \sum_{\mu} (1 - \cos(q_{\mu}a)) \right) \mathbb{I} + \frac{i}{a} \sum_{\mu} \gamma^{\mu} \sin(q_{\mu}a).\end{aligned}\quad (4.3.1)$$

By inverting this operator, we will see how the $q_{\mu} = (0, 0, 0, 0)$ momentum mode is recovered and the other $(2^D - 1)$ modes decouple from the theory,

$$\widetilde{M}_W^{-1}(q) = \frac{\left(m + \frac{1}{a} \sum_{\mu} (1 - \cos(q_{\mu}a)) \right) \mathbb{I} - ia^{-1} \sum_{\mu} \gamma^{\mu} \sin(q_{\mu}a)}{\left(m + \frac{1}{a} \sum_{\mu} (1 - \cos(q_{\mu}a)) \right)^2 + a^{-2} \sum_{\mu} \sin^2(q_{\mu}a)}.\quad (4.3.2)$$

For the $q_{\mu} = (0, 0, 0, 0)$ mode, the cosine terms evaluate to 1 and (4.2.7) is immediately recovered. For all the other 15 momenta, the cosine function will evaluate

to -1 and the sum over μ will give us a multiplicative factor $l = 1 \dots 4$ for each component with momentum $\frac{\pi}{a}$. Furthermore, the sine functions will evaluate to zero, giving,

$$\begin{aligned} \widetilde{M}_W^{-1}(q) &= \frac{(m + \frac{2l}{a}) \mathbb{I} - ia^{-1} \sum_{\mu} \gamma^{\mu} \sin(q_{\mu} a)}{(m + \frac{2l}{a})^2 + a^{-2} \sum_{\mu} \sin^2(q_{\mu} a)}, \\ &= \mathbb{I} \left(m + \frac{2l}{a} \right)^{-1}, \end{aligned} \tag{4.3.3}$$

which is a constant. In essence, what has happened here is that the doublers have been given a very large mass compared to the $q_{\mu} = (0, 0, 0, 0)$ mode. In the continuum limit, the propagator evaluates to zero and therefore the doubler modes simply do not propagate. This is the sense in which they are ‘decoupled’ from the theory. One may think of these doubler modes as adding an infinitely large constant to the action which cancels when taking the correlation function, just as we saw for the normalisation constant in (2.3.5).

We have added a term to the momentum space Dirac operator, but we will be performing calculations in position space. Furthermore, because we constructed the Wilson with no gauge field, we must also ensure it is gauge invariant. Fourier transformation is simple; we simply redefine (4.2.4) so that it includes the Wilson

term, and work back to position space,

$$\begin{aligned}
M_W(x, y) &= \frac{1}{N^3 N_T} \sum_{p, q} e^{ipx} \delta_{p, q} \widetilde{M}_W^{-1}(q) e^{-iqy} \\
&= \frac{1}{\sqrt{N^3 N_T}} \sum_q e^{iqx} \widetilde{M}_W^{-1}(q) e^{-iqy} \\
&= \frac{1}{\sqrt{N^3 N_T}} \sum_q e^{iqx} \left[m\mathbb{I} + \frac{i}{a} \sum_\mu \gamma^\mu \sin(q_\mu a) + \mathbb{I} \frac{1}{a} \sum_\mu (1 - \cos(q_\mu a)) \right] e^{-iqy} \\
&= \frac{1}{\sqrt{N^3 N_T}} \sum_q e^{iqx} \left[m\mathbb{I} + \sum_\mu \frac{1}{2a} \gamma^\mu (e^{iaq_\mu} - e^{-iaq_\mu}) \right. \\
&\quad \left. + \sum_\mu \frac{1}{2a} \mathbb{I} (2 - (e^{iaq_\mu} + e^{-iaq_\mu})) \right] e^{-iqy} \\
&= \frac{1}{\sqrt{N^3 N_T}} \sum_q \left[m\mathbb{I} e^{iq(x-y)} + \sum_\mu \left(\frac{1}{2a} \gamma^\mu (e^{iq[(x+\hat{\mu})-y]} - e^{iq[(x-\hat{\mu})-y]}) \right. \right. \\
&\quad \left. \left. - \frac{1}{2a} (e^{iq[(x+\hat{\mu})-y]} - 2e^{iq(x-y)} + e^{iq[(x-\hat{\mu})-y]}) \right) \right].
\end{aligned}$$

We now perform the sum over q , which gives Kronecker delta functions in position space,

$$\begin{aligned}
M_W(x, y) &= \left[m\mathbb{I} \delta_{x, y} + \frac{1}{2a} \sum_\mu ((\gamma^\mu - \mathbb{I}) \delta_{x+\hat{\mu}, y} - (\gamma^\mu + \mathbb{I}) \delta_{x-\hat{\mu}, y} + 2\delta_{x, y}) \right], \\
&= \left[m\mathbb{I} \delta_{x, y} + \frac{1}{2a} \sum_\mu (\gamma^\mu (\delta_{x+\hat{\mu}, y} - \delta_{x-\hat{\mu}, y})) \right. \\
&\quad \left. - a \sum_\mu \left(\frac{1}{2a^2} \mathbb{I} (\delta_{x+\hat{\mu}, y} - 2\delta_{x, y} + \delta_{x-\hat{\mu}, y}) \right) \right].
\end{aligned}$$

We can instantly recognise the central term in the above as the naive central difference operator (4.1.4). The last term is the discretised version of the second order derivative ∂^2 , which is the central difference of two forward distance differential

operators,

$$\begin{aligned} \sum_{\mu} \mathbb{I} \left[\frac{1}{a} (\delta_{x+\hat{\mu},y} - \delta_{x,y}) - \frac{1}{a} (\delta_{x,y} - \delta_{x-\hat{\mu},y}) \right] &= a \sum_{\mu} \frac{1}{2a^2} \mathbb{I} (\delta_{x+\hat{\mu},y} - 2\delta_{x,y} + \delta_{x-\hat{\mu},y}) \\ &= -\frac{4}{a} \mathbb{I} \delta_{x,y} + a \sum_{\mu} \frac{1}{2a^2} \mathbb{I} (\delta_{x+\hat{\mu},y} + \delta_{x-\hat{\mu},y}) \end{aligned} \quad (4.3.4)$$

Notice the appearance of the $\frac{4}{a}$ term which will be incorporated into the mass term. We must now make this operator gauge invariant by inserting the appropriate link variables. Each Kronecker delta with an $x \pm \hat{\mu}$ index will need a link. Spin and colour indices will be reintroduced for completeness. Furthermore, we add an overall coefficient r to the additional operator, which is conventionally set to unity,

$$\begin{aligned} M_W(x, y) &= \left[\left(m + \frac{4r}{a} \right) \mathbb{I} \delta^{a,b} \delta_{\alpha,\beta} \delta_{x,y} \right. \\ &\quad + \frac{1}{2a} \sum_{\mu} ((\gamma^{\mu})_{\alpha\beta} (U_{\mu}^{ab}(x) \delta_{x+\hat{\mu},y} - U_{-\mu}^{ab}(x) \delta_{x-\hat{\mu},y})) \\ &\quad \left. - \frac{ar}{2} \sum_{\mu} \frac{1}{a^2} \mathbb{I} \delta^{a,b} \delta_{\alpha,\beta} (U_{\mu}^{ab}(x) \delta_{x+\hat{\mu},y} + U_{-\mu}^{ab}(x) \delta_{x-\hat{\mu},y}) \right]. \end{aligned} \quad (4.3.5)$$

This operator gives rise to an action that has $\mathcal{O}(a)$ errors, though we will postpone showing this until we come to the subsection on clover improved fermions, where we will show that this $\mathcal{O}(a)$ error can be removed to leave only $\mathcal{O}(a^2)$ errors (see section 4.5.) The choice of $r = 1$ comes from the continuum energy-momentum relation of the massless fermions. We expect physical states to obey the relation $E(\vec{p}) = |\vec{p}|$ and this is trivially satisfied for the $q_{\mu} = (0, 0, 0, 0)$ mode. The energy momentum relation for the other $2^D - 1 = 15$ modes for various values of r can be seen in figure 4.1. The dashed line represents the continuum on shell energy-momentum relation. Plot (a) clearly displays the doubler modes at the edge of the Brillouin zone, where $|\vec{p}|$ is maximal and $E(\vec{p})$ is zero. As r (or λ , as is used in the original paper) approaches unity, the energy of the doublers is shifted above the continuum value (b,c) and at $r = 1$, it can be shown that the energies become infinite and decouple. For $r \gg 1$ the doubler modes asymptotically approach the continuum

relation, known as ‘near-doubling’.

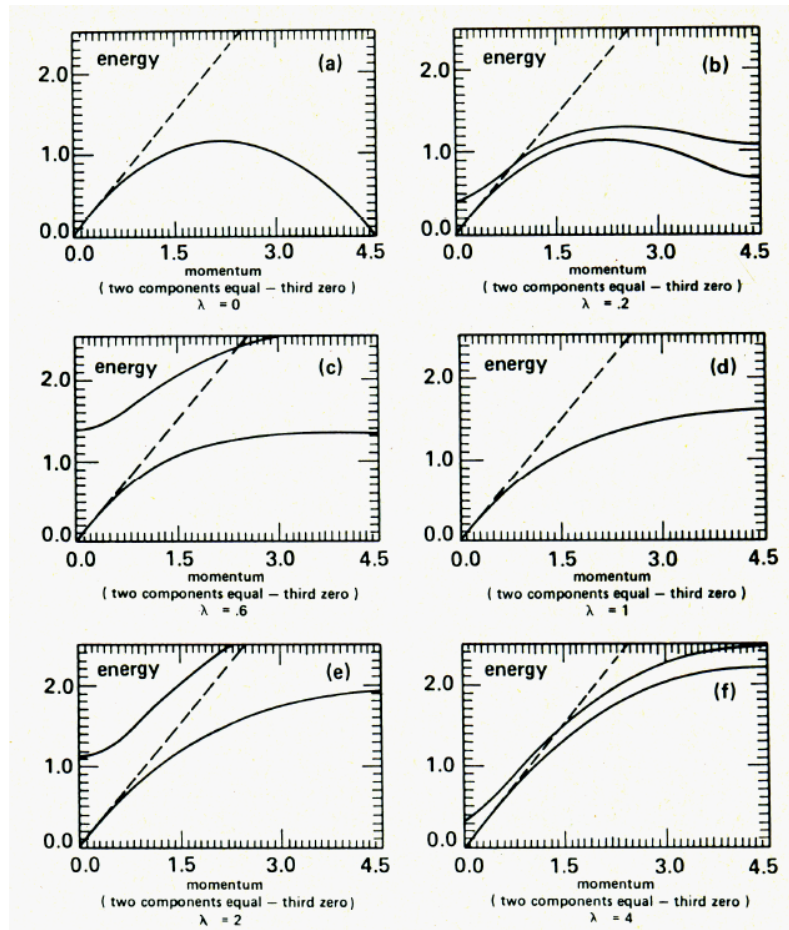


Figure 4.1: These plots show the behaviour of the energy-momentum relation for the 2^D modes of the naïve Wilson action. In Sheikholeslami and Wohlert’s paper, the symbol λ was used rather than r . (Figure from Sheikholeslami and Wohlert (5))

4.4 Wilson Gauge Action

The remaining task is to formulate a discretised action for the gluons (gauge fields.) We saw, in the classical, Minkowski space treatment, that the basic gauge invariant operator that involved only the gauge fields was,

$$\frac{1}{2}\text{Tr}[G_{\mu\nu}^2(x)]. \quad (4.4.1)$$

In Euclidean space, this becomes,

$$\frac{1}{2}\text{Tr}(G_{\mu\nu}(x)G_{\mu\nu}(x)). \quad (4.4.2)$$

Notice that all the indices in Euclidean space are either always covariant or contravariant. In fact, it really doesn't matter where the indices are, but it helps to remember that if one sees summed indices at the same height, the the metric must be Euclidean. Now, rather than trying to discretise (4.4.2) directly, we will take a more intuitive approach. We know that the gauge action must be gauge invariant, and we also know that we can build gauge invariant objects using Wilson lines. We may build such an object on the lattice using the link variables introduced in section 4.1. Recall the link gauge transformation property,

$$U_\mu(x) \rightarrow V(x)U_\mu(x)V^\dagger(x + \hat{\mu}). \quad (4.4.3)$$

Consider now some path $P[U]$ of connected links from x to y that undergoes a gauge transformation to $P[U']$,

$$\begin{aligned} P[U] &= U_{\mu_0}(x)U_{\mu_1}(x + \hat{\mu}_0) \dots U_{\mu_n}(y - \hat{\mu}_n), \\ \rightarrow P[U'] &= V(x)U_{\mu_0}(x) \underbrace{V^\dagger(x + \hat{\mu}_0)V^\dagger(x + \hat{\mu}_0)}_{=1} U_{\mu_1}(x + \hat{\mu}_0) \dots \\ &\quad \underbrace{V(y - \hat{\mu}_n)V^\dagger(y - \hat{\mu}_n)} U_{\mu_n}(y - \hat{\mu}_n)V^\dagger(y), \\ &= V(x)U_{\mu_0}(x)U_{\mu_1}(x + \hat{\mu}_0) \dots U_{\mu_n}(y - \hat{\mu}_n)V^\dagger(y), \\ &= V(x)P[U]V^\dagger(y). \end{aligned} \quad (4.4.4)$$

Note that on the links and on the $SU(3)$ gauge transformation matrices, there are two colour indices, which we have suppressed for clarity. Now, if we assert that the start and end points x, y be that same and take the trace over colour indices, we form a gauge invariant object P_{loop} made purely of gauge fields, precisely the object

we require for the gauge action,

$$\begin{aligned}
 \text{Tr}(P_{loop}[U']) &\rightarrow \text{Tr}(V(x)P_{loop}[U]V^\dagger(x)), \\
 &= \text{Tr}\left(\underbrace{V^\dagger(x)V(x)}_{=1}P_{loop}[U]\right), \\
 &= \text{Tr}(P_{loop}[U]).
 \end{aligned}
 \tag{4.4.5}$$

Any closed path will do, but it is sufficient to consider the simplest possible loop, known as a *plaquette*. A plaquette is an oriented loop of four link variables which form a square, as shown in figure 4.2. Note that we have employed the hermitian conjugate definition in some of the link variables.

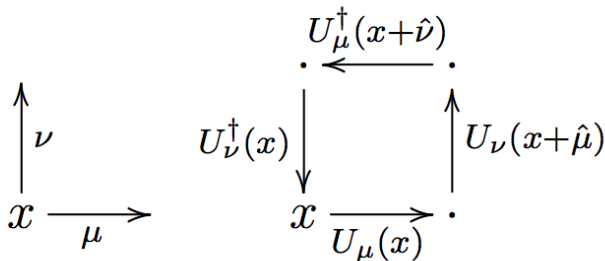


Figure 4.2: A schematic showing an oriented Wilson loop plaquette.

The plaquette has three variables associated with it; a starting lattice point, the μ, ν plane on which it resides, and an orientation, hence a convenient notation is,

$$P_{plaq}[U] \equiv U_{\mu\nu}(x) = U_\mu(x)U_\nu(x + \hat{\mu})U_\mu^\dagger(x + \hat{\nu})U_\nu^\dagger(x),
 \tag{4.4.6}$$

whereby the orientation of the plaquette is given by the order of the spacetime indices. The complex conjugate of $U_{\mu\nu}$ is the same loop with opposite orientation. Wilson's gauge action is a sum of the trace of all such plaquettes, which is therefore a sum over all lattice sites x and, at each site, a sum over all μ, ν for $\mu \neq \nu$. As always, we must check that the gauge action has the correct form in the continuum

limit. Recall the exponential definition of the link variable given in (4.1.9),

$$U_\mu(x) = \exp [igaA_\mu(x)].$$

We will use this, and the Baker-Campbell-Hausdorff formula,

$$e^A e^B = e^{A+B+\frac{1}{2}[A,B]+\dots}, \quad (4.4.7)$$

for the first two links in the plaquette and then again on the second two links, then again on the product, to expand the plaquette to $\mathcal{O}(a^2)$,

$$\begin{aligned} U_{\mu\nu}(x) &= \exp \left[igaA_\mu(x) + igaA_\nu(x + \hat{\mu}) - \frac{a^2 g^2}{2} [A_\mu(x), A_\nu(x + \hat{\mu})] + \mathcal{O}(a^3) \right] \\ &\times \exp \left[-igaA_\mu(x + \hat{\nu}) - igaA_\nu(x) - \frac{a^2 g^2}{2} [A_\mu(x + \hat{\nu}), A_\nu(x)] + \mathcal{O}(a^3) \right] \\ &= \exp \left[iga(A_\mu(x) + A_\nu(x + \hat{\mu}) - A_\mu(x + \hat{\nu}) - A_\nu(x)) \right. \\ &\quad \left. + \frac{a^2 g^2}{2} \left([A_\nu(x + \hat{\mu}), A_\mu(x + \hat{\nu})] + [A_\nu(x), A_\mu(x)] \right. \right. \\ &\quad \left. \left. - [A_\mu(x), A_\nu(x + \hat{\mu})] - [A_\mu(x + \hat{\nu}), A_\nu(x)] \right. \right. \\ &\quad \left. \left. + [A_\mu(x), A_\mu(x + \hat{\nu})] + [A_\nu(x + \hat{\mu}), A_\nu(x)] \right) + \mathcal{O}(a^3) \right]. \end{aligned} \quad (4.4.8)$$

We now Taylor expand the gauge fields with shifted lattice point arguments,

$$A_\mu(x + \hat{\nu}) = A_\mu(x) + a\partial_\nu A_\mu(x) + \frac{a^2}{2}\partial_\nu\partial_\rho A_\mu(x) + \mathcal{O}(a^3) \quad (4.4.9)$$

so that all gauge fields are expressed at the same spacetime point x . This will give rise to many cancellations, the most convenient of which are that all $\mathcal{O}(a^4)$ terms cancel each other, resulting in,

$$\begin{aligned} U_{\mu\nu}(x) &= \exp [ia^2 g (\partial_\mu A_\nu(x) - \partial_\nu A_\mu(x) + ig[A_\mu(x), A_\nu(x)]) + \mathcal{O}(a^5)] . \\ &= \exp [ia^2 g G_{\mu\nu}(x) + \mathcal{O}(a^5)] . \end{aligned} \quad (4.4.10)$$

Now, we want our lattice gauge action to approach the continuum gauge action in the limit $a \rightarrow 0$. The fact that we have the gluon field tensor G appearing in our definition of the plaquette is very encouraging, also that the finite corrections are $\mathcal{O}(a^5)$, as these terms, when summed over lattice points with a discrete measure of a^4 , will automatically disappear in the continuum limit. We now expand $U_{\mu\nu}(x)$ to second order in G and take the trace,

$$U_{\mu\nu}(x) = \left[\mathbb{I} + ia^2 g G_{\mu\nu}(x) - \frac{a^4 g^2}{2} G_{\mu\nu}^2 + \mathcal{O}(a^5) \right]. \quad (4.4.11)$$

Recall here that $G_{\mu\nu}(x)$ is hiding some notation. Expressed in terms of a sum over the generators of $SU(3)$,

$$G_{\mu\nu}(x) = \sum_a G_{\mu\nu}^a(x) \tau^a, \quad (4.4.12)$$

we see that we can use the traceless property of the τ^a generators to deduce that,

$$\text{Tr}[G_{\mu\nu}^a(x) \tau^a] = 0. \quad (4.4.13)$$

The trace of the two plaquette now reads as,

$$\begin{aligned} \text{Tr}[U_{\mu\nu}(x)] &= \text{Tr} \left[\mathbb{I} + ia^2 g G_{\mu\nu}(x) - \frac{a^4 g^2}{2} G_{\mu\nu}^2(x) + \mathcal{O}(a^6) \right] \\ &= \text{Tr}[\mathbb{I}] + \text{Tr}[ia^2 g \overline{G_{\mu\nu}(x)}] - \text{Tr}[a^4 g^2 G_{\mu\nu}^2(x)] + \mathcal{O}(a^6) \\ \frac{1}{g^2} \text{Tr}[\mathbb{I} - U_{\mu\nu}(x)] &= a^4 \frac{1}{2} \text{Tr}[G_{\mu\nu}^2(x)] + \mathcal{O}(a^6) \end{aligned} \quad (4.4.14)$$

Now, when we sum this quantity over all lattice points, and all spacetime indices, there is a subtlety we can exploit. Plaquettes are hermitian, and plaquettes on the same μ, ν plane of different orientation differ only by hermitian conjugation, therefore at each lattice point, there will be a sum,

$$\begin{aligned} \sum_{\mu \neq \nu} \text{Tr}[\mathbb{I} - U_{\mu\nu}(x)] &= \sum_{\mu < \nu} (\text{Tr}[\mathbb{I} - U_{\mu\nu}(x)] + \text{Tr}[\mathbb{I} - U_{\mu\nu}^\dagger(x)]), \\ &= 2 \sum_{\mu < \nu} \text{ReTr}[\mathbb{I} - U_{\mu\nu}(x)]. \end{aligned} \quad (4.4.15)$$

Notice how we pick up only the real part of the trace, and we limit the sum indices to $\mu < \nu$ and simply double the result. Putting everything together,

$$S_G[U] = \frac{2}{g^2} \sum_x \sum_{\mu < \nu} \text{ReTr}[\mathbb{I} - U_{\mu\nu}(x)] = a^4 \sum_x \sum_{\mu, \nu} \frac{1}{2} \text{Tr}[G_{\mu\nu}^2(x)] + \mathcal{O}(a^2) \quad (4.4.16)$$

We now have a gauge invariant, interacting lattice action that is free from doublers with $\mathcal{O}(a)$ discretisation error which approaches the continuum limit as $a \rightarrow 0$. We use the interacting fermion action (4.1.10) with the Wilson Dirac operator (4.3.5) and the Wilson gauge action (4.4.16), to define the Wilson lattice action,

$$S_{WLA}[\psi, \bar{\psi}, U] = S_F^I[\psi, \bar{\psi}, U] + S_G[U]. \quad (4.4.17)$$

This is a working model of lattice gauge theory that can be used to give credible results. However, the $\mathcal{O}(a)$ error on the action can be reduced to an $\mathcal{O}(a^2)$ with a variety of techniques. This work will utilise one such technique known as clover improvement.

4.5 Clover Improved Fermions

When trying to formulate a discretised action, we encountered the doubling problem and resolved it by adding a term to the Lagrangian that vanished in the continuum limit of $a \rightarrow 0$. It is instructive to write down the Wilson fermion action in the language of continuum operators to see why this technique works,

$$S_F^I[\psi, \bar{\psi}, U] = a^4 \sum_x \bar{\psi}(x) \left(\not{D} + m - \frac{ar}{2} D_\mu D_\mu \right) \psi(x), \quad (4.5.1)$$

In this form, it is clear that the Wilson term does indeed vanish in the continuum due to the coefficient of a . This rather subtle point of being allowed to add any term we wish to the action, provided it vanishes in the continuum, was alluded to at the start of subsection 4.1. There exists a systematised program of improvement, known as the *Symanzik improvement program* (6), and we can use it to define an improved operator known as the *clover* operator.

Consider some effective continuum action S_{EFF} that contains extra terms in

the Lagrangian of increasing physical dimension, but reduces to the continuum definition of the true action in the $a \rightarrow 0$ limit,

$$\begin{aligned} S_{EFF} &= \int d^4x (\mathcal{L}_0(x) + a\mathcal{L}_1(x) + a^2\mathcal{L}_2 + \dots) \\ &= \int d^4x \sum_{k=0}^N a^k \mathcal{L}_k(x). \end{aligned} \quad (4.5.2)$$

One can allow N to run to any arbitrary integer, and in fact, it can formally run to infinity. Now, we would like to remove the $\mathcal{O}(a)$ errors from the Wilson lattice action, so we will concentrate on the leading order correction $\mathcal{L}_1(x)$, which is a dimension-5 operator. In the continuum, there are 5 such operators therefore $\mathcal{L}_1(x)$ must be some linear combination of them,

$$\mathcal{L}_1^{(1)}(x) = \bar{\psi}(x)\sigma_{\mu\nu}G_{\mu\nu}\psi(x), \quad (4.5.3a)$$

$$\mathcal{L}_1^{(2)}(x) = \bar{\psi}(x)(\vec{D}_\mu\vec{D}_\mu + \overleftarrow{D}_\mu\overleftarrow{D}_\mu)\psi(x), \quad (4.5.3b)$$

$$\mathcal{L}_1^{(4)}(x) = m \left(\bar{\psi}(x)(\gamma_\mu(\vec{D}_\mu - \overleftarrow{D}_\mu))\psi(x) \right), \quad (4.5.3c)$$

$$\mathcal{L}_1^{(3)}(x) = m\text{Tr}[G^2], \quad (4.5.3d)$$

$$\mathcal{L}_1^{(5)}(x) = m^2\bar{\psi}(x)\psi(x), \quad (4.5.3e)$$

where $\sigma_{\mu\nu} = \frac{1}{2i}[\gamma_\mu, \gamma_\nu]$. To eliminate some of these terms, we can appeal to the continuum Dirac equation $(\gamma_\mu D_\mu + m)\psi = 0$ and the fact that some of these terms can be simply be redefined to deduce that $\mathcal{L}_1^{(1)}$ is sufficient for $\mathcal{O}(a)$ improvement. We must now find a discretised version of the field tensor $G_{\mu\nu}$. Many such versions exist, but one definition of particular use is the following,

$$\lim_{a \rightarrow 0} G_{\mu\nu}(x) = \frac{1}{8ia^2}(C_{\mu\nu}(x) - C_{\nu\mu}(x)), \quad (4.5.4)$$

where $C_{\mu\nu}(x)$ is the sum of four plaquettes in the μ, ν plane,

$$C_{\mu\nu}(x) \equiv U_{\mu,\nu}(x) + U_{\nu,-\mu}(x) + U_{-\mu,-\nu}(x) + U_{-\nu,\mu}(x). \quad (4.5.5)$$

A schematic of this sum of plaquettes is given in diagram 4.3,

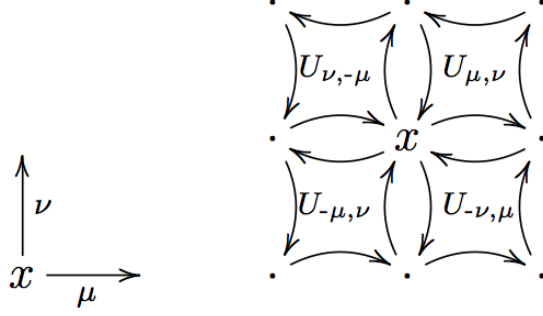


Figure 4.3: A schematic showing an oriented $C_{\mu\nu}(x)$ sum of plaquettes. The same plaquettes with loops in the opposite direction is $C_{\mu\nu}^\dagger(x) = C_{\nu\mu}$.

Showing that this definition of $G_{\mu\nu}(x)$ approaches the continuum definition is simple. From equation (4.4.10) we can deduce that each plaquette, regardless of its μ, ν orientation, approaches $G_{\mu\nu}(x)$ in the continuum limit, hence,

$$\begin{aligned} \frac{1}{8ia^2}(C_{\mu\nu}(x) - C_{\nu\mu}(x)) &= \frac{1}{8ia^2} (4\mathbb{I} + 4ia^2gG_{\mu\nu}(x) - 4\mathbb{I} + 4ia^2gG_{\mu\nu}^\dagger(x) + \mathcal{O}(a^6)) \\ &= \frac{1}{8ia^2}4ia^2g (G_{\mu\nu}(x) + G_{\mu\nu}^\dagger(x) + \mathcal{O}(a^4)), \end{aligned}$$

and using the fact that $G_{\mu\nu}(x)$ is hermitian,

$$\lim_{a \rightarrow 0} \frac{1}{8ia^2}(C_{\mu\nu}(x) - C_{\nu\mu}(x)) = gG_{\mu\nu}(x). \quad (4.5.6)$$

Let us now investigate the effect of adding this clover term to the Lagrangian. Using the language of continuum operators, we can express the Wilson gauge action including the clover term as,

$$S_{SW}[\psi, \bar{\psi}, U] = a^4 \sum_x \bar{\psi}(x) \left(\not{D} + m - \frac{ar}{2} \not{D} \not{D} \right) \psi(x) \quad (4.5.7)$$

The subscript SW on the action is reference to *Sheikholeslami* and *Wohlert* (5) who devised this technique in 1985. To show that the above is equivalent to the Wilson action and the clover term, we will use the two Euclidean gamma matrices

identities,

$$\{\gamma_\mu, \gamma_\nu\} = 2\delta_{\mu,\nu}\mathbb{I}, \quad \text{and} \quad [\gamma_\mu, \gamma_\nu] = 2i\sigma_{\mu\nu}, \quad (4.5.8)$$

such that, when these two identities are added,

$$\gamma_\mu\gamma_\nu = \delta_{\mu,\nu} + i\sigma_{\mu\nu} \quad (4.5.9)$$

we can deduce,

$$\begin{aligned} \not{D}\not{D} &= \gamma_\mu\gamma_\nu D_\mu D_\nu \\ &= (\delta_{\mu,\nu} + i\sigma_{\mu\nu})(D_\nu D_\mu - igG_{\mu\nu}) \quad \text{from eq. (3.3.4)} \\ &= D_\mu D_\mu - ig\text{Tr}[G_{\mu\nu}] + \frac{1}{2}(\gamma_\mu\gamma_\nu - \gamma_\nu\gamma_\mu)D_\nu D_\mu + g\sigma_{\mu\nu}G_{\mu\nu} \end{aligned}$$

Now, the trace in the above expression evaluates to zero, and the gamma matrices commute with the gauge covariant derivatives, so that expression evaluates to zero also, leaving,

$$\not{D}\not{D} = D_\mu D_\mu + g\sigma_{\mu\nu}G_{\mu\nu}. \quad (4.5.10)$$

One can easily see that substituting the above expression back into (4.5.7), the interacting Wilson fermion action plus the clover term is recovered,

$$\begin{aligned} S_F[\psi, \bar{\psi}, U] &= a^4 \sum_x \bar{\psi}(x) \left(\not{D} + m - \frac{ar}{2} D_\mu D_\mu - C_{SW} \frac{ar}{2} \sigma_{\mu\nu} g G_{\mu\nu} \right) \psi(x) \\ &= S_F^I[\psi, \bar{\psi}, U] + S_{SW}[\psi, \bar{\psi}, U] \end{aligned} \quad (4.5.11)$$

Notice the addition of another constant, C_{SW} . When setting this constant equal to r , the clover improvement corresponds to tree-level. That is, the correction to the gauge action that comes from loops and higher order terms are neglected. One can tune C_{SW} to further correct at higher loop order (?). We can now combine equations (4.5.11) and (4.4.16) to form a discretised, fully interacting, undoubled, $\mathcal{O}(a)$ improved QCD action on the lattice,

$$S[\psi, \bar{\psi}, U] = S_F[\psi, \bar{\psi}, U] + S_G[U]. \quad (4.5.12)$$

The next step is to incorporate this action into a path integral that can be performed on a computer. This will require numerical simulation of the gauge field evolution (chapter 5) together with the introduction of Grassmann calculus to deal with the fermionic integrals (appendix B) and a more specific definition of the operators.

CHAPTER 5

Numerical Simulation

We now have a discretised action that is free from doublers and is tree-level improved up to $\mathcal{O}(a^2)$. The path integral with this action, for some set of operators,

$$A = \prod_n \mathcal{O}_n, \tag{5.0.1}$$

may now be written down,

$$Z = \int \mathcal{D}\psi \mathcal{D}\bar{\psi} \mathcal{D}U e^{-S[\psi, \bar{\psi}, U]}, \tag{5.0.2}$$

so that the expectation value of A is

$$\langle A \rangle = \frac{1}{Z} \int \mathcal{D}\psi \mathcal{D}\bar{\psi} \mathcal{D}U e^{-S[\psi, \bar{\psi}, U]} A. \tag{5.0.3}$$

A natural question to ask at this point would be this: how can we compute the functional integrals on a computer? The answer must be given in multiple parts. The first part will deal with the simulation of a pure gauge theory which will cover the general technique for performing the functional integrals over the gauge field. Discussion of the Grassmann calculus necessary to perform the functional integrals over the fermion fields can be found in appendix B. Then, an approximation technique known as ‘quenching,’ where the physical interpretation is that only valence quarks are present in our simulation and there are no sea quarks, will be presented⁷. We shall next discuss operators on the lattice which correspond to the creation and annihilation operators of quantum field theory. At this point, we will be in a position to extract physical results from computational simulations, but further discussion on that point will be deferred to section 8 which is specific to the σ meson. We shall then finalise the section by dealing with dynamical fermions where sea quarks

⁷In the language of field theory, this is the same as saying that the masses of the sea quarks are infinitely heavy and are therefore forbidden from being produced by virtual gluons

and valence quarks are mass degenerate and virtual pair-production of quarks and antiquarks is allowed and simulated.

5.1 Simulation of a Pure Gauge Field

Consider the vacuum expectation value of some observable quantity O in a pure gauge theory on the lattice, i.e., no fermions present,

$$\langle O \rangle = \frac{1}{Z} \int \mathcal{D}[U] e^{-S_G[U]} O[U] \quad \text{such that} \quad Z = \int \mathcal{D}[U] e^{-S_G[U]} \quad (5.1.1)$$

A **Monte Carlo** simulation can approximate this observable by evaluating the observable $O[U]$ on a set of N gauge field configurations and taking the mean. The gauge field configurations are sampled from a set with some probability density function $P(U_n)$ that is proportional to $e^{-S_G[U_n]}$, the natural field theory analogue of the Boltzmann weighting factor in statistical mechanics,

$$\langle O \rangle = \lim_{N \rightarrow \infty} \frac{1}{N} \sum_n^N O[U_n]. \quad (5.1.2)$$

Now, in order to account for the weighting factor $e^{-S_G[U_n]}$, we must employ **importance sampling**. Consider the expectation value of some function $f(x)$ with an associated probability density function $\rho(x)$ over some interval (a, b) ,

$$\langle f(x) \rangle_\rho = \frac{\int_a^b dx \rho(x) f(x)}{\int_a^b dx \rho(x)} \quad (5.1.3)$$

This mean value is approximated by,

$$\langle f(x) \rangle_\rho = \lim_{N \rightarrow \infty} \frac{1}{N} \sum_n^N f(x_n), \quad \text{for } x_n \in (a, b), \quad (5.1.4)$$

and each x_n is sampled with a probability density,

$$dP(x) = \frac{\rho(x) dx}{\int_a^b dx \rho(x)}. \quad (5.1.5)$$

From these standard results we can read off that our U_n must be sampled from a probability distribution density,

$$dP(U) = \frac{e^{-S_G[U]} \mathcal{D}[U]}{\int \mathcal{D}[U] e^{-S_G[U]}}. \quad (5.1.6)$$

To realise this, the gauge field configurations are generated via a **Markov Chain** or **Markov Process**. In such a procedure, a gauge field configuration U transitions to the next configuration in the chain U' in one Markov step (or one step in computer time) by some conditional transitional probability,

$$P(U \rightarrow U') = T(U'|U), \quad (5.1.7)$$

which must satisfy,

$$0 \leq T(U'|U) \leq 1, \quad \text{and} \quad \sum_{U'} T(U'|U) = 1, \quad (5.1.8)$$

where the sum simply states that all other target configurations are accessible. Once the configuration had reached an equilibrium, the probability for the configuration to evolve *into* some U' in one Markov step must be the same as the probability of the configuration evolving *out of* U' at the same step. This leads to the following balance equation,

$$\sum_U T(U'|U)P(U) = \sum_U T(U|U')P(U). \quad (5.1.9)$$

We can evaluate the right hand side by relabelling $U \leftrightarrow U'$ in (5.1.8), which shows that the equilibrium distribution $P(U)$ is a fixed point in the Markov chain,

$$\sum_U T(U'|U)P(U) = P(U'). \quad (5.1.10)$$

In order for the balance equation to hold for all possible gauge field configuration, we can impose a sufficient (but not necessary) condition of *detailed balance*,

$$T(U'|U)P(U) = T(U|U')P(U). \quad (5.1.11)$$

which is the starting point for most simulation algorithms. We shall look at two such algorithms in detail as they are both employed in this analysis. Both are based on the **Metropolis algorithm**

5.1.1 Metropolis Algorithm for $SU(3)$

The Metropolis algorithm (8) was devised by Nicholas Constantine Metropolis in 1953. It advances the Markov chain from $U_{n-1} = U$ to $U_n = U'$ in the following way:

1. Select a candidate configuration for U' according to some selection probability $T_0(U|U')$
2. Accept the new configuration with the following acceptance probabilities:

$$T_{accept}(U|U') = \min \left(1, \frac{T_0(U|U')P(U')}{T_0(U'|U)P(U)} \right).$$

3. Repeat from 1.

The first step is straight forward; it instructs us to generate a candidate configuration from a known probability distribution. The second step contains the subtlety. If the right hand expression of the $\min(1, X)$ function is greater than 1, the candidate configuration is accepted with probability 1, ($X > 1$). This tends to bring the configuration closer to the equilibrium distribution. If right hand side is less than 1, ($X < 1$), the candidate configuration is accepted with a probability X . If the candidate configuration is accepted, it becomes the new starting point and the process is repeated. If the candidate configuration is rejected, then the old configuration becomes the next configuration in the Markov chain and the process is repeated.

We can apply this algorithm to the gauge fields of $SU(3)$ and the Wilson gauge action of lattice gauge theory. Recall the Wilson gauge action (4.4.16) from chapter 4,

$$S_G[U] = \frac{2}{g^2} \sum_x \sum_{\mu < \nu} \text{ReTr}[\mathbb{I} - U_{\mu\nu}(x)] \quad (5.1.12)$$

We shall consider the *local* change in the action, i.e., at particular lattice point, by changing one of the link variables $U_\mu(x) \rightarrow U_\mu(x)'$. In the 4-dimensional spacetime

of the lattice, this will affect 6 other plaquettes, though the link variables in those affected plaquettes will remain constant. This allows us to write down the action associated with a single link $U_\mu(x)$ *in terms of that link*,

$$S_{local}[U_\mu(x)] = \frac{2}{g^2} \text{ReTr}[6\mathbb{I} - U_\mu(x)B], \quad (5.1.13)$$

$$\text{such that } B = \sum_{\mu \neq \nu} (U_\nu(x + \hat{\mu})U_{-\mu}(x + \hat{\mu} + \hat{\nu})U_{-\nu}(x + \hat{\nu}) \\ + U_{-\nu}(x + \hat{\mu})U_{-\mu}(x + \hat{\mu} - \hat{\nu})U_\nu(x - \hat{\nu})). \quad (5.1.14)$$

This allows us to write the total change in in the action from one gauge field configuration to another, if the only thing we change is a single link variable,

$$\Delta S[U] = S_{local}[U_\mu(x)'] - S_{local}[U_\mu(x)] = -\frac{2}{g^2} \text{ReTr}[(U_\mu(x)' - U_\mu(x))B]. \quad (5.1.15)$$

This is already suggestive of the Metropolis algorithm, as we clearly want our gauge fields to fluctuate about the classical (extremised) configuration. Indeed, the classical value of the action would be the equilibrium gauge field configuration.

The next thing to do is to decide on a selection procedure for $U_\mu(x)'$. A typical strategy is to choose some element X of $SU(3)$ close to the identity and make the candidate link,

$$U_\mu(x)' = XU_\mu(x) = (\mathbb{I} + i\alpha^a \tau^a)U_\mu(x), \quad (5.1.16)$$

where the constants $\alpha^a \in \mathbb{R}$ are small and τ^a are the group generators of $SU(3)$. We choose X to be close to the identity so keep the rejection rate down. Of course, one is free to choose any acceptance rate one wishes, depending on the needs of the calculation. Now, $SU(3)$ has 8 free parameters and generating random elements can prove computationally costly. One method of avoiding this cost is to construct three elements $R, S, T \in SU(2)$ close to the identity, and create the element X via,

$$R = \begin{pmatrix} r_{11} & r_{12} & 0 \\ r_{21} & r_{22} & 0 \\ 0 & 0 & 1 \end{pmatrix}, \quad S = \begin{pmatrix} s_{11} & 0 & s_{12} \\ 0 & 1 & 0 \\ s_{21} & 0 & s_{22} \end{pmatrix}, \quad T = \begin{pmatrix} 1 & 0 & 0 \\ 0 & t_{11} & t_{12} \\ 0 & t_{21} & t_{22} \end{pmatrix}, \quad X = RST. \quad (5.1.17)$$

Now, any element of $SU(2)$ may be expressed as a 2×2 matrix with two complex elements $a, b \in \mathbb{C}$ subject to the constraint $|a|^2 + |b|^2 = 1$,

$$\begin{pmatrix} a & b \\ -b^* & a^* \end{pmatrix} \begin{pmatrix} a^* & -b \\ b^* & a \end{pmatrix} = \begin{pmatrix} |a|^2 + |b|^2 & 0 \\ 0 & |a|^2 + |b|^2 \end{pmatrix} = \mathbb{I}. \quad (5.1.18)$$

The four real elements of the $SU(2)$ matrix can be expressed as,

$$a = x_0 + ix_3, \quad b = x_2 + ix_1, \quad (5.1.19)$$

or, more compactly,

$$\begin{pmatrix} a & b \\ -b^* & a^* \end{pmatrix} = x_0 \mathbb{I} + i\vec{x} \cdot \vec{\sigma}, \quad (5.1.20)$$

where $\vec{\sigma}$ are the Pauli matrices. To construct an element of $SU(2)$ close to the identity, one may choose four random numbers $-\frac{1}{2} < y_i < \frac{1}{2}$ and construct the elements $x_0 \dots x_3$ via,

$$\vec{x} = \epsilon \frac{\vec{y}}{|\vec{y}|}, \quad x_0 = \frac{y_0}{|y_0|} (1 - \epsilon)^{\frac{1}{2}}. \quad (5.1.21)$$

The real parameter ϵ controls how close to the identity one wishes to generate the $SU(2)$ elements, and in turn the $SU(3)$ elements. This gives us step 1 of the Metropolis algorithm.

In practise, we wish to have a symmetric selection probability $T_0(U|U') = T_0(U'|U)$ for our candidate gauge fields so we generate a large set of $X \in SU(3)$ and include their inverses X^\dagger in the selection set. Although we may assign different selection probabilities to different X , we assign the *same* selection probability to any particular X and its inverse X^\dagger . Furthermore, this simplifies the second step in the Metropolis algorithm, to

$$T_{accept} = \min \left(1, \frac{P(U')}{P(U)} \right). \quad (5.1.22)$$

Now, we use as our probability measure the the ‘Boltzmann weighting factor’ $\exp(-S[U])$ hence we have a relevant expression, using (5.1.15), for step two of

Metropolis.

$$T_{\text{accept}} = \min(1, \exp(-\Delta S)). \quad (5.1.23)$$

We may now write down the Metropolis steps for simulating an $SU(3)$ gauge field:

1. From some gauge field configuration, choose a site x and a lattice direction μ and generate a candidate link via $U_\mu(x)' = XU_\mu(x)$.
2. Compute the local change in the action using (5.1.15). If the action is reduced, i.e. if $\Delta S < 0$, accept the candidate link. If $\Delta S > 0$, generate a random number $0 < r \leq 1$ and accept the candidate gauge link if $r \leq \exp(-\Delta S)$.
3. Repeat from step 1.

As one can imagine, the Metropolis algorithm can be computationally expensive. Even for moderate size lattices, the number of spacetime point and directions make performing such an algorithm over *all* links (which is equivalent to a single step in the entire gauge field evolution) a daunting task. Nonetheless, Metropolis is the starting point for two very important algorithms in lattice gauge theory, namely the heatbath (9) and the Hybrid Monte-Carlo (10)

5.1.2 Heatbath Algorithm

The heatbath combines steps 1. and 2. of Metropolis in to a single step. The candidate link $U_\mu(x)'$ is chosen according to some local probability distribution defined by the staples B ,

$$dP(U) = dU \exp\left(\frac{2}{g^2} \text{ReTr}[UB]\right). \quad (5.1.24)$$

A heatbath algorithm for $SU(3)$ does not exist, but we can ‘pseudo-heatbath’ the $SU(3)$ elements by applying the heatbath procedure to the three $SU(2)$ subgroups (5.1.17). The sum of the staples B in $SU(2)$ may be written in the form,

$$B = bV \quad \text{such that} \quad b = (\det[B])^{\frac{1}{2}}, \quad (5.1.25)$$

which means V is a properly normalised element of $SU(2)$. We can now invoke the invariant property of the Haar measure by making the transformation $X = UV$,

$$dP(X) = dX \exp\left(\frac{2b}{g^2} \text{ReTr}[X]\right), \quad (5.1.26)$$

so that candidate links can be constructed via,

$$U_\mu(x)' = XV^\dagger = XB^\dagger \frac{1}{b}. \quad (5.1.27)$$

The task now is to generate matrices X that are distributed according to (5.1.26). We do this by rewriting the Haar measure in terms of the four real components of X ,

$$dX = \frac{1}{\pi^2} d^4x \delta(x_0^2 + |\vec{x}|^2 - 1). \quad (5.1.28)$$

We use the Dirac delta identity,

$$\delta(x^2 - \alpha^2) = \frac{1}{2|\alpha|} [\delta(x + \alpha) + \delta(x - \alpha)], \quad (5.1.29)$$

to rewrite the measure as,

$$dX = \frac{1}{\pi^2} d^4x \frac{\theta(1 - x_0^2)}{2(1 - x_0^2)^{\frac{1}{2}}} \left[\delta\left(|\vec{x}| - (1 - x_0^2)^{\frac{1}{2}}\right) + \delta\left(|\vec{x}| + (1 - x_0^2)^{\frac{1}{2}}\right) \right], \quad (5.1.30)$$

where θ is the Heaviside step function,

$$\theta(x) = \begin{cases} 0 & \text{if } x < 0 \\ 1 & \text{if } x > 0 \end{cases}$$

and,

$$\frac{\partial}{\partial x} \theta(x) = \delta(x). \quad (5.1.31)$$

Now, we can rewrite the measure d^4x as a measure over the 3-vector \vec{x} , x_0 , and the solid angle Ω , which will also immediately allow us to eliminate the right-hand delta

function in (5.1.30),

$$\begin{aligned} dX &= d|\vec{x}||\vec{x}|^2 d^2\Omega dx_0 \\ \Rightarrow dX &= \frac{1}{2\pi^2} d^2\Omega dx_0 (1-x_0^2)^{\frac{1}{2}} \theta(1-x_0^2). \end{aligned} \quad (5.1.32)$$

Noting that $|x_0| \leq 1$ for our candidate $SU(2)$ elements, we can eliminate the Heaviside step function. Using an explicit expression for the solid angle $d^2\Omega = (d\cos\theta)(d\phi)$ and also noting that $\text{ReTr}(X) = 2x_0$, we can write down the distribution measure $dP(X)$,

$$dP(X) = \frac{1}{2\pi^2} (d\cos\theta)(d\phi) (1-x_0^2)^{\frac{1}{2}} \exp\left(\frac{4bx_0}{g^2}\right), \quad (5.1.33)$$

which reduces the problem to the determination of three real parameters x_0, θ , and ϕ . A procedure for determining these numbers can be found in (11) and (12). The $SU(2)$ heatbath algorithm may now be expressed:

1. Identify a lattice point x and direction μ . Compute $b = (\det[B])^{\frac{1}{2}}$ from the surrounding staples and compute $V = \frac{1}{b}B$.
2. Determine an $SU(2)$ group element X .
3. Update the link: $U_\mu(x)' = XV^\dagger$.

Notice how the link is updated at each step giving a new link at each step in the Markov chain. To apply this to an $SU(3)$ theory, we must apply the above $SU(2)$ formulation to the subgroups of $SU(3)$. The ‘pseudo-heatbath’ algorithm generates three $SU(2)$ matrices R, S, T as before, (c.f. (5.1.17)) but this time, after each multiplication, the staples must be recalculated to compute the weights for the next candidate $SU(2)$ matrix. If we multiply in the order R , then S , then T , this means that the Boltzmann weights for R will be UB , the weights for S will be RUB , and the weights for T , will be $SRUB$. Hence, the new $SU(3)$ link will be,

$$U_\mu(x)' = TSRU_\mu(x). \quad (5.1.34)$$

This algorithm is perfectly suited to simulating a pure gauge field. One can systematically update all gauge links on the lattice and thereby simulate the quantum fluctuations of a pure gauge field. However, when one introduces fermions to the lattice, the situation becomes more complex as the updating procedure for generating new link variables will now not be weighted by the sum of the staples only, but also by the dynamics of the fermions. One can essentially ‘turn off’ the fermions while updating the gauge field and use heatbath to save on computer time. This is known as the **quenched**⁸ approximation. Although this approximation is manifestly physically unsound, it can still give good results (13). We use the quenched approximation in our preliminary analysis.

We shall now present the introduction of fermions on the lattice and show how one can employ the quenched approximation, or make the fermions dynamical, whereupon a new simulation algorithm is needed.

5.2 Fermions on the Lattice.

In order to see how fermions on the lattice can be simulated, let us take another look at the expectation value of some product of operators on the lattice 5.0.3,

$$\langle A[\psi, \bar{\psi}, U] \rangle = \frac{1}{Z} \int \mathcal{D}U e^{-S_G[U]} \mathcal{D}\psi \mathcal{D}\bar{\psi} e^{-S_F[\psi, \bar{\psi}, U]} A[\psi, \bar{\psi}, U]. \quad (5.2.1)$$

Let us consider a two flavour theory with (*u*)up- and (*d*)down-type quarks, and let us also consider a pair of pseudo-scalar operators P_{\pm} of the form,

$$P_+^{\dagger}(x) = P_-(x) = \bar{u}(x)\gamma_5 d(x), \quad P_-^{\dagger}(x) = P_+ = \bar{d}(x)\gamma_5 u(x). \quad (5.2.2)$$

This is actually the creation of a positively charged pion at $x = (\vec{x}, 0)$ and its subsequent destruction at $y = (\vec{y}, t)$. Using the Berezin calculus in Appendix B, we can perform the integrals over the fermions fields analytically, which will leave us

⁸The term ‘quenched’ comes from the practice of heating metals with impurities and rapidly cooling them, thereby freezing in a favourable crystalline configuration of the impurities to induce hardness in the final state.

with the purely bosonic gauge field integration,

$$\begin{aligned} & \langle \bar{d}(y)\gamma_5 u(y)\bar{u}(x)\gamma_5 d(x) \rangle \\ &= -\frac{1}{Z} \int \mathcal{D}U e^{-S_G[U]} \det[M_u] \det[M_d] \text{Tr} [\gamma_5 M_u^{-1}(y, x)\gamma_5 M_d^{-1}(y, x)], \\ \text{where } Z &= \int \mathcal{D}U e^{-S_G[U]} \det[M_u] \det[M_d], \end{aligned} \quad (5.2.3)$$

and M is the Dirac operator of the theory. The fermion determinants are dependent on the gauge fields and therefore the lattice links U , hence one must use as a weighting factor in any gauge field simulation the following probability measure,

$$P(U) \propto \frac{e^{-S_G[U]} \det[M_u] \det[M_d]}{\int \mathcal{D}U e^{-S_G[U]} \det[M_u] \det[M_d]}. \quad (5.2.4)$$

A small lattice (in terms of modern lattice calculations) of spacetime dimension $L = 8, T = 16$ will have $3_{colour} \times 4_{spin} \times 8^3 \times 16 \approx 10^5$ complex entries, making the brute force calculation of the determinant prohibitively expensive. A simple solution to this problem is to set the fermion determinants to unity, reducing the Boltzmann weighting factor to that of a pure gauge theory and reducing computation time significantly. This amounts to setting the masses of sea quarks in our theory to infinity, as can be seen from the hopping parameter expansion.

5.2.1 Hopping Parameter

The Wilson-Dirac operator M_W (4.3.5) can be rewritten in the following form,

$$\begin{aligned} M_W(x, y) &= C(\mathbb{I} - \kappa H), \quad \kappa = \frac{1}{2(ma + 4)}, \quad C = m + \frac{4}{a}, \\ H_{\alpha\beta}^{ab}(x, y) &= \sum_{\mu=\pm 1}^{\pm 4} (\mathbb{I} - \gamma_\mu)_{\alpha\beta} U_\mu^{ab}(x) \delta_{x+\hat{\mu}, y}. \end{aligned} \quad (5.2.5)$$

We can allow the constant factor C to be absorbed by the fields in a redefinition $\psi \rightarrow C^{\frac{1}{2}}\psi$ and then expand the Wilson-Dirac propagator M_W^{-1} in powers of the

hopping parameter κ ,

$$M_W^{-1}(x, y) = (\mathbb{I} - \kappa H)^{-1} = \sum_{n=0}^{\infty} \kappa^n H^n. \quad (5.2.6)$$

The definition of the hopping expansion is such that for a given pair of lattice points (x, y) , the propagator is a sum of fermion lines starting at y and ending at x . The length of the path is given by n and, by the nature of the definition of the hopping term, back-tracking paths are prohibited. One can also expand the determinant of the Wilson-Dirac operator in terms of the hopping parameter,

$$\begin{aligned} \det[M_W(x, y)] &= \det[\mathbb{I} - \kappa H(x, y)] = \exp(\text{Tr}[\ln(\mathbb{I} - \kappa H(x, y))]) \\ &= \exp\left(-\sum_{n=1}^{\infty} \frac{1}{n} \kappa^n \text{Tr}[H^n(x, y)]\right) \end{aligned} \quad (5.2.7)$$

The trace here runs over spin, colour, and position indices, hence will only give a non-zero value when $y = x$, i.e., for **fermion loops**. These fermion loops are the sea quarks (or virtual quarks) of the QCD path integral. As mentioned at the start of this chapter, the quenched approximation ignores the effects of these sea quarks and, from the previous section, we can see that this can be realised by setting the fermion determinants in the path integral to unity. One could also argue that in the case of finite lattice spacing a , one is setting the masses of the sea quarks to be infinitely large c.f. (5.2.5) and thereby setting the hopping parameter to zero in the case of the expansion of the determinant.

5.2.2 Pseudo-Fermions

As we saw in the previous section, we can circumvent the problem of calculating the fermion determinants of the path integral by simply setting them to unity, but this comes at the cost of losing all the dynamical properties of the fermions. In order to include the dynamical nature, we must include their effects when we simulate our gauge fields, and we are led to the weighting factor of (5.2.4). Now, in the modified minimal subtraction renormalisation scheme it is perfectly acceptable to impose degeneracy on the up and down quarks. Typical values for the renormalised mass

for both quarks is around 5MeV. This mass degeneracy has a very neat consequence on the path integral of a theory with two mass degenerate flavours $m_u = m_d = m_l$,

$$\begin{aligned}
\det[M_u] \det[M_d] &\rightarrow \det[M] \det[\gamma_5 M^\dagger \gamma_5], \quad (\text{using } \gamma_5 M^\dagger \gamma_5 = M) \\
&= \det[M] \det[\gamma_5^2] \det[M^\dagger], \\
&= \det[M] \det[M^\dagger], \\
&= \det[MM^\dagger].
\end{aligned} \tag{5.2.8}$$

This form of the determinant is useful and we will come back to it later. Its interpretation as a probability measure means it must be real and positive. The Dirac operators for fermions with finite mass are non-singular (invertible) and therefore we may always perform a similarity transformation to a unitary basis V ,

$$M = V^\dagger \Lambda V, \tag{5.2.9}$$

where Λ is the diagonal matrix of eigenvalues of M . Taking the determinant of the product MM^\dagger now reads as,

$$\begin{aligned}
\det[MM^\dagger] &= \det[V^\dagger \Lambda V V^\dagger \Lambda^* V] \\
&= \det[V^\dagger] \det[\Lambda \Lambda^*] \det[V] \\
&= (\pm 1)^2 \prod_i |\Lambda_i|^2
\end{aligned} \tag{5.2.10}$$

which will always give a real and positive number, hence we are justified in using as part of a probability measure. However, an unfortunate property of Grassmann valued variables $\theta, \bar{\theta}$ is that the function $\exp(-\bar{\theta}_i M_{ij} \theta_j)$ is not positive definite. We can remedy this by noting that the Grassmann valued result⁹,

$$\begin{aligned}
\int \prod_{i=1}^N d\bar{\theta}_i d\theta_i \exp(-\bar{\theta}_i A_{ij} \theta_j) &= -(A_{12} A_{21} - A_{11} A_{22}) \int d\bar{\theta}_1 \bar{\theta}_1 \int d\theta_1 \theta_1 \int d\bar{\theta}_2 \bar{\theta}_2 \int d\theta_2 \theta_2 \\
&= \det[A],
\end{aligned} \tag{5.2.11}$$

⁹This is for $N = 2$, but the result holds for all N . See appendix B, equation B.3.6

is in analogy with the result for complex valued variables z, \bar{z} ,

$$\begin{aligned}
\int \prod_{i=1}^N d\bar{z}_i dz_i \exp(-\bar{z}_i A_{ij} z_j) &= \int \prod_{i=1}^N d\bar{z}_i dz'_i \exp(-\bar{z}_i z'_i) \quad \text{where } z'_i = A_{ij} z_j \\
&= \frac{1}{|\det[A]|} \int \prod_{i=1}^N d\bar{z}_i dz_i \exp(-\bar{z}_i z_i) \\
&= \frac{\pi^N}{|\det[A]|}.
\end{aligned} \tag{5.2.12}$$

This allows us to employ pseudo-fermions ϕ in the probability measure as we can make the equality (for the case $m_u = m_d$),

$$\begin{aligned}
\int D[\psi] D[\bar{\psi}] \exp(-\psi_u M \psi_u - \psi_d M \psi_d) &= \pi^{-N} \int D[\phi_{\text{Re}}] D[\phi_{\text{Im}}] \exp(\phi^\dagger (MM^\dagger)^{-1} \phi) \\
&= |\det[MM^\dagger]|
\end{aligned} \tag{5.2.13}$$

Notice the inverse of MM^\dagger appears in the bosonic integral. The determinant of the product MM^\dagger is used to define the *effective fermion action*,

$$\det(MM^\dagger) = \exp(\text{Tr}[\ln(MM^\dagger)]) = \exp(-S_F^{\text{eff}}[U]), \tag{5.2.14}$$

so that we now have a total action,

$$\begin{aligned}
S[U] &= S_G[U] + S_F^{\text{eff}}[U] \\
&= S_G[U] + \phi^\dagger (MM^\dagger)^{-1} \phi
\end{aligned} \tag{5.2.15}$$

which we may use in the probability weighting (5.2.4). For the accept/reject step of Metropolis, we must compute the total change in the action due to changing the gauge field $U \rightarrow U'$,

$$\exp(-S[U'] + S[U]) = \exp(-S_G[U'] + S_G[U]) \exp(-S_F^{\text{eff}}[U'] + S_F^{\text{eff}}[U]) \tag{5.2.16}$$

There are two ways in which one could implement this using the techniques described so far. The first would be to use the Metropolis algorithm for individual

gauge links, but this would require us to compute the inverse of MM^\dagger for every gauge link update. Acceptance rates would be good, but the computational effort required to calculate the inverses makes this technique extremely expensive from a computational point of view.

Another technique would be to change all link variables for every inversion of MM^\dagger , known as a global update. One would then ease the computational burden by requiring much fewer inversions, but the cost is that the action will change by a much larger amount at each update, so the acceptance rate suffers badly. In order to keep the simulation going, one would need to perform a great deal of Metropolis updates, and thus the computational burden reappears. In order to formulate an efficient, dynamical simulation of the gauge fields, one must use a different approach, one such is the hybrid Monte-Carlo.

5.3 Hybrid Monte-Carlo Algorithm

The hybrid Monte-Carlo algorithm (HMC) (10) offers us a way to evolve entire gauge field configurations with dynamical fermions while keeping the acceptance rates high. It takes, as a starting point, the concept of molecular dynamics from classical mechanics with coordinates Q and conjugate momentum P . These variables are dependent on spacetime (or lattice points) and therefore the notation $Q = Q(x)$ and $P = P(x)$ is implicit.

Consider then the expectation value of some operator $O(Q)$ over a bosonic path integral,

$$\langle O \rangle = \frac{\int D[Q] \exp(-S[Q]) O[Q]}{\int D[Q] \exp(-S[Q])}. \quad (5.3.1)$$

We can, without any loss of generality, introduce a quadratic (conjugate) momentum term in the exponential and integrate over the momentum variables,

$$\langle O \rangle = \frac{\int \mathcal{D}[Q] \mathcal{D}[P] \exp\left(-\frac{1}{2}P^2 - S[Q]\right) O[Q]}{\int \mathcal{D}[Q] \mathcal{D}[P] \exp\left(-\frac{1}{2}P^2 - S[Q]\right)}, \quad (5.3.2)$$

which leaves the expectation value unchanged as the Gaussian integrals in P will simply cancel. However, we can also identify the argument of the exponential as the non-relativistic ‘Hamiltonian’ of some system with canonical coordinates Q , canonical momentum P , and ‘potential’ $S[Q]$,

$$\mathcal{H}(P, Q) = \frac{1}{2}P^2 + S[Q], \quad \text{where} \quad P^2 \equiv \sum_x P^2(x). \quad (5.3.3)$$

We can even go so far as to introduce a fictitious time variable τ and generate equations of motion for this Hamiltonian,

$$\frac{\partial Q}{\partial \tau} = \frac{\partial \mathcal{H}}{\partial P}, \quad \frac{\partial P}{\partial \tau} = -\frac{\partial \mathcal{H}}{\partial Q} = -\frac{\partial S}{\partial Q}. \quad (5.3.4)$$

Now, as we can see from (5.3.2), we can extract observables from this path integral over Q and P that are equivalent to the original path integral observables extracted from (5.3.1). Furthermore, if we evolve the Hamiltonian through the parameter τ , we can generate configurations in the phase space of Q and P , that lie on a constant hypersurface because the Hamiltonian is a constant of the motion. This means that new configurations will always be accepted in a Metropolis step, provided the equations of motion can be solved exactly. Of course, on a computer, the calculus is done numerically with some step size $\epsilon = \Delta\tau$ and evolution will introduce errors of order $\mathcal{O}(\epsilon^2)$. This evolution of the Hamiltonian over a finite set of discrete points is known as a *trajectory*. The errors that are introduced over a trajectory are ‘corrected’ by a Metropolis step in the HMC algorithm. Large errors will induce a small acceptance probability, and conversely, errors that ‘correct’ previous deviations by bringing the Hamiltonian back to its equilibrium position will always be accepted in the Metropolis step.

In order to satisfy the detailed balance condition, one must ensure that the integration measure $\mathcal{D}[Q]\mathcal{D}[P]$ remain invariant and that any trajectory be reversible, both of which are enforced by the Störmer-Verlet (leapfrog) integration scheme. Our canonical coordinates will be the gauge links $U_\mu(x)$,

$$U_\mu(x) = \exp(i\omega_\mu^a(x)T^a) \equiv \exp(iQ), \quad (5.3.5)$$

where a runs over the $SU(3)$ generators T^a and $\omega_\mu^a(x)$ parameterise the coordinates Q . We use T^a here to represent the generators rather than τ^a to avoid an obvious ambiguity with the Hamiltonian evolution parameter τ . There are also eight real canonically conjugate momentum variables associated with the $\omega_\mu^a(x)$,

$$P_\mu(x) = P_\mu^a(x)T^a. \quad (5.3.6)$$

According to (5.3.3), we define the square of the momentum as,

$$\frac{1}{2} \sum_{x,\mu,a} (P_\mu^a(x)T^a)^2 = \sum_{x,\mu} \text{Tr}[P_\mu(x)^2], \quad (5.3.7)$$

where we make use of the relation $\text{Tr}[T^a T^b] = \frac{1}{2}\delta^{ab}$ c.f. (3.3.11). This allows us to compute the derivate of Q with respect to τ ,

$$\dot{Q} \equiv \frac{\partial Q}{\partial \tau} = \frac{\partial \mathcal{H}}{\partial P} = P. \quad (5.3.8)$$

The next task is to compute the derivative of the action with respect to Q , which we have established as elements of $SU(3)$. The rule for differentiating a function $f(U)$ with respect to $U = \exp(i\omega^a T^a)$ is to simply differentiate $f(U)$ with respect to the real parameter ω^a , multiply by the generator T^a , and sum over a ,

$$\nabla^a f(U) = \frac{\partial f(U)}{\partial \omega^a} = \frac{\partial}{\partial \omega} f(e^{i\omega T^a} U) \Big|_{\omega=0}. \quad (5.3.9)$$

We shall therefore define the function $F(U, \phi)$ as the $SU(3)$ group differential of the action (5.2.15),

$$F(U, \phi) = \nabla^a (S_G(U) + \phi^\dagger (MM^\dagger)^{-1} \phi) T^a. \quad (5.3.10)$$

For the pure gauge action $S_G[U]$ one finds, using the local definition of the action (5.1.13),

$$\begin{aligned} \frac{2}{g^2} \nabla^a \text{Tr}[UB + B^\dagger U^\dagger] T^a &= \frac{2}{g^2} \text{Tr}[iT^a(UB - B^\dagger U^\dagger)] T^a \\ &= \frac{i}{g^2} (UB - B^\dagger U^\dagger), \end{aligned} \quad (5.3.11)$$

which uses the traceless and hermitian nature of $i(UB - B^\dagger U^\dagger)$ and the identity,

$$T^j \text{Tr}[T^j c_k T^k] = \frac{1}{2} c_j T^j. \quad (5.3.12)$$

For the effective fermion action, we employ the identity,

$$\frac{\partial M^{-1}}{\partial \omega} = -M^{-1} \left(\frac{\partial M}{\partial \omega} \right) M^{-1}, \quad (5.3.13)$$

to find that,

$$\begin{aligned} \nabla^a (\phi^\dagger (MM^\dagger)^{-1} \phi) &= -\phi^\dagger (MM^\dagger)^{-1} (\nabla^a (MM^\dagger)^{-1}) (MM^\dagger)^{-1} \phi \\ &= - (MM^\dagger)^{-1} \phi)^\dagger \left(\frac{\partial M}{\partial \omega^a} M^\dagger + M \frac{\partial M^\dagger}{\partial \omega^a} \right) (MM^\dagger)^{-1} \phi)^\dagger. \end{aligned} \quad (5.3.14)$$

This means that at each step in the trajectory (or equivalently, each step in the leapfrog integration) one must calculate the derivative of the Dirac operator M with respect to the gauge links, and also compute the inverse of MM^\dagger . Differentiation of the Dirac operator (and its conjugate) is straightforward as M is linear in the gauge links c.f. Wilson action (4.3.5) and the clover action (4.5.11); the inversion is the most computationally expensive part.

We may now write down the HMC algorithm:

1. Generate a pseudo-fermion field $\phi = Mz$ from the distribution $\exp(-z^\dagger z)$.
2. From the initial gauge field configuration, generate the $P_\mu^a(x)$ according to the distribution $\exp(-\text{Tr}[P^2])$.
3. Perform the leapfrog integration over $n = \epsilon^{-1}$ steps. We denote the value of a variable at each step as a subscript:

$$\begin{aligned} \text{(a)} \quad P_{\frac{1}{2}} &= P_0 - \frac{\epsilon}{2} F(U, \phi) \Big|_{U_0}. \\ \text{(b)} \quad \text{For } k = 1 \dots n-1: \\ U_k &= \exp\left(i\epsilon P_{k-\frac{1}{2}}\right) U_{k-1} \quad P_{k+\frac{1}{2}} = P_{k-\frac{1}{2}} - \epsilon F(U, \phi) \Big|_{U_k}. \\ \text{(c)} \quad U_n &= \exp\left(i\epsilon P_{n-\frac{1}{2}}\right) U_{n-1} \quad P_n = P_{n-\frac{1}{2}} - \frac{\epsilon}{2} F(U, \phi) \Big|_{U_n}. \end{aligned}$$

4. Perform a Metropolis step on the candidate configuration. Accept with probability

$$T_{accept} = \min(1, \exp(-\Delta\mathcal{H})).$$

When we take measurements of observable quantities using gauge field configurations that have been generated using the HMC algorithm, the fluctuations in that observable will closely resemble the quantum fluctuations that would appear in a real measurement. Furthermore, the expectation values of those observable are simply the respective averages of those measurements. It is intriguing that, in order to numerically approximate a non-Abelian quantum gauge theory, we must use a classical equation of motion 5.3.3 to guide us through configuration space. This somewhat counter-intuitive fact is the governing principle of Bohmian mechanics in which the evolution of a quantum mechanical wave function is itself governed by the evolution of classical degrees of freedom in a configuration space. Indeed, equation 5.3.10 defines a function F which can be interpreted as a classical force guiding the evolution of the QCD system with the gauge action $S_G(U)$ and $\phi^\dagger(MM^\dagger)\phi$ acting as classical potentials.

Though it is easy to draw parallels between Bohmian mechanics and the Hybrid Molecular Dynamics algorithm, these parallels alone do not give us enough cause to abandon the Copenhagen interpretation and rethink the fundamentals of quantum mechanics. However, the QCD Lagrangian is widely accepted to be the governing equation of strong dynamics in the standard model, and the path integral that instructs us how to use the Lagrangian has remained analytically unsolved since its inception some 50 years ago. Whether or not one agrees with the principles of Bohmian mechanics, we must use them to extract the non-perturbative physics of non-Abelian quantum gauge theories.

5.4 *Caveat Emptor: A Note on Exceptional Configurations*

The previous section on the HMC introduces M^{-1} into the numerical part of the simulation¹⁰, and as such a new obstacle is encountered. Consider the Dirac operator as function of the gauge links, $M(U) = \not{D}(U) + m$, and its spectrum of k

¹⁰Albeit in the form $(MM^\dagger)^{-1}$

eigenvalues $\lambda_k(U)$,

$$M(U)\psi_k = (\not{D}(U) + m)\psi_k = (\lambda_k(U) + m)\psi_k. \quad (5.4.1)$$

The m here refers to the bare quark mass in the QCD Lagrangian. If any $\lambda_k(U)$ approaches the value $-m$, then the entire matrix operator M becomes nearly defective. To see this, we express the matrix inverse M^{-1} through its eigendecomposition,

$$M(U)^{-1} = \sum_{k,l} (\lambda_k(U) + m)^{-1} \psi_k \phi_l^\dagger, \quad \psi_k^\dagger \phi_l = \delta_{k,l}. \quad (5.4.2)$$

In the case where $\lambda_k(U) + m = 0$, the matrix $M(U)$ will have no inverse. In a numerical calculation with double floating point precision, the chances of this happening exactly are very small indeed. However, near misses are not so unlikely and when they happen, the configurations from which $M(U)$ is defined are said to be exceptional. Thankfully, the HMC algorithm can autonomously (in the Kantian sense!) omit these configurations from the ensemble via the final Metropolis step. This happens because the action S associated with Dirac operator formed from an exceptional configuration will change wildly, much more so than the tamer quantum fluctuations we simulate with the random pseudo-fermion fields. Therefore, the $\Delta\mathcal{H}$ calculated from the HMC evolution will be abnormally large, and the probability of acceptance T_{accept} will diminish towards zero. Colloquially, it is said that the HMC pushes the gauge field evolution away from exceptional configurations with the pseudo-fermion force. Judicious choices of the HMC simulation parameters can prevent them from appearing in dynamical ensembles. One must choose a matrix inverse residue tolerance that is not too small, but small enough to get accurate results. This means increasing the number of Leap-Frog steps to accommodate for any errors introduced with loose residue tolerance. Furthermore, a small lattice spacing is much more preferable to a coarse one as coarse lattices have large variations in the link variables, which gives a wide range over which the gauge links can fluctuate. This will tend to cause the HMC to ‘bump’ into exceptional configurations more frequently, thus lowering the acceptance rate.

The problem of exceptional configurations therefore lies squarely in the quenched

approximation. The reason that we must highlight this effect is because in the quenched approximation, no such Metropolis step exists and the gauge fields are free to evolve as close to, or as far from, the points where $\lambda_k(U) + m = 0$ as the Heat-Bath algorithm dictates. This should come as no surprise as the quenched approximation is really just a pure $SU(3)$ Yang-Mills gauge field evolution algorithm with no fermion mass in sight. That is, of course, until one places a fermion mass in the Dirac operator when calculating correlation functions (and therefore matrix inverses) as we shall see in the next chapter. This is why the ‘buyer must beware’ of the cheapness of the quenched approximation, rather than the more computationally expensive HMC.

CHAPTER 6

Correlation Functions and Propagators

6.1 A Pseudo-scalar Correlation Function

In order to study a 0^{++} scalar state such as the σ meson, we must create a state on the lattice with the same quantum numbers. One such state is $\pi_+\pi_-$, which we can create by inserting a π_+ at $(0, 0)$ and a π_- at $(\vec{x}, 0)$. We then destroy the pions at (\vec{y}, t) and (\vec{z}, t) respectively, and study the decay of its correlation function as a function of time,

$$C_{2\pi}(t) = \langle \Omega | T \{ \hat{\pi}_-(\vec{z}, t) \hat{\pi}_+(\vec{y}, t) \hat{\pi}_-(\vec{x}, 0) \hat{\pi}_+(\vec{0}, 0) \} | \Omega \rangle, \quad (6.1.1)$$

where,

$$\begin{aligned} \hat{\pi}_+^\dagger(\vec{x}, t) &= \bar{u}(\vec{x}, t) \gamma_5 d(\vec{x}, t) = \hat{\pi}_-(\vec{x}, t), \\ \hat{\pi}_-^\dagger(\vec{x}, t) &= \bar{d}(\vec{x}, t) \gamma_5 u(\vec{x}, t) = \hat{\pi}_+(\vec{x}, t). \end{aligned} \quad (6.1.2)$$

The time ordering operator $T\{\dots\}$ arranges the field operators in decreasing temporal value from left to right, i.e., latest to the left. For notational convenience, we now drop the hats on operators and switch to a 4-vector notation with the understanding that the points y and z are located at timeslice $t \geq 0$, and x and 0 are located at $t = 0$. The correlation function expressed in terms of quark operators now reads as,

$$C_{2\pi}(t) = \langle \Omega | T \{ \bar{u}(z) \gamma_5 d(z) \bar{d}(y) \gamma_5 u(y) \bar{d}(x) \gamma_5 u(x) \bar{u}(0) \gamma_5 d(0) \} | \Omega \rangle \quad (6.1.3)$$

If we insert a complete set of intermediate states, labelled by the state n and three-momentum \vec{k} ,

$$\mathbb{I} = \sum_{n, \vec{k}} |n, \vec{k}\rangle \langle n, \vec{k}| \quad (6.1.4)$$

between the operators at $t = 0$ and $t \geq 0$, we can see that the quark operators will have a non-zero overlap with all intermediate momentum states. By Fourier transforming the operators to momentum space, we see explicitly that there will be a contribution from higher energy intermediate states,

$$\sum_{\vec{k}} e^{-i\vec{k}\cdot\vec{x}} \bar{u}(\vec{k}, t) |n, \vec{k}\rangle = \sum_{\vec{k}} e^{-i\vec{k}\cdot\vec{x}} |u, \vec{k}\rangle \quad (6.1.5)$$

The culprit is the sum over \vec{k} . We can sidestep this somewhat by projecting all operators onto zero-momentum states in the hope that this state will have the greatest overlap with the ground state of the system. Indeed, we can project the operators onto any momentum (or set of momenta) that we wish. For the initial calculations in this project, we chose to start with zero-momentum operators, as that is the intuitive choice for a ground state calculation. The Fourier transformed operators projected onto zero-momentum have a simple form,

$$\begin{aligned} \bar{u}(\vec{p}, t) &= \sum_{\vec{x}} e^{-i\vec{p}\cdot\vec{x}} \bar{u}(\vec{x}, t), \\ \Rightarrow \bar{u}(\vec{0}, t) &= \sum_{\vec{x}} \bar{u}(\vec{x}, t), \end{aligned} \quad (6.1.6)$$

hence summing over all spatial lattice sites should give us good overlap with the ground state energy of the system.

Now, in accordance with Wick's theorem¹¹, we must take this time ordered product and contract the operators among themselves to create the normal ordered product with all possible contractions,

$$T\{\psi(x_1)\psi(x_2)\dots\psi(x_n)\} = N\{\psi(x_1)\psi(x_2)\dots\psi(x_n) + \text{all possible contractions}\}. \quad (6.1.7)$$

Wick's theorem is presented in more detail in (3). For a simple example, consider a two-point function,

$$T\{\psi(x_1)\psi(x_2)\} = N\{\psi(x_1)\psi(x_2) + \overline{\psi(x_1)\psi(x_2)}\}, \quad (6.1.8)$$

¹¹see appendix B.3, eqns. B.3.17, B.3.18

the ‘bridge’ notation instructs us to replace the fields with the propagator from x_b to x_a ,

$$\overline{\psi(x_a)\psi(x_b)} \equiv M^{-1}(x_a, x_b). \quad (6.1.9)$$

This very neat theorem tells us how to translate a time ordered product of operators into a product of propagators. The normal ordered term (the term with no ‘bridge’) is ordered such that it produces a 0 when applied to the $|\Omega\rangle$ vacuum state. Any term with uncontracted operators will similarly give 0, leaving only products of propagators.

Due to the fermion nature of the quarks, the operators are Grassman valued and there are some subtleties we must be aware of. For example, we may contract a barred operator only with an unbarred one. This is because a barred operator creates a field quantum, or particle, from the $|\Omega\rangle$ ket, and an unbarred operator destroys that particle at $\langle\Omega|$. If the barred operator is already to the right of the unbarred operator, we need only bring them next to each other, as they will then already be in normal order. Further, because of the Grassman algebra which the operators obey, each time we use the anti-commutation relation to move an operator, a minus sign is picked up, which gives the overall parity of the correlation function value. We therefore restrict the contractions to be between barred and unbarred operators of the same flavour (even though we will impose mass degeneracy between up- and down-type quarks) and we will keep track of the number of minus signs we pick up.

The correlation function (6.1.3) will admit four unique time orderings. That is, there are four unique ways to contract the operators among themselves which preserve the time ordering, yielding four different quark propagator diagrams. Each contraction contributes to the correlation function value so we assign each one a subscript from 0...3. We will go through the explicit calculation of the $C_1(t)$ contraction to highlight the general procedure. Spin and colour indices will be suppressed until they are required.

1. Identify the quark operators we wish to contract,

$$C_1(t) = \langle\Omega|T\{\overline{u}(z)\gamma_5 d(z)\overline{d}(y)\gamma_5 u(y)\overline{d}(x)\gamma_5 u(x)\overline{u}(0)\gamma_5 d(0)\}|\Omega\rangle$$

2. Move the barred operator to the right of the unbarred operator,

$$C_1(t) = \langle \Omega | \overbrace{u(y)\bar{u}(z)}^{(-1)^3} \gamma_5 \underbrace{d(z)\bar{d}(y)}_{(-1)^0} \gamma_5 \underbrace{d(0)\bar{d}(x)}_{(-1)^3} \gamma_5 \overbrace{u(x)\bar{u}(0)}^{(-1)^0} \gamma_5 | \Omega \rangle$$

3. Count the number of minus signs picked up to give the overall parity,

$$(-1)^3(-1)^0(-1)^3(-1)^0 = (-1)^6 = +1$$

4. Fourier transform the operators to zero momentum,

$$C_1(t) = \sum_{\vec{x}, \vec{y}, \vec{z}} \langle \Omega | u(y)\bar{u}(z)\gamma_5 d(z)\bar{d}(y)\gamma_5 d(0)\bar{d}(x)\gamma_5 u(x)\bar{u}(0)\gamma_5 | \Omega \rangle$$

5. Replace the operators with the relevant propagator.

$$C_1(t) = \sum_{\vec{x}, \vec{y}, \vec{z}} \langle \Omega | M^{-1}(y, z)\gamma_5 M^{-1}(z, y)\gamma_5 M^{-1}(0, x)\gamma_5 M^{-1}(x, 0)\gamma_5 | \Omega \rangle \quad (6.1.10)$$

We have dropped the u and d subscripts on the propagators as we may now impose mass degeneracy on the quarks. We can use the correlation function in its current form if we wish, but notice how there are four instances of γ_5 which will require extra operations on the machine during computation. We can remove these γ_5 matrices, now that we have imposed mass degeneracy, by employing γ_5 -conjugation on the propagators. To see how this works, we must reintroduce spin and colour indices to avoid ambiguity in notation,

$$(M^{-1})_{\alpha\beta}^{ab}(x, y) = \gamma_5 [(M^{-1})_{\alpha\beta}^{ab}]^\dagger(y, x)\gamma_5 \quad (6.1.11)$$

This rather messy layout deserves some explanation. The propagator on the left-hand side starts at y and ends at x . The propagator on the right is the hermitian conjugate of a propagator that starts at x and ends at y . The conjugation acts **only** on the spin and colour indices of the propagator, the start and end points are fixed by the above definition. In essence, equation (6.1.11) tells us that if we have the

propagator that starts at x and ends at y , take the hermitian conjugate, then left and right multiply by γ_5 , we will produce the propagator that starts at y and ends at x . Using γ_5 -conjugation on the second and fourth propagators, and reintroducing the spin and colour indices, the $C_1(t)$ correlation function becomes,

$$C_1(t) = \sum_{x,y,z} \langle \Omega | (M^{-1})_{\alpha\beta}^{ab}(y, z) \gamma_5 \gamma_5 [(M^{-1})_{\alpha\beta}^{ab}]^\dagger(y, z) \gamma_5 \gamma_5 (M^{-1})_{\rho\sigma}^{cd}(0, x) \gamma_5 \gamma_5 [(M^{-1})_{\rho\sigma}^{cd}]^\dagger(0, x) \gamma_5 \gamma_5 | \Omega \rangle,$$

whereupon we now recognise that there are two traces over the spin colour indices and the γ_5 products cancel to the identity. We now use the same technique from equation (2.3.7) to extract the ground state energy. We recast the operators at z and y into the Schrödinger picture, Wick rotate to Euclidean time, and insert a complete set of eigenstates labelled by four-momenta k ,

$$\begin{aligned} C_1(\tau) &= \sum_{x,y,z} \sum_k \langle \Omega | e^{\hat{H}\tau} (M^{-1})_{\alpha\beta}^{ab}(y, z) e^{-\hat{H}\tau} e^{\hat{H}\tau} [(M^{-1})_{\alpha\beta}^{ab}]^\dagger(y, z) e^{-\hat{H}\tau} | k \rangle \\ &\quad \times \langle k | (M^{-1})_{\rho\sigma}^{cd}(0, x) [(M^{-1})_{\rho\sigma}^{cd}]^\dagger(0, x) | \Omega \rangle, \\ &= \sum_{x,y,z} \langle \Omega | (M^{-1})_{\alpha\beta}^{ab}(y, z) [(M^{-1})_{\alpha\beta}^{ab}]^\dagger(y, z) | 0 \rangle \\ &\quad \times \langle 0 | (M^{-1})_{\rho\sigma}^{cd}(0, x) [(M^{-1})_{\rho\sigma}^{cd}]^\dagger(0, x) | \Omega \rangle + \text{Excited States}, \end{aligned} \quad (6.1.12a)$$

$$C_1(\tau) = \sum_{x,y,z} \text{Tr} [M^{-1}(y, z) (M^{-1})^\dagger(y, z)] \text{Tr} [M^{-1}(0, x) (M^{-1})^\dagger(0, x)]. \quad (6.1.12b)$$

The quark propagator diagram for the $C_1(t)$ correlation function is shown in figure 6.2. All four contractions and the resulting correlation functions are given below and the corresponding diagrams are given in figures 6.1, 6.2, and 6.3. Note that the product of propagators in $C_3(t)$ and $C_2(t)$ are hermitian conjugate (up to cyclic order) and therefore the traces of both these correlation functions are identical. In practice, this allows us to calculate either one and simply double the result. We could calculate both and make a slight improvement on the error, but the computer

time required does not justify performing the same calculation twice over simply doubling the result from one. Notice also that these two contributions come with an overall minus sign. The correlation function we wish to measure is the sum of these four contributions,

$$C_{sum}(t) = C_0(t) + C_1(t) - 2C_2(t) \quad (6.1.13)$$

Now, looking closely at the sources in the four correlation functions in (6.1.14),

$$C_3(t) = \langle \Omega | T \{ \bar{u}(z) \gamma_5 d(z) \bar{d}(y) \gamma_5 u(y) \bar{d}(x) \gamma_5 u(x) \bar{u}(0) \gamma_5 d(0) \} | \Omega \rangle$$

$$\Rightarrow \lim_{\tau \rightarrow \infty} C_3(\tau) = - \sum_{x,y,z} \text{Tr} [M^{-1}(x,z) (M^{-1})^\dagger(y,z) M^{-1}(y,0) (M^{-1})^\dagger(x,0)] \quad (6.1.14a)$$

$$C_2(t) = \langle \Omega | T \{ \bar{u}(z) \gamma_5 d(z) \bar{d}(y) \gamma_5 u(y) \bar{d}(x) \gamma_5 u(x) \bar{u}(0) \gamma_5 d(0) \} | \Omega \rangle$$

$$\Rightarrow \lim_{\tau \rightarrow \infty} C_2(\tau) = - \sum_{x,y,z} \text{Tr} [M^{-1}(y,z) (M^{-1})^\dagger(x,z) M^{-1}(x,0) (M^{-1})^\dagger(y,0)] \quad (6.1.14b)$$

$$C_1(t) = \langle \Omega | T \{ \bar{u}(z) \gamma_5 d(z) \bar{d}(y) \gamma_5 u(y) \bar{d}(x) \gamma_5 u(x) \bar{u}(0) \gamma_5 d(0) \} | \Omega \rangle$$

$$\Rightarrow \lim_{\tau \rightarrow \infty} C_1(\tau) = \sum_{x,y,z} \text{Tr} [M^{-1}(y,z) (M^{-1})^\dagger(y,z)] \text{Tr} [M^{-1}(0,x) (M^{-1})^\dagger(0,x)] \quad (6.1.14c)$$

$$C_0(t) = \langle \Omega | T \{ \bar{u}(z) \gamma_5 d(z) \bar{d}(y) \gamma_5 u(y) \bar{d}(x) \gamma_5 u(x) \bar{u}(0) \gamma_5 d(0) \} | \Omega \rangle$$

$$\Rightarrow \lim_{\tau \rightarrow \infty} C_0(\tau) = \sum_{x,y,z} \text{Tr} [M^{-1}(x,z) (M^{-1})^\dagger(x,z)] \text{Tr} [M^{-1}(y,0) (M^{-1})^\dagger(y,0)] \quad (6.1.14d)$$

one can see that there are only two sources; one at 0 and one at z . The source at 0 gives rise to what is called a *point-to-all* propagator. The source is fixed at 0 and the sinked to all other points the lattice. The source at z is an *all-to-all* propagator. It has sources at all points on the lattice, but set of sources on a particular time slice τ have sinks only to the same time-slice ($M^{-1}(y,z)$) and to the $\tau = 0$ time slice ($M^{-1}(x,z)$). It is the source at z which takes take up most of the

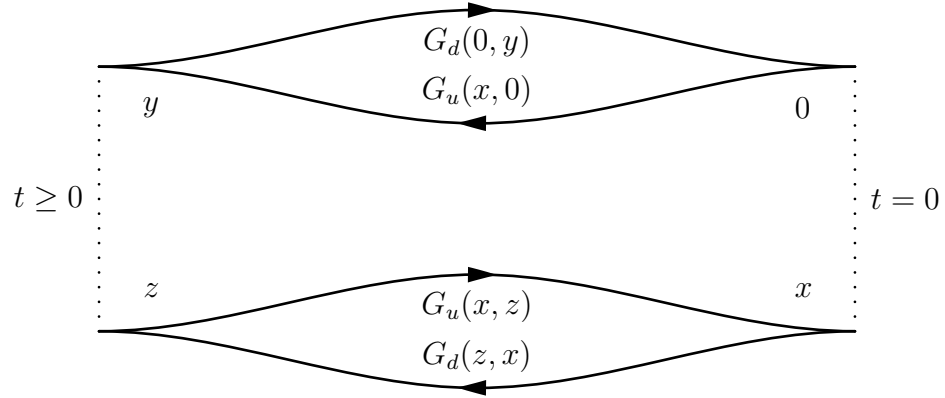


Figure 6.1: Quark propagator diagram for the $C_0(t)$ correlation function.

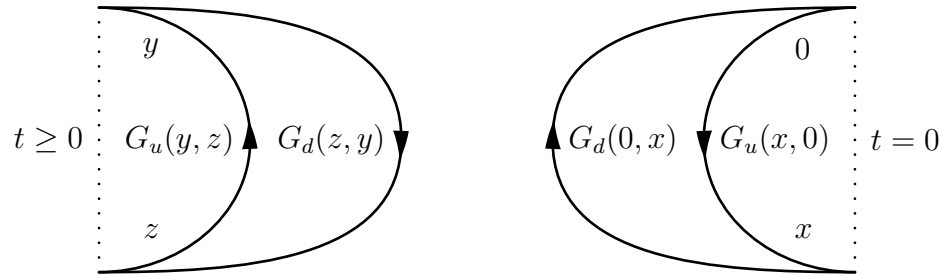


Figure 6.2: Quark propagator diagram for the $C_1(t)$ correlation function.

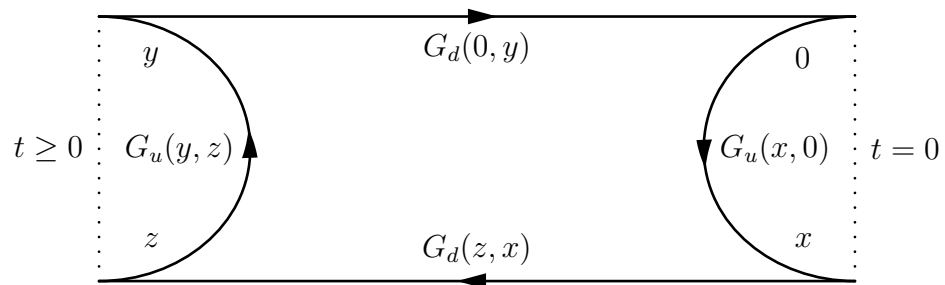


Figure 6.3: Quark propagator diagram for the $C_2(t)$ correlation function.

computational burden and so it is vital that we use techniques that will give us accurate results that are not prohibitively expensive.

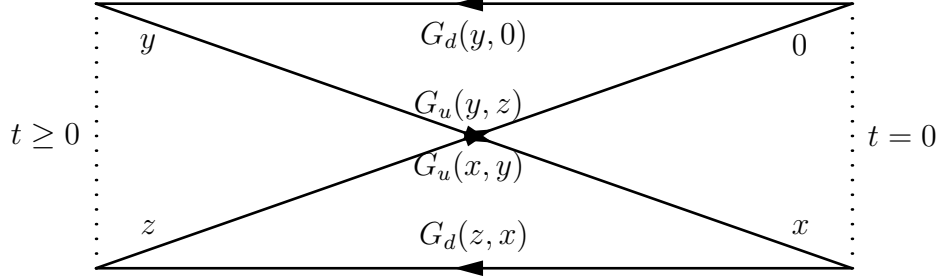


Figure 6.4: Quark propagator diagram for the $C_4(t)$ correlation function.

6.2 Signal to Noise Improvement Strategies

6.2.1 Isospin Projection

The $\pi\pi \rightarrow \pi\pi$ operator of the previous section has sufficient overlap with the $I = 0, 0^{++}$ state to calculate correlation functions in that channel. The positive and negatively charged pions are $|I = 0, I_z = \pm 1\rangle$ states respectively, so the direct product of the $I_z \pm 1$ states naturally has $I_z = 0$.

In order to construct an operator with full overlap of the $I = 0, 0^{++}$ channel one must include the $|I = 0, I_z = 0\rangle$ state in the operator. This corresponds to the neutral pion which has quark content,

$$\hat{\pi}_0^\dagger(\vec{x}, t) = \frac{1}{\sqrt{2}}(\bar{u}(\vec{x}, t)\gamma_5 u(\vec{x}, t) - \bar{d}(\vec{x}, t)\gamma_5 d(\vec{x}, t)). \quad (6.2.1)$$

We must then ascertain how much of each of these operators we must include in the $I = 0, I_z = 0$ operator, which can be easily looked up from Clebsch-Gordan tables. The full operator that constructs an $I = 0$ state at $t = 0$ takes the form,

$$O_{I=0}^\dagger(\vec{x}, t; \vec{y}, t) = \frac{1}{\sqrt{3}}(\hat{\pi}_+^\dagger(\vec{x}, t)\hat{\pi}_-^\dagger(\vec{y}, t) - \hat{\pi}_0^\dagger(\vec{x}, t)\hat{\pi}_0^\dagger(\vec{y}, t) + \hat{\pi}_-^\dagger(\vec{x}, t)\hat{\pi}_+^\dagger(\vec{y}, t)), \quad (6.2.2)$$

and from here one must substitute in the quark operators and perform all possible Wick contraction on the correlation function,

$$C_{I=0}(t) = \langle \Omega | O_{I=0}(\vec{z}, t; \vec{y}, t) O_{I=0}^\dagger(\vec{0}, 0; \vec{x}, 0) | \Omega \rangle. \quad (6.2.3)$$

Thankfully, the many dozens of quark propagator diagrams that are generated from this fearsome correlation function cancel due to the presence of minus signs and $C_{I=0}(t)$ can be expressed in terms of the three quark propagator diagrams already calculated, name the Direct 6.1, Vacuum, 6.2, Box 6.3, and a fourth diagram which is generally given the name Cross, 6.4 whose correlation function we denote as $C_4(t)$. The coefficients for each of these correlation functions is given by,

$$C_{I=0}(t) = 2C_0(t) + 3C_1(t) - 6C_2(t) + C_4(t). \quad (6.2.4)$$

We note here, purely out of interest, that this definition of the $I = 0$ correlation function differs from 6.1.13 (up to an irrelevant overall coefficient of 3) by,

$$C_0(t) \rightarrow \frac{2}{3}C_0(t) + \frac{1}{3}C_4(t), \quad (6.2.5)$$

indicating that provided this new $C_4(t)$ correlation function value does not deviate too wildly from the $C_0(t)$ value, then 6.1.13 does indeed have good overlap with the full $I = 0$ projection. The $C_4(t)$ correlation function requires no extra matrix inversions as it can be constructed from sources at $t = 0$ alone, but some extra burden on the spin-colour trace routines will appear.

6.2.2 Vacuum Expectation Value Removal

The Direct 6.1 and Vacuum 6.2 diagrams are each composed of 2 quark propagator loops. This dictates that we must remove the vacuum expectation value (VEV) from the correlation function to get the truly vacuum disconnected part of the correlation function. For example, the vacuum diagram with gauge averaged $\langle \dots \rangle_U$ correlation function,

$$\langle C_1(t) \rangle_U = \left\langle \sum_{x,y,z} \text{Tr} [M^{-1}(y,z)(M^{-1})^\dagger(y,z)] \text{Tr} [M^{-1}(0,x)(M^{-1})^\dagger(0,x)] \right\rangle_U, \quad (6.2.6)$$

with the VEV removed will evaluate to,

$$\langle C_1(t) \rangle_U \Big|_{VEV} = \left\langle \sum_{x,y,z} (\text{Tr}[M^{-1}(y,z)(M^{-1})^\dagger(y,z)] - \langle \text{Tr}[M^{-1}(y,z)(M^{-1})^\dagger(y,z)] \rangle_U) \right. \\ \left. (\text{Tr}[M^{-1}(0,x)(M^{-1})^\dagger(0,x)] - \langle \text{Tr}[M^{-1}(0,x)(M^{-1})^\dagger(0,x)] \rangle_U) \right\rangle_U. \quad (6.2.7)$$

6.2.3 Fierz Rearrangement

Two distinct mesonic operators creating or destroying states, each the same time slice, are subject to mathematical rearrangement via the Fierz identity,

$$(\bar{u}_1 \Gamma^A u_2)(\bar{u}_3 \Gamma^B u_4) \sum_{C,D} K^{AB}{}_{CD} (\bar{u}_1 \Gamma^C u_4)(\bar{u}_3 \Gamma^D u_2), \quad (6.2.8)$$

where Γ^A are any of the 16 linearly independent Dirac gamma matrix products, $K^{AB}{}_{CD}$ are coefficients set by the completeness relations of Γ^A , and u are fermionic operators. There is also an analogous Fierz relationship for the 8 $SU(3)$ generators which is convolved with the spinorial one shown explicitly here. This greatly complicates the calculation of mesonic correlation functions as one ought to calculate all the relevant operators allowed by Fierz rearrangement to ensure no spurious operator mixing occurs.

Mercifully, one can simply create two hadronic states at t and $t + 1$, and similarly destroy those states at $t + \delta t$ and $t + 1 + \delta t$ respectively, and elegantly sidestep the entire affair of Fierz rearrangement.

6.3 Propagator Construction and Approximation

As shown in the previous section, the task of computing Euclidean correlation functions on the lattice is essentially the task of matrix inversion. For a lattice with spatial dimension L^3 and temporal extent T , the all-to-all propagators are $N \times N$ complex matrices where $N = 3_{col} \times 4_{spin} \times L^3 T$. For a moderate lattice of $L^3 T = 8^3 16$, this corresponds to a real matrix which, when using double precision, is of size 144GB. N will scale with the 4th power of L as $L^3 T = 2L^4$ so a more

realistically sized matrix of $L = 16$ will require over 35TB of memory. Furthermore, this matrix must be inverted over many hundreds of gauge field configurations to accurately approximate the path integral. Evidently, accurate approximations are required.

We shall present here four methods for calculating this inverse. The first is known as the point source method and it is exact. All the information contained in the inverse can be calculated using points sources, though this renders it the most expensive. The second is the stochastic source method which is an approximation. In this case, all of the information is approximated to arbitrary accuracy. The third, more novel method, is to use gauge connected momentum sources. In contrast to the other two methods, only information in the propagator pertaining to particular physical momentum modes is extracted. Given that we want only the information from low momentum modes when we calculate the ground state properties of hadrons on the lattice, this is the method of choice used in this investigation. The fourth is via singular value decomposition and it has some interesting properties in and of itself, as well as being the best possible way of approximating a matrix that obeys γ_5 -hermiticity. As well as being the most optimal way to approximate the full all-to-all propagator, it still approximates all momentum modes and therefore includes unwanted information. For that reason, we delay a full numerical study into singular value decomposition and push on with gauge connected momentum sources.

6.3.1 Point Sources

To illustrate the point source method, consider the all-to-all propagator matrix, which is the inverse of some Dirac operator M . We can write the following equation,

$$M_{\alpha\beta}^{ab}(y, x)\chi_{\beta}^b(x) = \phi_{\alpha}^a(y), \quad (6.3.1)$$

and assert that the vector $\phi_{\alpha}^a(y)$ is equal to $(1, 0, 0, \dots, 0)^{\top}$, i.e.,

$$\phi_{\alpha}^a(y) = \delta(0, a)\delta(0, \alpha)\delta(0, y) = \begin{cases} 1 & \text{if } a, \alpha, y = 0, \\ 0 & \text{otherwise.} \end{cases}$$

That is, we place a unit source at a single space time point, and also zero out 11 of the 12 spin-colour components of the Dirac vector. With this definition of ϕ , we can write down a simple expression for the $a, \alpha, y = 0$ column of the inverse matrix,

$$\chi_\beta^b(x) = (M^{-1})_{\beta\alpha}^{ba}(y, x)\phi_\alpha^a(y), \quad (6.3.2a)$$

$$= (M^{-1})_{\beta 0}^{b0}(0, x), \quad (6.3.2b)$$

i.e., when using a point source in the vector ϕ , the solution vector χ is a single column of the inverse matrix M^{-1} . We therefore must solve the system of linear equations,

$$\begin{pmatrix} M_{00} & \cdots & M_{N0} \\ \vdots & \ddots & \vdots \\ M_{0N} & \cdots & M_{NN} \end{pmatrix} \begin{pmatrix} \chi_0 \\ \vdots \\ \chi_N \end{pmatrix} = \begin{pmatrix} 1 \\ \vdots \\ 0 \end{pmatrix}, \quad (6.3.3)$$

and, if we desire the full inverse matrix M^{-1} , place the point source in ϕ at every possible point in the vector and calculate all the corresponding χ . This, recall, will require $3 \times 4 \times L^3 \times T$ calls to the inverter.

This point source method is an extreme form of dilution. Dilution is a method whereby only a certain sub-volume of a given vector space is populated per inversion. Spin and colour dilution in lattice QCD are so common that they are written in to the routines at such a deep level that the user has no high-level control over it and it is performed as a matter of course¹². Given that quark sources are defined by the direct product of spin, colour, and position space variables, full dilution of all three of these spaces gives the aforementioned $3_{colour} \times 4_{spin} \times (L^3 T)_{spacetime}$ possible point sources. This dilution gives rise to excellent noise suppression and is well documented in (14). The fully diluted propagator takes the form,

$$\sum_c \sum_\gamma \sum_{x_0 \in x} M^{-1}(y, x_0)_{\beta\alpha}^{ba} \delta^{ac} \delta_{\alpha\gamma} = M^{-1}(y, x)_{\beta\gamma}^{bc}$$

Although a rather simple way to calculate the propagator matrix M^{-1} , the

¹²See for example the Columbia Physics System

triple sum over spin, colour, and spacetime gives rise to, for most researchers, a prohibitively large number of inversions and approximations must be made instead.

6.3.2 Stochastic Sources

In what follows, spin and colour indices will be suppressed until necessary. Consider, rather than the point sources in the previous section, a set of column vectors $\eta_i(x)$ that satisfy the following properties,

$$\lim_{N \rightarrow \infty} \frac{1}{N} \sum_{i=0}^{N-1} \eta_i(x) \eta_i^\dagger(y) = \delta(x, y), \quad \lim_{N \rightarrow \infty} \frac{1}{N} \sum_{i=0}^{N-1} \eta_i(x) = 0. \quad (6.3.4)$$

i.e., the N -averaged sum of outer products of these vectors will approach the identity matrix, and the sum of all the elements of any vector (or its conjugate) will sum to zero in the same limit. Now, consider the system of linear equations 6.3.1 with $\phi(x)$ replaced by an $\eta_i(x)$. We solve for $\chi_i(y)$ and take the outer product $\chi_i(y) \eta_i^\dagger(x)$,

$$\chi_i(y) = M^{-1}(y, x) \eta_i(x), \quad (6.3.5)$$

$$\begin{aligned} \frac{1}{N} \sum_{i=0}^{N-1} \chi_i(y) \eta_i^\dagger(z) &= \frac{1}{N} \sum_{i=0}^{N-1} M^{-1}(y, x) \eta_i(x) \eta_i^\dagger(z), \\ \lim_{n \rightarrow \infty} \frac{1}{N} \sum_{i=0}^{N-1} \chi_i(y) \eta_i^\dagger(z) &= M^{-1}(y, z). \end{aligned} \quad (6.3.6)$$

In the last line, we used the property that in the limit of infinite distinct vectors, the sum of projectors $\eta_i(x) \eta_i^\dagger(z)$ approaches the identity. We can introduce the spin and colour components to stochastic sources and use dilution in the same way as was done for point sources. Each stochastic vector is fully spin, color, and time diluted, thereby increasing the number of inversions to $N \times 12 \times T$. One can also partition the lattice space into sub-volumes and partially dilute in position space¹³. Including spin, colour, and temporal dilution regimes, the stochastic all-to-all propagator is

¹³The degree of choice involved in partitioning the spatial lattice is rather large and no definitive dilution regime exists at this time, which might be grounds for a separate study

defined as,

$$\lim_{n \rightarrow \infty} \frac{1}{N} \sum_{i=0}^{N-1} \sum_{t_0=0}^{T-1} \sum_c \sum_{\gamma} \chi_i(\mathbf{y}, t) {}^b_{\beta} \eta_i^{\dagger}(\mathbf{z}, t_0) {}^a_{\alpha} \delta^{ac} \delta_{\alpha\gamma} = M^{-1}(\mathbf{y}, t; \mathbf{z}, t_0) {}^{bc}_{\beta\gamma}, \quad (6.3.7)$$

This result may also be viewed as the arithmetic sum of a set of projection operators acting on M^{-1} , though in this case, the basis set $\eta_i(x)$ is not necessarily orthogonal. The conditions 6.3.4 ensure that each projection contains a component of the target matrix M^{-1} , and that in the arithmetic mean, these components will add constructively. Furthermore, the off-diagonal components of the projectors will add destructively. In the limit of sufficiently large N , the ‘signal’ will outweigh the ‘noise’ and an acceptable approximation to the target matrix can be calculated.

An important point to note is that although one is free to use γ_5 -conjugation 6.1.11 to obtain propagators in the opposite direction, one may not take the trace of the product of propagators (as is done in 6.1.14) that have been calculated using the same set of random vectors as this will introduce bias. Consider the trace of $M^{-1}M^{-1\dagger}$ where both matrices are constructed using the same set of random vectors $\eta_i(x)$,

$$\begin{aligned} \text{Tr}[M^{-1}(M^{-1})^{\dagger}] &= M^{-1}(x, y)M^{-1}(x, y)^{\dagger} \\ &\approx \frac{1}{N^2} \sum_{i,j} M^{-1}(x, y) \underbrace{\eta_i(y)\eta_i^{\dagger}(z)\eta_j(z)\eta_j^{\dagger}(y)}_{\text{off-diags} > 0} (M^{-1}(x, y))^{\dagger}. \end{aligned} \quad (6.3.8)$$

The bias comes from the fact that the off diagonal terms in the square of an approximation to the identity matrix will always be positive. The solution is to use a different set of random vectors $\xi(x)$ for the other propagator,

$$\begin{aligned} \text{Tr}[M^{-1}(M^{-1})^{\dagger}] &= M^{-1}(x, y)(M^{-1}(y, x))^{\dagger} \\ &\approx \frac{1}{N^2} M^{-1}(x, y) \underbrace{\eta_i(y)\eta_i^{\dagger}(z)\xi_j(z)\xi_j^{\dagger}(y)}_{\text{off-diags} \approx 0} (M^{-1}(x, y))^{\dagger}. \end{aligned}$$

Indeed, for every propagator in a given quark diagram, independent sources must be used in their calculation.

The natural question to ask is this: how many random vectors are required for an accurate approximation to the propagator M^{-1} ? We attempted to answer this question by calculating correlation functions for small lattices with both point sources and stochastic sources and looking for convergence of the two as a function of N and under different dilution scheme. We found that an unacceptable number of inversions were required to arrive at an answer in reasonable time. As such, a new technique was devised, based on the momentum source method.

6.3.3 Momentum Sources

Recall that one can think of the summands of the stochastic propagator as vectors in a high dimensional space, each of which has a component that lies along M^{-1} , and a component that is orthogonal with the set of outer products $\eta(\vec{x})\eta^\dagger(\vec{y})$ acting as projection operators. Can one construct a better source type and project M^{-1} along a more desirable direction? Consider plane waves of momentum \mathbf{p} ,

$$\begin{aligned} \rho_{\mathbf{p}}(\mathbf{x}) &= e^{-i\mathbf{p}\cdot\mathbf{x}}. \\ \frac{1}{V_p} \sum_{\mathbf{p}} \rho_{\mathbf{p}}(\mathbf{x})\rho_{\mathbf{p}}^\dagger(\mathbf{y}) &= \frac{1}{V_p} \sum_{\mathbf{p}} e^{-i\mathbf{p}\cdot(\mathbf{x}-\mathbf{y})} = \delta(\mathbf{x}, \mathbf{y}) \end{aligned} \quad (6.3.9)$$

$$\sum_{\mathbf{p}} \rho_{\mathbf{p}}(\mathbf{x}) = 0 \quad (6.3.10)$$

Notice that when consider 3-momentum modes, we need only consider values on a particular time slice. V_p is the volume of the reciprocal lattice. We proceed by inverting $M(\mathbf{x}, t_0; \mathbf{y}, t)\chi(\mathbf{y}, t) = \rho_{\mathbf{p}}(\mathbf{x}, t_0)$ over all momentum modes \mathbf{p}

$$\begin{aligned} \frac{1}{V_q} \sum_{\mathbf{p} \in q} \phi_{\mathbf{p}}(\mathbf{y}, t)\rho_{\mathbf{p}}^\dagger(\mathbf{z}, t_0) &= \frac{1}{V_q} \sum_{\mathbf{p}} M^{-1}(\mathbf{y}, t; \mathbf{x}, t_0)\rho_{\mathbf{p}}(\mathbf{x}, t_0)\rho_{\mathbf{p}}^\dagger(\mathbf{z}, t_0) \\ &= M^{-1}(\mathbf{y}, t, \mathbf{z}, t_0). \end{aligned} \quad (6.3.11)$$

The complete set of momentum modes \mathbf{p} at each time slice form a complete basis for the propagator matrix, hence we recover the full propagator after inverting over all L^3T momentum modes. Momentum sources are, therefore, just as inefficient as point sources. It is tempting to assert that one can invert only over some subset \mathbf{q} of

the momentum modes and project the full propagator onto the that desired subset, but this cannot be done in a gauge covariant fashion. As such, all previous studies involving momentum sources have come hand-in-hand with gauge fixing in an attempt to ameliorate the effects of the extra gauge noise introduced. This approach does work, but is presented in the literature *ad hoc* with little rigorous justification. Furthermore, the canonical momentum modes in 6.3.11 have no gauge field information associated with them, so they cannot be the physical momentum modes of the $SU(3)$ non abelian gauge theory of QCD. We present next a prescription for constructing physical, gauge connected momentum modes $\tilde{\mathbf{p}}$ along with mathematical justification for gauge fixing.

6.3.4 Truncated Singular Value Decomposition

One way of decomposing a matrix is in terms of its Singular Value Decomposition (SVD)¹⁴. The singular values σ_l are non-negative, real numbers and the right and left singular vectors ν_l and μ_l obey the following relations,

$$M(y, x)\nu_l(x) = \sigma_l\mu_l(y), \quad (6.3.12)$$

$$M^\dagger(y, x)\mu_l(x) = \sigma_l\nu_l(y). \quad (6.3.13)$$

One can express the matrix M in terms of the diagonal matrix of singular values Σ and the unitary matrices V and U which are composed of the column vectors ν_l and μ_l respectively,

$$M(y, x) = U(y)\Sigma V^\dagger(x), \quad (6.3.14)$$

from which the inverse is,

$$M^{-1}(y, x) = V(x)\Sigma^{-1}U^\dagger(y). \quad (6.3.15)$$

The matrices U and V are composed of orthonormal basis vectors μ_l and ν_l . In the general case of an arbitrary complex matrix, there is no analytic relation between

¹⁴In the literature (especially computer science and data analysis) SVD is known as principal component analysis

U and V , but due to the γ_5 hermiticity of the Dirac matrix M ,

$$M(y, x) = \gamma_5 M^\dagger(x, y) \gamma_5, \quad (6.3.16)$$

we can discern a very simple relation between ν_l and μ_l using the above property on 6.3.12 and 6.3.13,

$$\begin{aligned} M(y, x) \nu_l(x) &= \sigma_l \mu_l(y) \\ \gamma_5 M^\dagger(x; y) \gamma_5 \nu_l(x) &= \sigma_l \mu_l(y), \\ M^\dagger(x, y) \gamma_5 \nu_l(x) &= \sigma_l \gamma_5 \mu_l(y), \\ \Rightarrow \gamma_5 \nu_l(x) &= \mu_l(x) \quad \text{and} \quad \gamma_5 \mu_l(x) = \nu_l(x), \end{aligned} \quad (6.3.17)$$

from which we make the simple identification,

$$\begin{aligned} M^{-1}(y, x) &= V(x) \Sigma^{-1} V^\dagger(y) \gamma_5 \\ &= \gamma_5 U(x) \Sigma^{-1} U^\dagger(y). \end{aligned} \quad (6.3.18)$$

Due to γ_5 -hermiticity, one can completely describe the propagator exclusively in terms of either $V(x)$ or $U(x)$. This affords us a speedy method for identifying the right singular vectors. To do this¹⁵ we find the *eigenpairs* of the manifestly hermitian matrix $\gamma_5 M(y, x)$. Left multiplying 6.3.12 with γ_5 reveals that,

$$\gamma_5 M(y; x) \nu_l(x) = \sigma_l \gamma_5 \mu_l(y) = \sigma_l \nu_l(y), \quad (6.3.19)$$

so the right singular vectors of values of $M(y, x)$ form the eigenpairs of $\gamma_5 M(y, x)$.

Also, 6.3.17 tells us that the right and left singular vectors of $M(y, x)$ are also the right and left singular vectors of γ_5 , each of which are degenerate with a singular value of unity, which afford us the identities,

$$\gamma_5 = U \mathbb{I} V^\dagger = V \mathbb{I} U^\dagger. \quad (6.3.20)$$

¹⁵One could also find the eigenvalues of $M^\dagger M$ and take the positive square root of the corresponding eigenvalues to get the right singular pair ν_l and σ_l , but the matrix product $M^\dagger M$ has a worse condition number than $\gamma_5 M$.

and,

$$\mathbb{I} = V^\dagger \gamma_5 U = U \gamma_5 V^\dagger. \quad (6.3.21)$$

By equating the eigen-decomposition,

$$M^{-1}(y; x) = \sum_k \frac{\rho_k(x) \eta_k(y)}{\lambda_k} = R \Lambda^{-1} L, \quad (6.3.22)$$

and 6.3.15 we can define an approximation of M^{-1} defined over the entire eigenspace from a truncation in singular values. We denote the approximation to a matrix with a tilde and a truncated matrix with subscript t ,

$$\begin{aligned} R(y) \Lambda^{-1} L(x) &= V(y) \Sigma^{-1} U^\dagger(x), \\ \Rightarrow \widetilde{M}^{-1}(y, x) &= \widetilde{L}(y) \widetilde{\Lambda}^{-1} \widetilde{R}(x) = V_t(y) \Sigma_t^{-1} U_t^\dagger(x). \end{aligned} \quad (6.3.23)$$

The truncated matrices U_t and V_t^\dagger (and the full ones) span separate subspaces with basis vectors μ_l and ν_l for $l \leq t$ where t is the rank of the truncated SVD matrices. Provided that enough of the low singular values are included in the truncation, a good approximation to the full eigenvector expansion 6.3.22 (and thence the full propagator matrix) can be obtained.

A robust definition of how well one matrix approximates another is via the Frobenius norm or $L_{2,2}$ norm,

$$\|M - M_t\|_2 \equiv \sqrt{\sum_a \sum_b |(M - M_t)_{ab}|^2} \quad (6.3.24)$$

which is the natural matrix extension of the Euclidean vector norm. However, one clearly cannot measure this value for all matrices $M(y; x)$ in a lattice QCD calculation. A conservative way of ensuring that the Frobenius norm is kept acceptably low is to treat the spectrum of inverse singular values σ_l^{-1} as a probability density function. One then asserts that to achieve a good approximation, one must include some fraction (95% would give a 3σ C.L.) of the PDF in the SVD truncation, which in turn defines t .

6.3.5 Correlation Functions Using S.V.D Propagators

Due to the fact that the propagator is constructed from a lower rank matrix generated from the vectors $\nu_t = \gamma_5 \mu_t$ and real numbers σ_t , one can construct correlation functions directly from this data without having to first construct and store the tensor product $\widetilde{M}^{-1}(y; x) = U_t(x) \Sigma^{-1} V_t^\dagger$. Consider first the gauge averaged $\langle \dots \rangle_U$ correlation function for a single pseudoscalar π with degenerate quark masses, created at t_0 and destroyed at t ,

$$C_\pi(t) = \left\langle \text{ReTr} \left(M^{-1}(\mathbf{y}, t; \mathbf{x}, t_0) \gamma_5 M^{-1}(\mathbf{x}, t_0; \mathbf{y}, t) \gamma_5 \right) \right\rangle_U. \quad (6.3.25)$$

by substituting 6.3.15 we see that,

$$C_\pi(t) = \left\langle \text{ReTr} \left(U(\mathbf{y}, t) \Sigma^{-1} U^\dagger(\mathbf{x}, t_0) U(\mathbf{x}, t_0) \Sigma^{-1} U^\dagger(\mathbf{y}, t) \right) \right\rangle_U \quad (6.3.26)$$

This rather neat result tells us that the correlation function can be calculated directly from the matrices U and Σ ¹⁶ by performing the matrix products of those portions of the singular vectors pertaining to the source and sink times t_0 and t respectively. Furthermore, we know that we can truncate the matrix Σ^{-2} at some point and capture most of the relevant information of the matrix M . More complicated correlation functions can be constructed in much the same manner. This means that the process of using an iterative matrix inverter such as bi-conjugate gradient stabilised to calculate the full rank inverse, then performing full rank matrix multiplications to acquire the real trace for Fourier transformation, can be replaced by using an eigen-solver on the matrix $\gamma_5 M$ to find the t lowest singular value pairs, then performing rank t matrix multiplications to acquire an approximation to the real trace. Indeed, the Eckart-Young-Mirsky theorem of low rank matrix approximations (15) proves unequivocally that the t truncated SVD of a matrix M is the best possible approximation of M at rank t , therefore utilising SVD in the construction of propagators (at least for γ_5 hermitian propagators) would be the optimal choice.

¹⁶Or equivalently V and Σ using $\gamma_5 \gamma_5$ insertions.

CHAPTER 7

High Frequency Decoupling and Gauge Fixing

7.1 Smearing

7.1.1 Source Smearing

Point sources in position space are highly localised, which makes them plane waves in momentum space. Each momentum mode therefore is equally populated, which gives rise to severe contamination from high momentum modes. By ‘smearing’ the point source to give it a Gaussian structure, the higher momentum modes are truncated with a natural Gaussian weighting. We ‘smear’ the position space point source with a gauge covariant operator, which gives the fermion field a Gaussian profile. By defining a gauge covariant differential operator,

$$\tilde{\Delta}^{ab}(\mathbf{x}, \mathbf{y}) = \sum_{n=1}^3 [U_n^{ab}(\mathbf{x})\delta_{\mathbf{x}+\hat{n},\mathbf{y}} + U_n^{ab\dagger}(\mathbf{x}-\hat{n})\delta_{\mathbf{x}-\hat{n},\mathbf{y}} - 2\delta^{a,b}\delta_{\mathbf{x},\mathbf{y}}],$$

and in turn defining a smearing kernel S ,

$$S^{ab}(\mathbf{x}, \mathbf{y}) = \delta_{\mathbf{x},\mathbf{y}}\delta^{a,b} + \frac{\omega^2}{4N}\tilde{\Delta}^{ab}(\mathbf{x}, \mathbf{y}), \quad (7.1.1)$$

we can, by successive application of S to a position space point source,

$$S^{ab}(\mathbf{x}, \mathbf{y})^N \delta_\alpha^b(\mathbf{y}, x_0) = \psi_\alpha^a(\mathbf{x}),$$

create a Gaussian shaped profile $\psi_\alpha^a(\mathbf{x})$ from the point source. This Gaussian profile in position space carries over to momentum space, and thence truncates the high momentum modes. Figure 7.1 shows a slice of such a Gaussian profile, which was constructed smearing a point source at lattice point $(\mathbf{x}, t) = (7, 7, 7, 0)$ where only the $\alpha = a = 0$ spin-colour entry was populated. The z -axis values are the norm of the complex 12-dimensional spin-colour vector associated with each point in that plane. The values of N and ω are chosen to give the desired value of κ (see

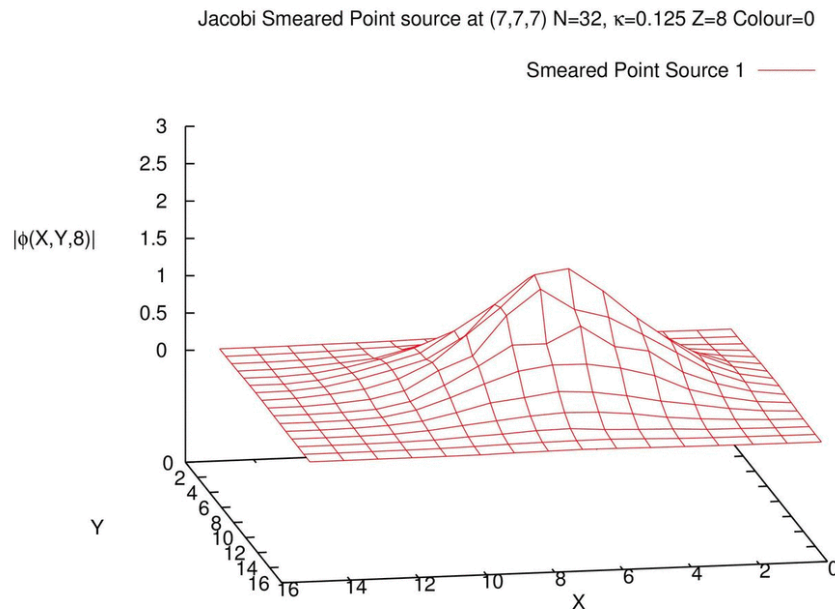


Figure 7.1: Gaussian profile of a covariantly smeared point source.

subsection 5.2.1). One could form an all-to-all propagator using the point source method and smearing each point, thereby improving the signal to noise ratio of the ground state over the excited states. Indeed, one can apply the smearing operator to stochastic sources and arrive at a good approximation with the high momentum modes similarly suppressed.

Not yet seen in the literature is a calculation where the smearing operator is applied to a momentum source. We have found that by taking a zero momentum source and then applying the smearing operator, an all-to-all propagator is formed which gives rise to correlation function values (after gauge fixing) that have remarkably good signal to noise ratios and produce effective mass plateaux with very little excited state contamination. This is not surprising given the mechanism by through which the smearing operator suppresses excited states.

Consider N successive applications of the smearing kernel 7.1.1 with $\omega = 2$.

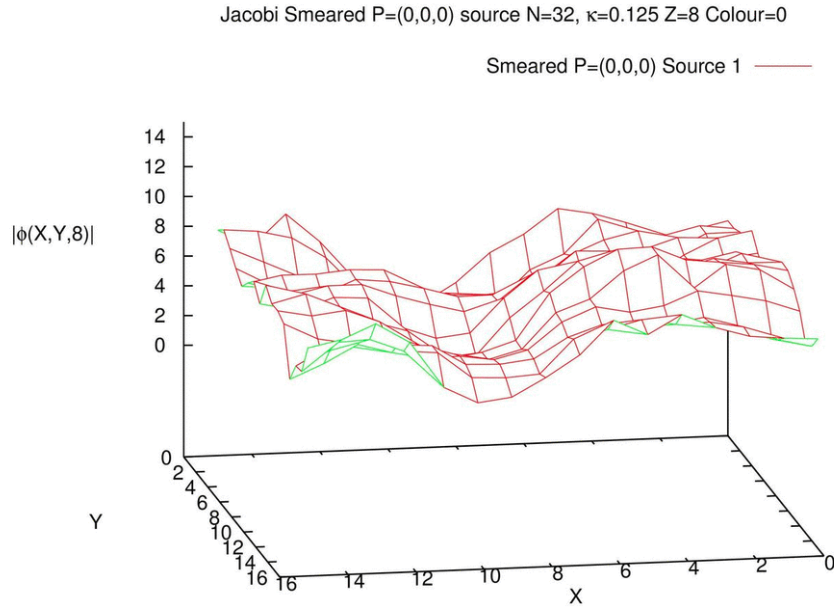


Figure 7.2: A covariantly smeared $\mathbf{p} = (0, 0, 0)$ momentum source.

For sufficiently large N , we can approximate the exponential,

$$\lim_{N \gg 1} S^{ab}(\mathbf{x}, \mathbf{y})^N \approx \exp(\tilde{\Delta}). \quad (7.1.2)$$

If we switch to continuum language and suppress colour indices, we see that we can write $\tilde{\Delta}$ in terms of the gauge covariant differential operator,

$$\begin{aligned} \tilde{\Delta} &= (\partial_i + iA_i(\mathbf{x}))(\partial_i + iA_i(\mathbf{x})) \\ &= (\partial^2 + i(\partial_i A_i(\mathbf{x})) + iA_i(\mathbf{x})\partial_i + iA_i(\mathbf{x})\partial_i - A^2(\mathbf{x})). \end{aligned} \quad (7.1.3)$$

Consider now the operator acting on plane wave $\psi(\mathbf{x}) = \exp(i\mathbf{p} \cdot \mathbf{x})$ of momentum

\mathbf{p} which will give,

$$\begin{aligned}
\exp(\tilde{\Delta}) \exp(i\mathbf{p} \cdot \mathbf{x}) &= \exp\left(\partial_i^2 + i(\partial_i A_i(\mathbf{x})) + i2A_i(\mathbf{x})\partial_i - A^2(\mathbf{x})\right) \exp(i\mathbf{p} \cdot \mathbf{x}) \\
&= \exp\left(-\mathbf{p}^2 + i(\partial_i A_i(\mathbf{x})) - 2A_i(\mathbf{x})p_i - A^2(\mathbf{x})\right) \exp(i\mathbf{p} \cdot \mathbf{x}) \\
&= \exp\left(-(p_i + A_i(\mathbf{x}))(p_i + A_i(\mathbf{x})) + i\partial_i A_i(\mathbf{x})\right) \exp(i\mathbf{p} \cdot \mathbf{x}).
\end{aligned} \tag{7.1.4}$$

In the last line we used the fact that $A_i(\mathbf{x})$ commutes with \mathbf{p} as the momentum appearing in the plane wave function is not an operator. This gives, in terms of the gauge connected momentum modes $\tilde{\mathbf{p}}_i = \mathbf{p}_i + A_i(\mathbf{x})$,

$$\exp(\tilde{\Delta}) \exp(i\mathbf{p} \cdot \mathbf{x}) = \exp(i\partial_i A_i(\mathbf{x})) \exp(-\tilde{\mathbf{p}}^2) \exp(i\mathbf{p} \cdot \mathbf{x}). \tag{7.1.5}$$

i.e., our source function is naturally weighted by the size of the square of the physical momentum mode $|\tilde{\mathbf{p}}(\mathbf{x})|^2$ with the addition of a local $SU(3)$ phase factor.

This continuum analysis carries over to the lattice too. Applying the smearing kernel S to a momentum mode (again, suppressing colour indices) gives,

$$\begin{aligned}
S(\mathbf{x}, \mathbf{y}) \exp(i\mathbf{p} \cdot \mathbf{y}) &= e^{i\mathbf{p} \cdot \mathbf{x}} + \frac{1}{N} \left[\sum_i \left(U_i(\mathbf{x}) e^{i\mathbf{p} \cdot (\mathbf{x} + \hat{i})} + U_i^\dagger(\mathbf{x} - \hat{i}) e^{i\mathbf{p} \cdot (\mathbf{x} - \hat{i})} - 2e^{i\mathbf{p} \cdot \mathbf{x}} \right) \right], \\
&= \left(\mathbb{I} + \frac{1}{N} \left[\sum_i \exp(ia(p_i + A_i(\mathbf{x}))) + \exp(-ia(p_i + A_i(\mathbf{x} - \hat{i}))) - 2\mathbb{I} \right] \right) e^{i\mathbf{p} \cdot \mathbf{x}}.
\end{aligned} \tag{7.1.6}$$

We express the gauge field derivative in discrete lattice units $a\Delta A_i(\mathbf{x}) = A_i(\mathbf{x}) - A_i(\mathbf{x} - \hat{i})$ and use the definition of gauge connected momenta,

$$S(\mathbf{x}, \mathbf{y}) \exp(i\mathbf{p} \cdot \mathbf{y}) = \left(\mathbb{I} + \frac{1}{N} \left[\sum_i \exp(ia\tilde{p}_i) + \exp(-ia\tilde{p}_i) \exp(ia^2\Delta A_i(\mathbf{x})) - 2\mathbb{I} \right] \right) e^{i\mathbf{p} \cdot \mathbf{x}}. \tag{7.1.7}$$

We now see that in the limit of $a \rightarrow 0$, $\Delta A_i(\mathbf{x}) \rightarrow \partial A_i(\mathbf{x}) = 0$ and if we gauge fix to Coulomb gauge $\partial A_i(\mathbf{x}) = 0$ the phase term involving will be sent to unity¹⁷. Let

¹⁷Of course on the lattice, when the gauge fixing is applies, it is the discrete differential $\Delta A_i(\mathbf{x})$ that is made to vanish, regardless of the lattice spacing

us now assert that we have fixed to Coulomb gauge fixed and expand to first order,

$$\begin{aligned}
S \exp(i\mathbf{p} \cdot \mathbf{x}) &= \left(\mathbb{I} + \frac{1}{N} \left[\sum_i \exp(ia\tilde{p}_i) + \exp(-ia\tilde{p}_i) - 2\mathbb{I} \right] \right) e^{i\mathbf{p} \cdot \mathbf{x}}, \\
&= \left(\mathbb{I} + \frac{1}{N} \left[\sum_i 2 \cos(a\tilde{p}_i) - 2\mathbb{I} \right] \right) e^{i\mathbf{p} \cdot \mathbf{x}}, \\
&= \left(\mathbb{I} - \frac{1}{N} (a^2 \tilde{\mathbf{p}}^2 + \mathcal{O}(a^4)) \right) e^{i\mathbf{p} \cdot \mathbf{x}}. \tag{7.1.8}
\end{aligned}$$

Repeated application of the smearing kernel N times and ignoring terms of order a^4 will give us the same result that we derived in the continuum, without the phase term,

$$\begin{aligned}
S^N \exp(i\mathbf{p} \cdot \mathbf{x}) &\approx \left(\mathbb{I} - \frac{1}{N} a^2 \tilde{\mathbf{p}}^2 \right)^N e^{i\mathbf{p} \cdot \mathbf{x}}, \\
&\approx \exp(-a^2 \tilde{\mathbf{p}}^2) \exp(i\mathbf{p} \cdot \mathbf{x}). \tag{7.1.9}
\end{aligned}$$

In figure 7.2, we see the profile of the smeared momentum source with the same conditions as the point source in figure 7.1. The profile is smoothly varying over the x - y plane, and indeed the same smooth behaviour is observed over the x - z and z - y planes. We can also express 7.1.9 purely in terms of gauge connected momenta,

$$\begin{aligned}
S^N \exp(i\mathbf{p} \cdot \mathbf{x}) &\approx \exp(-a^2 \tilde{\mathbf{p}}^2) \exp(i\tilde{\mathbf{p}} - A(\mathbf{x})) \cdot \mathbf{x}), \\
&\approx \exp(-A(\mathbf{x}) \cdot \mathbf{x}) \exp(-a^2 \tilde{\mathbf{p}}^2) \exp(i\tilde{\mathbf{p}} \cdot \mathbf{x}), \tag{7.1.10}
\end{aligned}$$

which shows explicitly that in order to construct high frequency suppressed, gauge connected momentum sources on the lattice, one must transform to a gauge where $\partial_i A_i(\mathbf{x}) = 0$ and $A_i(\mathbf{x})x_i = 0$ are simultaneously satisfied. This leads to the condi-

tion,

$$\begin{aligned}
\partial_j(A_i(\mathbf{x})x_i) &= (\partial_j A_j(\mathbf{x}))x_i + A_i(\mathbf{x})\delta_{ij}, \\
&= A_j(\mathbf{x}), \\
&= 0.
\end{aligned}
\tag{7.1.11}$$

which can be satisfied only in a free field theory.

7.1.2 Sink Smearing

Smearing the sources allows us to decouple the sources from high momentum modes and we can do exactly the same at the sinks. In the context of figure 6.3, we would be placing a smeared zero momentum source at both 0 and Z , thus projecting the pion wave functions at those points to zero momentum. The pions at X and Y are sinks and we have no control over the profile of the fermion wave functions there (that is governed by the dynamics of QCD). We can, however, smear those sinks so that whatever the profile is, it is decoupled from the unphysical high momentum modes and we can then project the sink onto any desired momentum using Fourier transformation. Because we use sources that are assumed to couple very strongly to the zero momentum mode, we may omit them from the Fourier transform concentrate on the spatial sink indices at X and Y ; a 6D transformation.

By using point or stochastic sources, we produce a source at Z that couples significantly to non-zero momentum modes and we are then forced to include that spatial point in the Fourier transformation, which is then 9D. This then becomes a computational obstacle as even a modest lattice of size $L = 16$ requires an array of size $2 \times 8 \times 16^9 = 16^{10}$ bytes, which is over a Terabyte of RAM (2 from the complex nature of the array elements and 8 bytes for double precision float) On the other hand, a 6D transform requires only 16^7 bytes, which is only 250MB.

7.1.3 Link Smearing

The general idea behind link smearing is to take a link variable $U_\mu(x)$ and use the surrounding links to generate a new link that respects continuity of the gauge field. Link variables that deviate from neighbouring links in a coarse manner can

introduce noise in the calculation of correlation function values. Even worse, high frequency gluon modes, represented by link variables that are far from the identity on the $SU(3)$ manifold, can enhance excited fermion state contamination when forming an operator. For example, the clover term that appears in the action 4.5.7 and the gauge links in the smearing operator 7.1.1 can affect the action associated with the fermion sources on which they act. Many such procedures to ameliorate this effect exist, namely APE smearing (16), stout smearing (17) and HEX smearing (18) which is a combination of the two. APE smearing code was available to us, but it contains a projection step back to $SU(3)$ in the process which may or may not introduce nonphysical effects. We therefore opted to construct stout smearing code for this study.

Consider a link variable $U_\mu(x)$ and the associated, so called ‘staples’ of links,

$$C_\mu(x) = \sum_{\nu \neq \mu} \rho_{\mu\nu} \left(U_\nu(x) U_\mu(x + \hat{\nu}) U_\nu^\dagger(x + \hat{\mu}) + U_\nu^\dagger(x - \hat{\nu}) U_\mu(x - \hat{\nu}) U_\nu(x - \hat{\nu} + \hat{\mu}) \right), \quad (7.1.12)$$

where $\hat{\mu}, \hat{\nu}$ are unit vectors in the μ, ν directions respectively. The coefficients $\rho_{\mu\nu}$ are parameters that can be tuned, but are usually set to $\rho_{\mu\nu} = \text{diag}(0, 1, 1, 1)$ with the temporal coordinate set to zero. By defining the manifestly traceless, hermitian matrix $Q_\mu(x)$ as,

$$Q_\mu(x) = \frac{1}{2}(\Omega_\mu^\dagger(x) - \Omega_\mu(x)) - \frac{i}{6}\text{Tr}(\Omega_\mu^\dagger(x) - \Omega_\mu(x)) \quad (7.1.13)$$

where,

$$\Omega_\mu(x) = (C(x)U^\dagger(x))_\mu, \quad (7.1.14)$$

one can define a new link variable,

$$U_\mu^{(n+1)}(x) = \exp(iQ_\mu(x))U_\mu^{(n)}(x) \quad (7.1.15)$$

that is an element of $SU(3)$, without the need for a projection step back down to $SU(3)$. This process can be iterated indefinitely, always keeping the new links on the $SU(3)$ manifold.

7.2 Gauge Fixing

An unfortunate problem that comes with using momentum sources is that they are not gauge invariant, as is made patently clear by the presence of the phase term in 7.1.7. However, we can completely eliminate this phase term by applying the Coulomb gauge fixing condition,

$$\partial_i A_i(x) = 0 \quad \text{for } i = 1, 2, 3. \quad (7.2.1)$$

In the continuum, this can be achieved by minimising the gauge functional.

$$\mathcal{F}[A(\mathbf{x})] \equiv \int dx \text{Tr}(A_i^a(\mathbf{x})\tau^a A_i^b(\mathbf{x})\tau^b), \quad (7.2.2)$$

which translates to maximising the lattice functional,

$$\mathcal{F}[U_\mu(\mathbf{x})] \equiv \sum_{\mathbf{x}, i < j} \text{Tr}(U_{ij}(\mathbf{x})), \quad (7.2.3)$$

independently at each time slice, where (in analogy with 4.4.6)

$$U_{ij}(\mathbf{x}) = U_i(\mathbf{x})U_j(\mathbf{x} + \hat{i})U_i^\dagger(\mathbf{x} + \hat{j})U_j^\dagger(\mathbf{x}). \quad (7.2.4)$$

The gauge fixing condition is a global condition, but clearly, if 7.2.3 is maximised at each time slice, then a global maximum is achieved.

An even further problem associated with gauge fixing is the presence of Gribov copies, a phenomenon first noted in 1978 when V.N. Gribov attempted to set out rules for quantising a non-Abelian Gauge theory (19). The conditions required for the presence of a Gribov copy are as follows. It what follows, dependence of spacetime as assumed and therefore suppressed in the notation. Consider two gauge fields A_μ^a and A'_μ connected by a locally defined gauge transformation,

$$A'_\mu = U A_\mu U^\dagger + \frac{i}{g}(\partial_\mu U)U^\dagger \quad (7.2.5)$$

Further consider that these two gauge fields satisfy a gauge fixing condition, $\partial_\mu A_\mu =$

$\partial_\mu A'_\mu = 0$. Application of the differential operator to 7.2.5 gives,

$$\partial_\mu A'_\mu = \partial_\mu U A_\mu U^\dagger + U A_\mu (\partial_\mu U^\dagger) + \frac{i}{g} [(\partial_\mu^2 U) U^\dagger + (\partial_\mu U)(\partial_\mu U^\dagger)] = 0. \quad (7.2.6)$$

Defining the gauge transformations as infinitesimal $U = \mathbb{I} + \alpha$ we see that,

$$\partial_\mu (\partial_\mu \alpha + ig[\alpha, A_\mu]) = 0. \quad (7.2.7)$$

We can recognise here the gauge covariant differential operator $D_\mu = \partial_\mu + igA_\mu$ which further tells us that,

$$\partial_\mu D_\mu \alpha = 0. \quad (7.2.8)$$

When we apply a transverse gauge condition such as Coulomb gauge $\partial_i A_i$ then the spatial part of the operator $\partial_\mu D_\mu$ becomes hermitian and the null space (kernel) is given by $\partial_i \psi$. These constant eigenvectors are not fixed by the gauge fixing condition and Gribov copies appear in the space orthogonal to the null space. In other words, the gauge fixing condition allows for multiple gauge field configurations that wholly exist outside of the null space, so the gauge fixing condition does not uniquely define the gauge.

In many instances, the literature will assert that, after gauge fixing, the noise induced from these Gribov copies is much smaller than the statistical noise associated with calculations of observable quantities (20, 21, 22). An analytical study (23) and an $SU(3)$ lattice study from 1993 (24) shed some light on the matter in general, as does (25), but definitive data is still lacking. A specific study (26) in the Coulomb gauge agrees that noise can be low, but suggests that on larger lattices it may become significant. With this in mind, we extended the method outlined in (24) for measuring both the density of Gribov copies present in a given gauge ensemble, and also ratio of copies to the Fundamental Modular Region. We also performed our preliminary quenched calculations on both gauge fixed and non-gauge fixed ensembles in an attempt to see how much noise is induced by omitting gauge fixing. Some calculations (27, 28) report that results can be obtained without gauge

fixing, so may see how much noise is suppressed by the gauge fixing procedure.

7.2.1 Gribov Density

The Fundamental Modular Region (FMR) of a gauge field is that configuration where the global gauge fixing condition is maximised globally. For example, if we were to take the Coulomb gauge fixing condition 7.2.1 as the defining condition, and we were to apply some gauge fixing routine after performing a gauge rotation, we would find several different values of link trace maximum. It is accepted that the configurations associated with the global maximum (or maximal value) are those which lie in the FMR. If after some significant number of iterations of gauge rotation and subsequent gauge fixing one sees a certain maximal value appear multiple times, one can be assured to a confidence level that one has identified the FMR.

The study undertaken as part of this thesis took a number of pure $SU(3)$ Yang-Mills (quenched) ensembles, catalogued in table (lattice table) and performed the following steps in order to identify the FMR for a given time slice:

- apply a gauge fixing algorithm to a gauge configuration, identify the link trace 7.2.3
- reload the lattice and apply a gauge field transformation parameterized by an angle $\frac{2\pi n}{N}$ where n is rotation number and N is the total number of gauge fixing attempts to be performed. Identify the new plaquette trace.
- continue until $(N - 1)$ rotations have been performed.

In order to ensure that a distinct Gribov copy has been identified, one must test to make sure that the stopping condition of the gauge fixing algorithm is small enough so that the variance of the plaquette trace across different Gribov copies is well defined. We found that a tolerance of 10^{-8} in the link trace from gauge fixing was more than enough to differentiate between different values of the link trace from differing Gribov copies, which was of order 10^{-5} or bigger. One can then plot the frequency of each distinct Gribov copy against the value of the real trace of the link to form a histogram that characterises the density of Gribov copies of that time slice.

The Coulomb gauge fixing condition is applied to lattice time slices independently, so for 100 configuration of size L^3T , one has $100T$ such histograms to consider. However, considering each of these time slices individually would ignore the fact that they all came from the same ensemble, which had only two input parameters, L and β ¹⁸. Furthermore, 100 data points per time slice is not always enough to make a well defined histogram with which to describe the density of Gribov copies. Figure 7.3 shows, as an example, the distribution of the binned values of the global maximum of the link trace for a $\beta = 6.20$, $L = 12$ lattice. The distribution fits a Gaussian very well and this is observed for all values of β and L . It also shows that we cannot compare the raw values of link traces with those from another time slice without somehow normalising all the values.

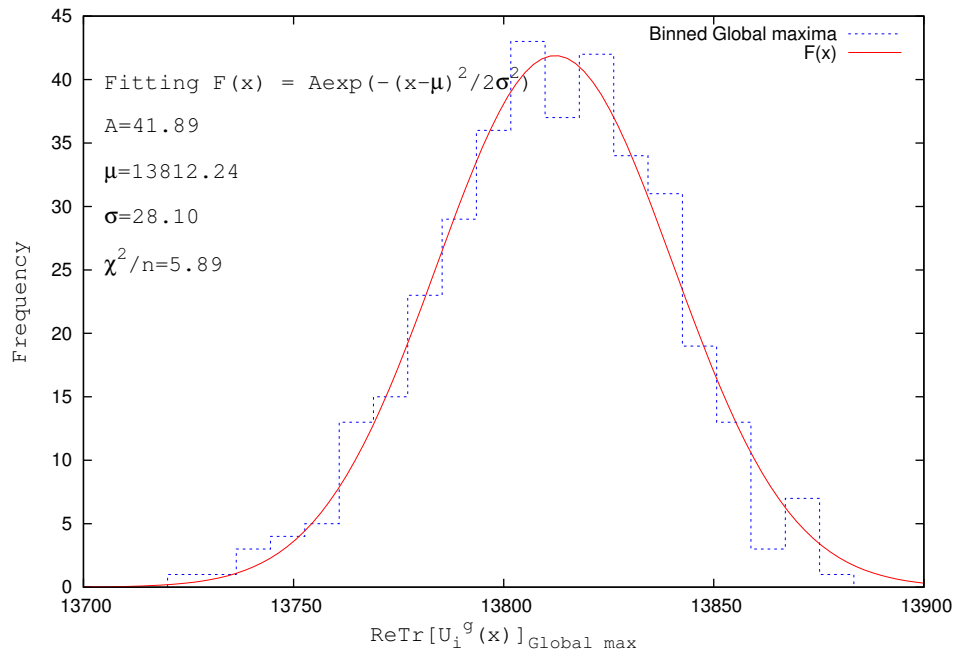


Figure 7.3: Gaussian profile of a the distribution of absolute link traces.

We therefore opted to define, for each time slice, a variable derived from the global maximum of the link trace U_i^g and the link trace from Gribov copies U_i (which

¹⁸Throughout this work we use lattices of size $T = 2L$ so L defines T .

is necessarily of a lower value) as,

$$X = 1 - \frac{\sum_{\mathbf{x},i} \text{ReTr}(U_i(\mathbf{x}))}{\sum_{\mathbf{x},i} \text{ReTr}(U_i^g(\mathbf{x}))}. \quad (7.2.9)$$

At each time slice, the global maximum maps to $X = 1$ and all other values to $X < 1$. This allows us to combine all the link trace data into a single histogram with only β and L as the parameters. We bin the data with some suitable width and observe an exponential attenuation in the frequency with X . This indicates that Gribov copies tend to cluster (at least so far as the link trace is concerned) around the FMR. We can measure this attenuation by fitting a linear decay, an example of which is shown in 7.4. Each value of β will give a different value of the gradient α , which we then plot which we then plot as a function of β . Three volumes were analyzed in this fashion, $L = 10, 12, 14$, and the results are plotted in 7.5, 7.6, and 7.7.

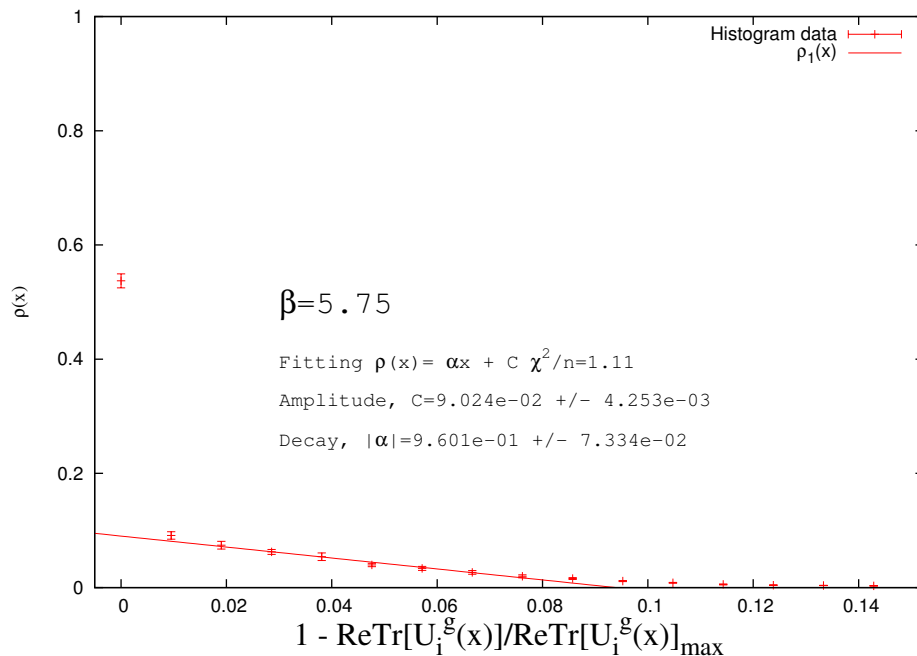


Figure 7.4: An example of how the attenuation of Gribov density is measured. This plot is from an $L = 12, \beta = 5.75$ lattice. The α parameter is extracted using a linear decay.

We also record how many times the gauge fixing routine finds a global maxi-

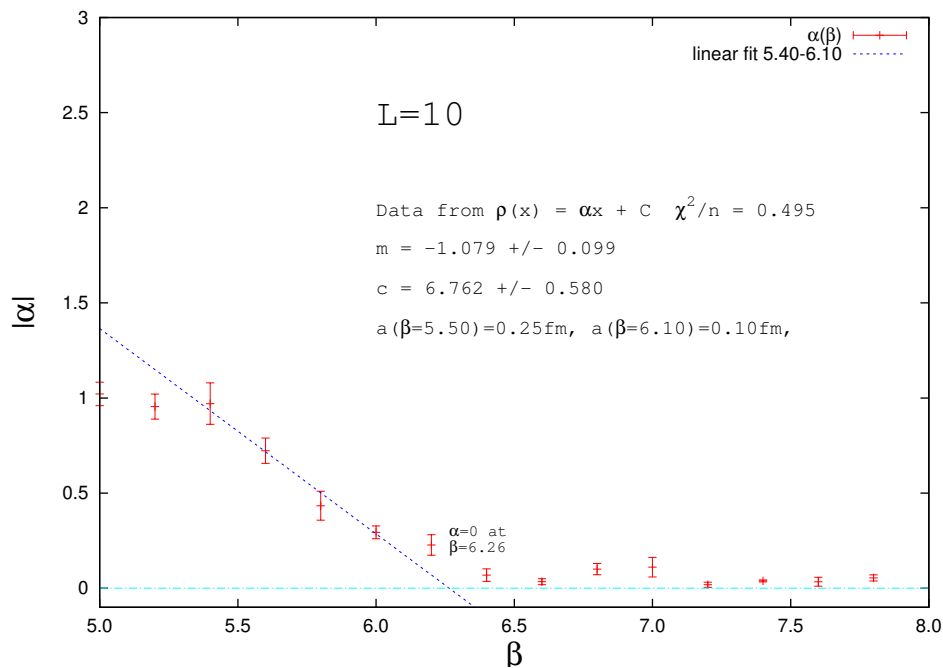


Figure 7.5: Evolution of Gribov density with β for $L=10$ in pure $SU(3)$.

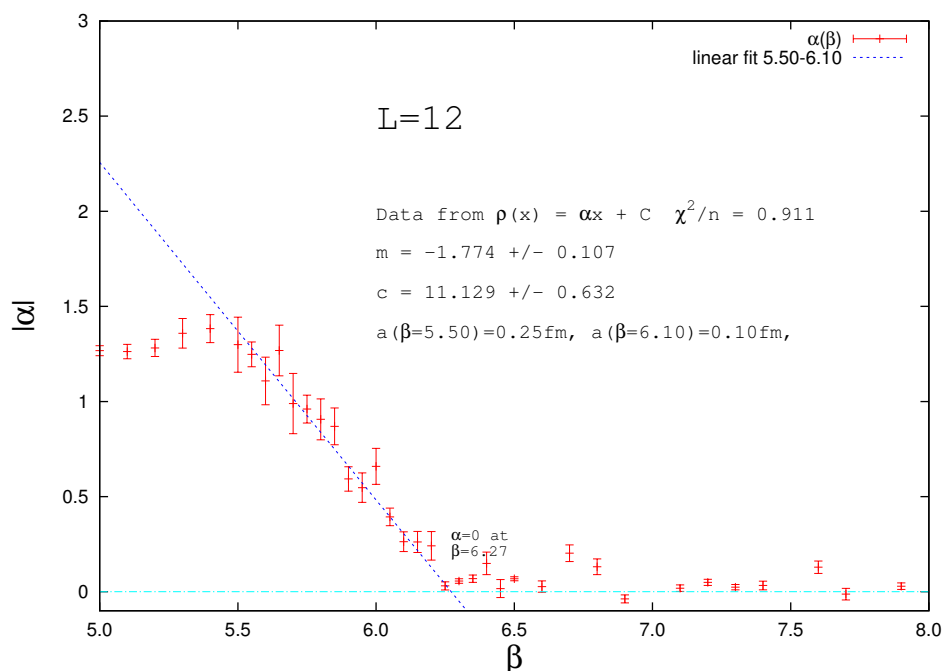


Figure 7.6: Evolution of Gribov density with β for $L=12$ in pure $SU(3)$.

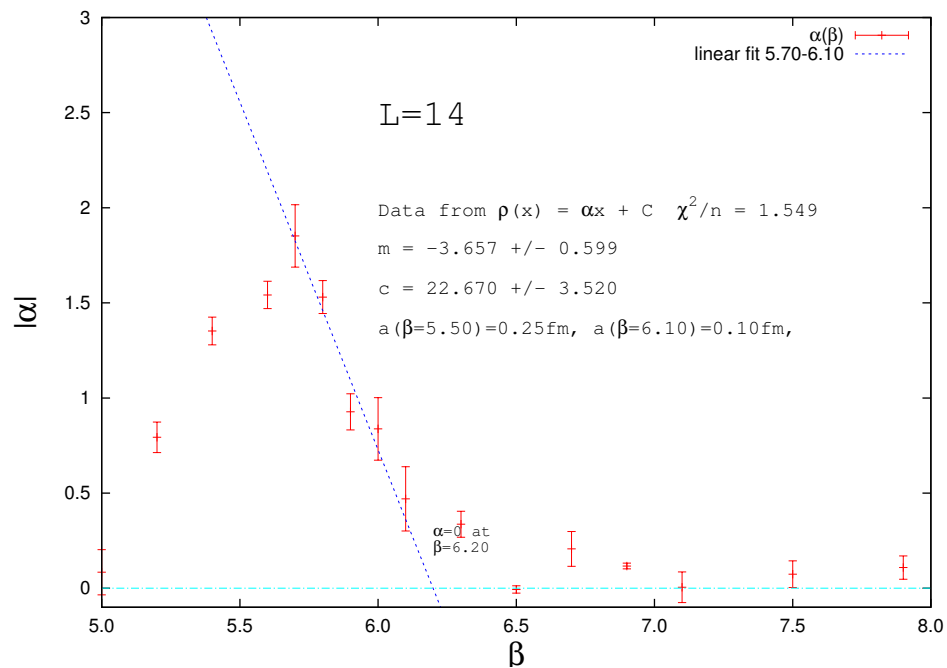


Figure 7.7: Evolution of Gribov density with β for $L=14$ in pure $SU(3)$.

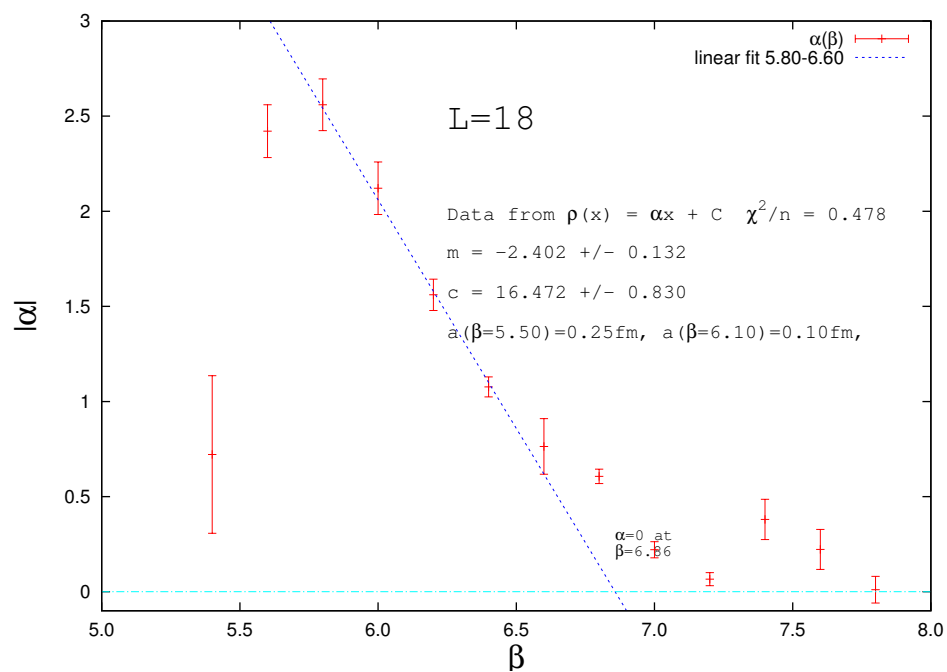


Figure 7.8: Evolution of Gribov density with β for $L=18$ in pure $SU(3)$.

mum (#FMR) compared to the total number of rotations (#ROT). For each value of β at a given L we plot this ratio and fit a very simple linear function over the range $5.40 < \beta < 6.10$. Results are shown in 7.9, 7.10, and 7.11. These observa-

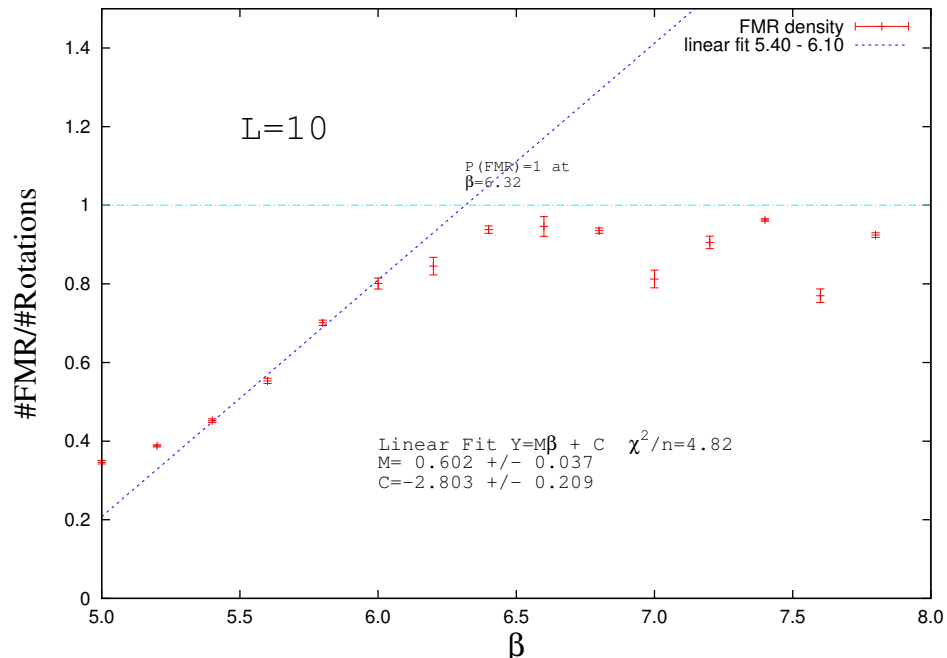


Figure 7.9: The probability of finding the FMR in pure $SU(3)$ for $L=10$.

tions are still in a very raw form and as such interpretation is tricky. However, one can still tentatively surmise some features:

- For each lattice size, there is a region over which the probability of finding the FMR is linearly increasing function, and this coincides with a decrease in the density of Gribov copies outside the FMR.
- The value of β to which this linear behaviour extrapolates is around the $\beta = 6.35$ mark. This may be a universal value for $SU(3)$ Yang-Mills, or it may change with lattice volume. More data is necessary.
- Around this value of $\beta = 6.35$, the Gribov copies tend to condense around the FMR, with the behaviour of a second order phase transition in $\alpha(\beta)$. This thermodynamic interpretation may coincide with deconfinement, so an

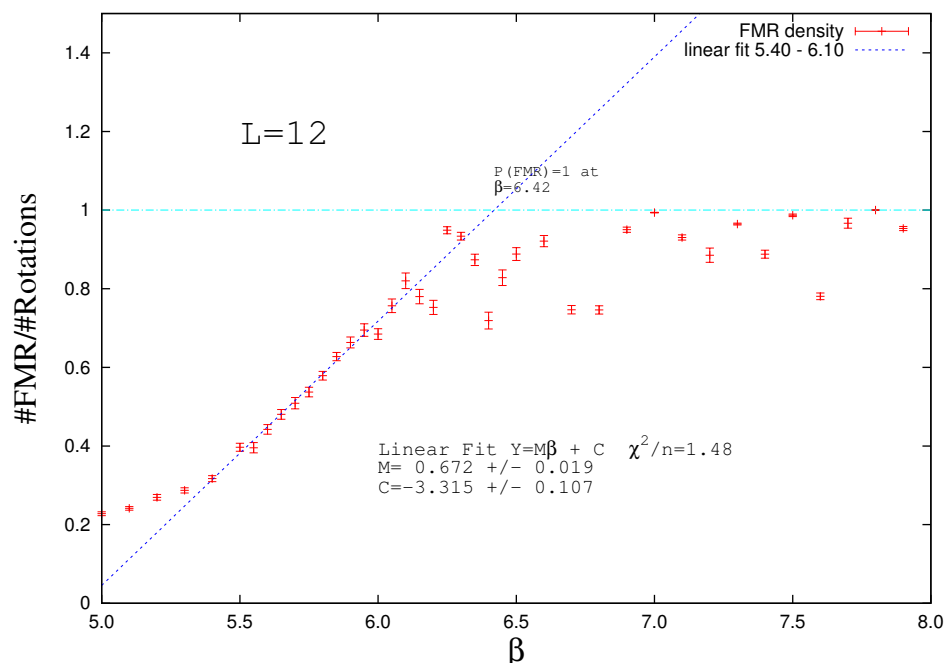


Figure 7.10: The probability of finding the FMR in pure $SU(3)$ for $L=12$.

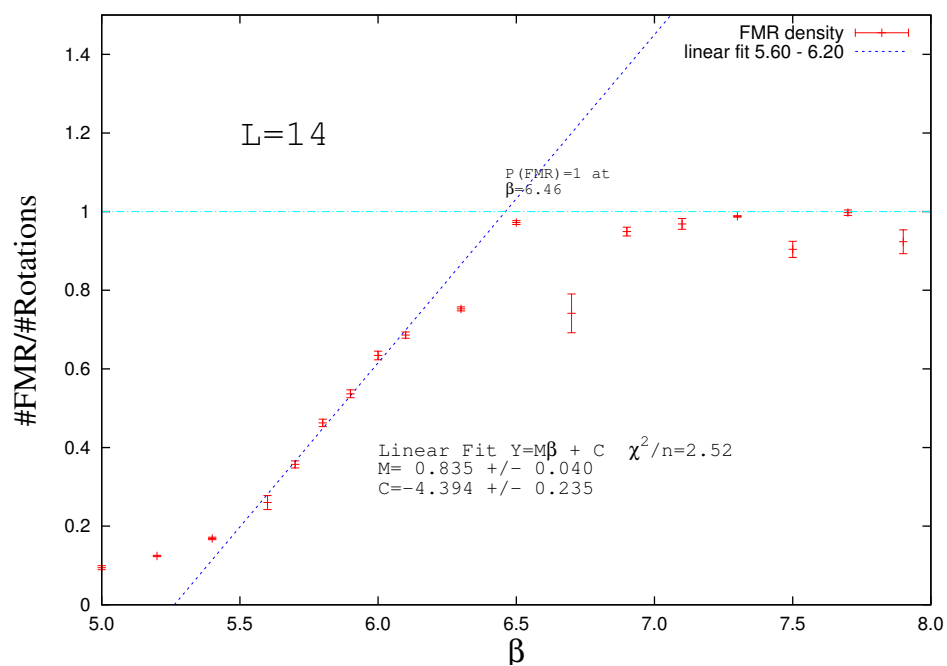


Figure 7.11: The probability of finding the FMR in pure $SU(3)$ for $L=14$.

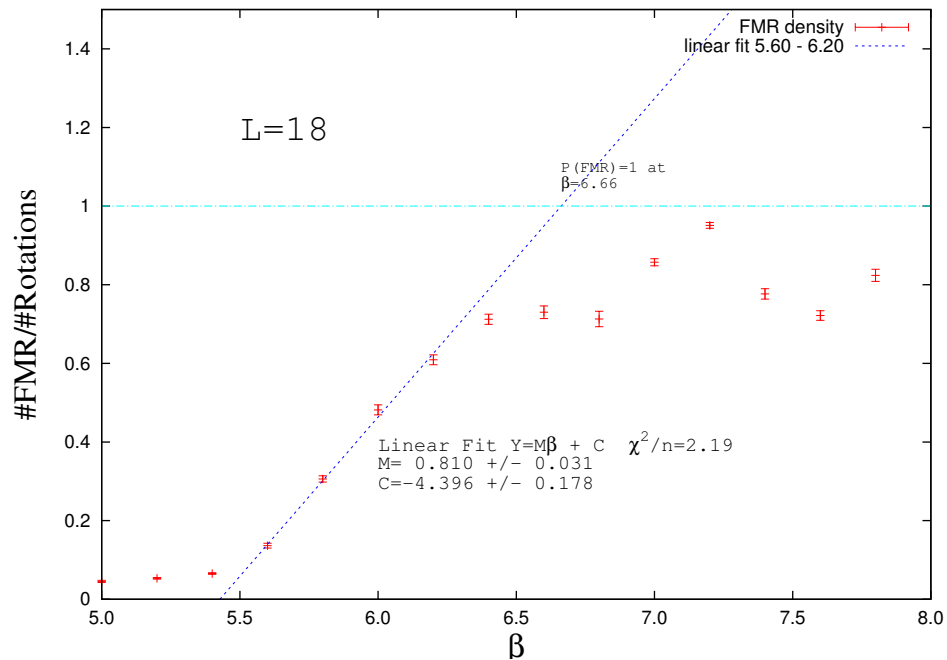


Figure 7.12: The probability of finding the FMR in pure $SU(3)$ for $L=18$.

independent measurement locating the deconfinement phase transition is necessary.

In future studies one might perform the same analysis on larger (smaller) lattices over suitable ranges of β and attempt to extrapolate the features in the plots above to the continuum, which may give us information about Gribov density in a continuum $SU(3)$ Yang-Mills theory. The same study can be performed on dynamical lattices too wherein contact can be made with QCD. In the Gribov-Zwanziger scenario (29, 30), the gluon propagator is suppressed in the infra-red limit which precipitates confinement. They also predict that continuum gauge field configurations will have Gribov copies that cluster around the first Gribov Horizon and the boundary of the FMR. This behaviour is corroborated in the plots above. As β increases, the lattice spacing shrinks and becomes more continuum like. As a result, more configurations are seen in the FMR as the Gribov copies migrate towards it, and fewer are left outside of it making it difficult to see the underlying structure. In any case, it is hoped that the observations presented here will generate interest and yield more concrete results as more data is gathered.

CHAPTER 8

Extracting Physics and the σ Meson

In this section an overview of the σ meson in QCD will be given in both experimental and theoretical contexts. Then, it will be shown how the lattice techniques given in previous sections are employed to extract the relevant physics necessary to make quantitative statements about the nature of the σ .

8.1 Theoretical Background

The standard model, and QCD in particular, has given us a superb mathematical tool with which to categorise and study the great number of particle states seen in collider experiments. Well known, and well established particles, such as the pion, rho, proton, and neutron to name but a few, are excellently described by quarks interacting via a non-Abelian $SU(3)$ gauge theory. Along with these well known states there are numerous particle resonances that are officially recognised by the Particle Data Group, but knowledge of these particles outside the confines of particle physics is not so well established.

The reason for this obscurity is because of our ignorance of the precise composition of these particles. Consider the the group of particles known as the ‘pseudoscalar nonet’ in figure 8.1. The quark content of these particles can be easily discerned from the quantum numbers they exhibit. This systematic grouping of particles is possible because of the underlying quark structure, and as such, we reverse the logic and make accurate statements about the quark content of the mesons just by noting their respective quantum numbers. The mass hierarchy of the pseudoscalars is also well described by the $SU(3)$ quark model as the lightest mesons are the pions which form an isospin triplet in the central horizontal line. This means they have no net strange quark content. Conversely, the K mesons, which contain strange quarks, are significantly heavier than the pions. Heavier still are the η mesons which have significant $s\bar{s}$ content in and are thus the heaviest. The amount of $s\bar{s}$ content in the

η, η' pair is given by the mixing angle $\phi_{PS} \approx 40$ (31) and the equations,

$$\begin{aligned}\eta &= \cos(\phi_{PS}) \left(\frac{|u\bar{u}\rangle + |d\bar{d}\rangle}{\sqrt{2}} \right) - \sin(\phi_{PS}) |s\bar{s}\rangle, \\ \eta' &= \sin(\phi_{PS}) \left(\frac{|u\bar{u}\rangle + |d\bar{d}\rangle}{\sqrt{2}} \right) + \cos(\phi_{PS}) |s\bar{s}\rangle.\end{aligned}\quad (8.1.1)$$

which neatly explains the observed mass splitting in the η system.

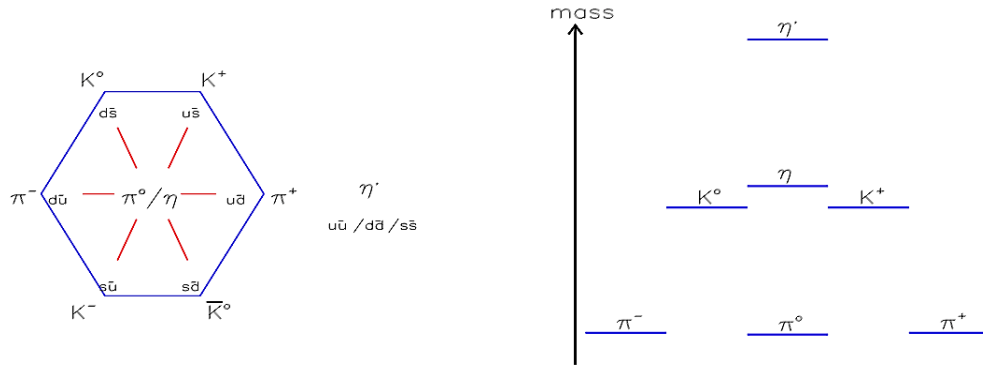


Figure 8.1: In the arrangement shown, the mesons exhibit S strange quark content in the horizontal lines, Q electromagnetic charge in the diagonal lines, and I isospin in the vertical. Figure taken from (32)

Unfortunately, we are not always able to make such clean cut insights when we try to group particles in this manner. The most taxing set of particles is known as the ‘scalar mesons’ shown in figure 8.2. As before, a triplet of a_0 states in the central horizontal show that they must have zero strange quark content, but measurements show that they have the heaviest mass in the nonet! The next lightest masses are the κ mesons which have non-zero strange quark content, and then lightest of all is the σ meson, or $f_0(500)$. One may be tempted to suggest that the $f_0(500) - f_0(980)$ mass splitting is due to a mixing angle, analogous to the η, η' system. But the $f_0(980)$ is very nearly mass degenerate with the $a_0(980)$, which must have $|u\bar{u}\rangle + |d\bar{d}\rangle$ quark content by observing its quantum numbers, so the mixing angle must be very small and would not be able to account the large $f_0(500) - f_0(980)$ mass splitting. Even more confusing is the evidence that both the $f_0(980)$ (33) and $a_0(980)$ (34) couple

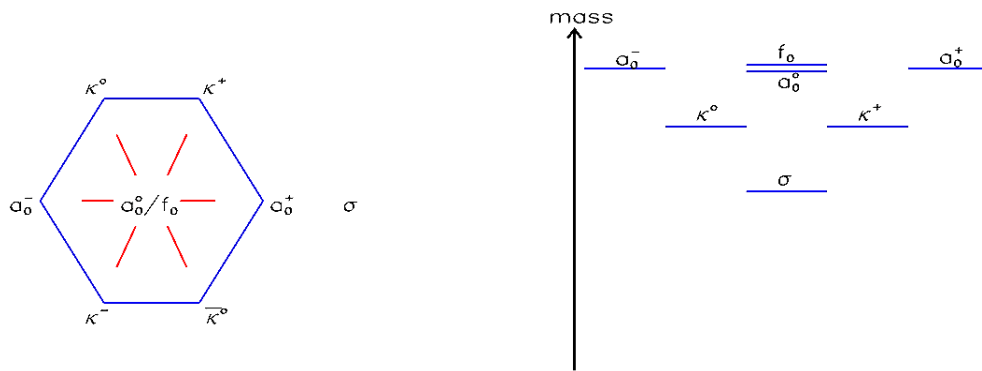


Figure 8.2: In the arrangement shown, the mesons exhibit the properties shown by the horizontal and diagonal lines. Q is electromagnetic charge and S is strange quark content. Figure taken from (32)

strongly to $K\bar{K}$ in their respective decay chains, suggesting that they both have a large $s\bar{s}$ quark content. This is at odds with the naive assumption that the scalars can be adequately described by simple $q\bar{q}$ states.

This therefore motivates an *ab initio* investigation using lattice gauge theory as a mathematical tool to capture the non perturbative aspects of the QCD Lagrangian in the scalar sector. On the lattice we may choose our operators and dynamics in such a way that we can make claims about the quark content of the particles we observe.

8.2 Experimental Evidence of the σ Meson

In 2004, the BES collaboration published data of 58 million J/ψ events detected in the BESII detector where the decay $J/\psi \rightarrow \omega\pi^+\pi^-$ was studied. An invariant mass plot of the $\pi^+\pi^-$ that scattered off the ω is shown in figure 8.3.

The detection algorithms and cut parameters of the detector are rather complicated. The omega meson ω has a very short lifetime compared to the neutral and charged pions, and in turn, the neutral pion has a short lifetime compared to the charged pions. The ω meson's principal decay mode (Γ_0) is $\omega \rightarrow \pi^+\pi^- + \pi^0$ with a branching fraction $\Gamma_0/\Gamma = (89.2 \pm 0.7)\%$, and the next leading contribution

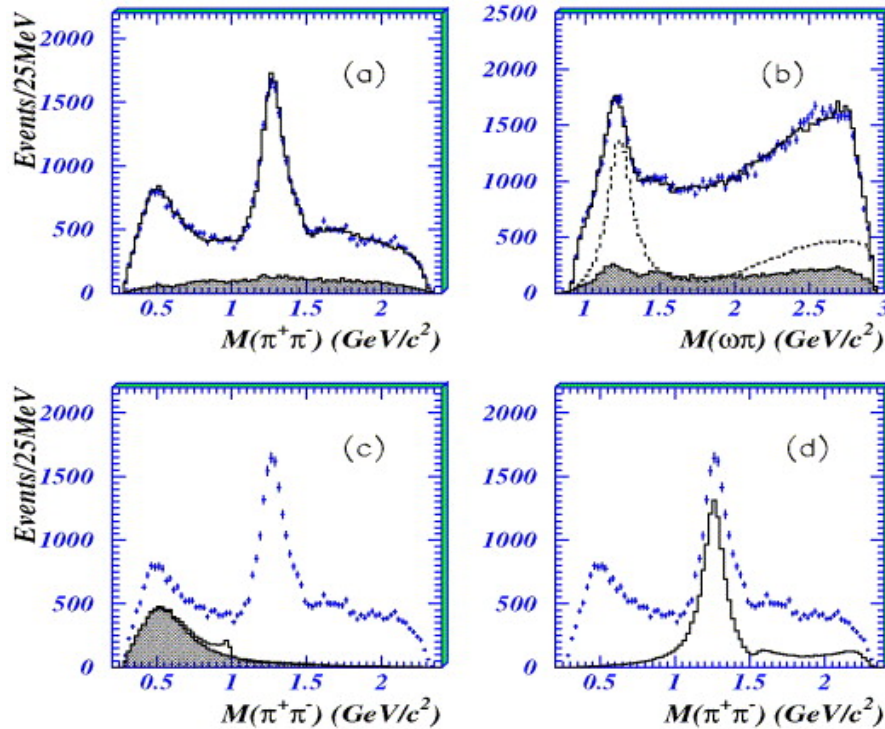


Figure 8.3: An invariant mass plot of the $\pi^+\pi^-$ from a $J/\psi \rightarrow \omega\pi^+\pi^-$ event at BESII. The upper left plot shows the invariant masses in the histogram and the shaded area is the expected background. In the lower left, we see the same histogram and the contribution from the sigma resonance alone. Figure taken from (1)

is $\omega \rightarrow \pi^0 + \gamma$ with fraction $\Gamma_1/\Gamma = (8.28 \pm 0.28)$. The π^0 decays practically exclusively into 2γ with a fraction $\Gamma_0/\Gamma = (98.823 \pm 0.034)$. The final state of a J/ψ event therefore is often a five particle system $J/\psi \rightarrow \omega + \pi^+\pi^- \rightarrow 2\pi^+2\pi^- + \gamma$ or a three particle, purely photon system $J/\psi \rightarrow \omega + \gamma \rightarrow 3\gamma$. By identifying an ω particle, one can attempt to identify a $\pi^+\pi^-$ pair and calculate the centre of mass energy of that pion pair. The shaded part of figure (a) in 8.3 shows the expected background 2π spectrum. The dashed line in the same plot represents the number of events (associated with J/ψ production) where an ω meson was detected and a $\pi^+\pi^-$ pair could be resolved. Two prominences can be seen in the data: The tall, narrow peak at ~ 1.3 GeV and the broader, short peak at ~ 600 MeV. The former is known as the $f_0(1370)$, the latter is known as the $f_0(500)$ or σ meson.

The interpretation of the σ meson as a particle resonance is, at this time, more speculative than concrete because of the three-body decay nature of the $\omega\pi^+\pi^-$ system. Even in the absence of any resonances in the isoscalar channel one would see a peak appear early in the $\pi^+\pi^-$ spectrum and then fall off with increasing energy. In order to establish the σ as a resonance, one must investigate the scattering phase shift of the $\pi^+\pi^-$ system to ascertain if there exists a resonance at the $\sim 500\text{MeV}$ energy level.

8.3 Effective Mass Plateaux

We tested the smeared momentum sources by comparing correlation function values and effective mass plots for a simple single hadron system. We chose the pseudo-scalar channel,

$$C_\pi(t) = \langle \Omega | T \{ \hat{\pi}_-(\mathbf{z}, t) \hat{\pi}_-^\dagger(\mathbf{0}, 0) \} | \Omega \rangle, \quad (8.3.1)$$

where the pseudo-scalar operators are defined as in (6.1.2) and flavour degeneracy is imposed after Wick contraction, leaving only one connected quark propagator diagram to evaluate. Due to translational invariance, we need only the point-to-all propagator for this calculation, so all correlation function values may be labelled by the lattice spacetime index of the sinks $z = (\mathbf{z}, t)$. This affords us an excellent method for making a comparative study between smeared momentum sources and gaussian sources.

8.3.1 Conventional method

Once a suitable number of gauge field configurations have been sampled, one can fit the decay of the correlation function value to extract the ground state energy of the system. Due to the periodic nature of the lattice in the temporal direction, the exponential decay will take the form,

$$C(\tau) = A[\exp(-E_0\tau) + \exp(-E_0(T - \tau))], \quad (8.3.2)$$

where A is an irrelevant constant. This is a hyperbolic cosine (cosh) function, though it is statistically better to fit the data in a different manner. We shall ‘fold’ each correlation function value in the following way,

$$C_{fold}(\tau) = \frac{C(\tau) + C(T - \tau)}{2} \quad \text{for } \tau = 1 \dots \left(\frac{T}{2} - 1\right), \quad (8.3.3)$$

and express $C_{fold}(\tau)$ as a single exponential function,

$$C_{fold}(\tau) = A \exp(-m\tau). \quad (8.3.4)$$

where we have simply relabelled the ground state energy $E_0 = m$. We then define the *effective mass* m_{eff} as,

$$m_{eff}(\tau) = -\ln \left[\frac{C_{fold}(\tau + 1)}{C_{fold}(\tau)} \right], \quad (8.3.5)$$

and plot m_{eff} as a function of τ . Plotting the data in this fashion will reveal that for small τ , $m_{eff}(\tau)$ decreases in value as τ increases, and then settles at some constant value out to the middle time slice (which is the region over which $C_{fold}(\tau)$ and therefore $m_{eff}(\tau)$ are defined). The reason for this behaviour is that correlation function values at small τ are contaminated by higher energy states (c.f. 6.1.12a as an example of a correlation function with excited state contaminations.) By plotting the effective mass and looking for a plateau in the $m_{eff}(\tau)$ function, i.e., the region where $m_{eff}(\tau)$ is approximately constant with respect to τ , we can identify the region where excited state contamination is negligible and the main contribution to the correlation function values comes from the ground state only. Had we simply performed a cosh fit to the raw $C(\tau)$ data, our calculated value of $E_0 = m$ would have been wrong due to our assumption that the exponential decay were parameterised by the ground state only.

Figure 8.4 shows the effective mass plateaux of a single pion correlation function on an $L = 16$ lattice, calculated using (a) unsmearred, and (b) smearred point sources. Figure 8.5 again shows the (a) unsmearred and (b) smearred zero momentum sources. One can see quite clearly the effective mass plateau is reached much more

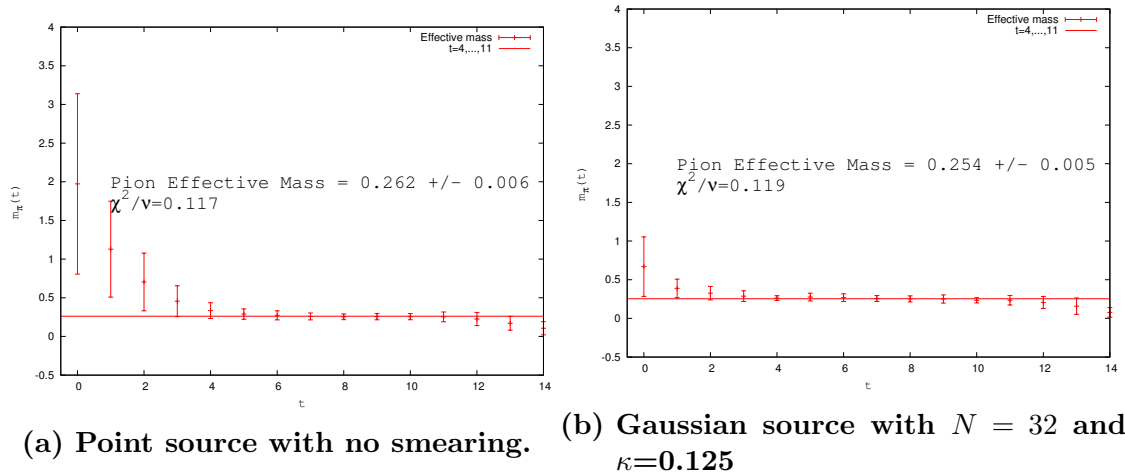


Figure 8.4: A comparison between smeared and unsmeared point sources for a single pion correlation function. In each calculation 48 unquenched gauge configurations trajectories were used, the Hopping parameter κ is 0.125 and stout link smearing was employed.

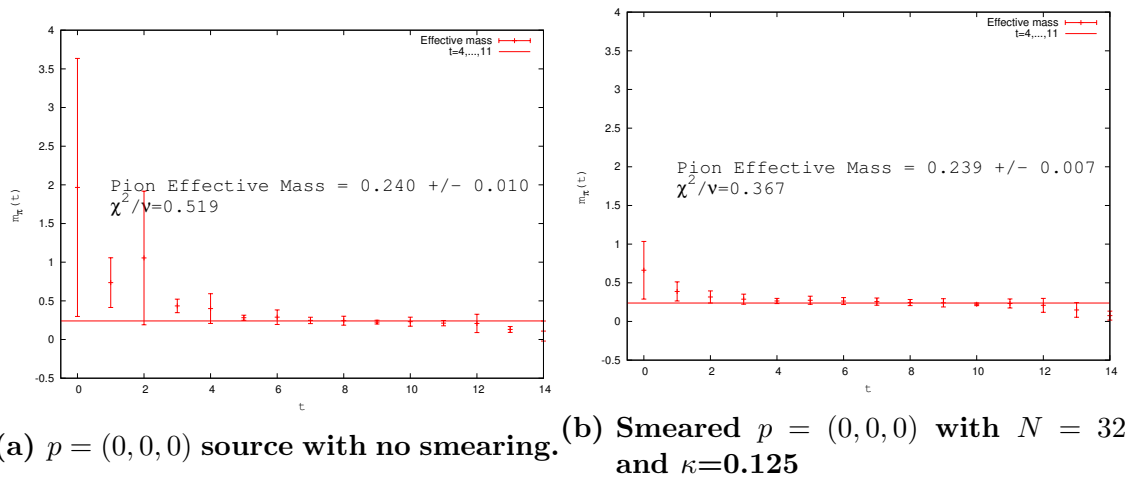


Figure 8.5: A comparison between smeared and unsmeared $p = (0,0,0)$ momentum sources for a single pion correlation function. In each calculation 48 unquenched gauge configurations trajectories were used and the Hopping parameter κ is 0.125 and stout link smearing was employed.

quickly when using the smeared source in both cases, and that the quality of the smeared fits are better.

8.3.2 Log-Normal Method

For each lattice timeslice t we plot a histogram of the correlation function values projected onto zero momentum from gauge configuration n . We find, in agreement with other studies (35, 36) that the correlation function values are log-normally distributed. The two parameters that define the normalised log-normal distribution,

$$f(C(t)) = \frac{1}{C(t)\sigma(t)\sqrt{2\pi}} \exp\left(\frac{-(\ln[C(t)] - \mu(t))^2}{2\sigma^2(t)}\right), \quad (8.3.6)$$

are the ‘scale’ parameter μ and ‘location’ parameter σ . These parameters respectively form the arithmetic mean and arithmetic standard deviation of a parent gaussian distribution from which the $C(t)$ are drawn.

It is illuminating to compare these two parameters for smeared momentum and point sources. Plotted in figures 8.6a and 8.6b are $\mu(t)$ and $\sigma(t)$ for both types of source over four different masses. What is clear is that the gradients of $\mu_{ps}(t)$ and $\mu_{mom}(t)$ are identical to within 0.1%. and give good agreement with the measured effective mass of the ground state, shown in figures 8.7a and 8.7b. This suggests that $\partial_t \mu(t)$, which in the present case will be the finite difference operator $\Delta_t \mu(t)$, is directly related to the ground state of the single hadron system being simulated. Indeed, if we define the gauge averaged correlation functions not as the arithmetic mean, but as the first moment of the log-normal distribution,

$$\langle C(t) \rangle_U = E[C(t)] = \exp\left(\mu(t) + \frac{\sigma^2(t)}{2}\right), \quad (8.3.7)$$

then a natural definition of the effective mass in terms of $\mu(t)$ and $\sigma(t)$ can be found

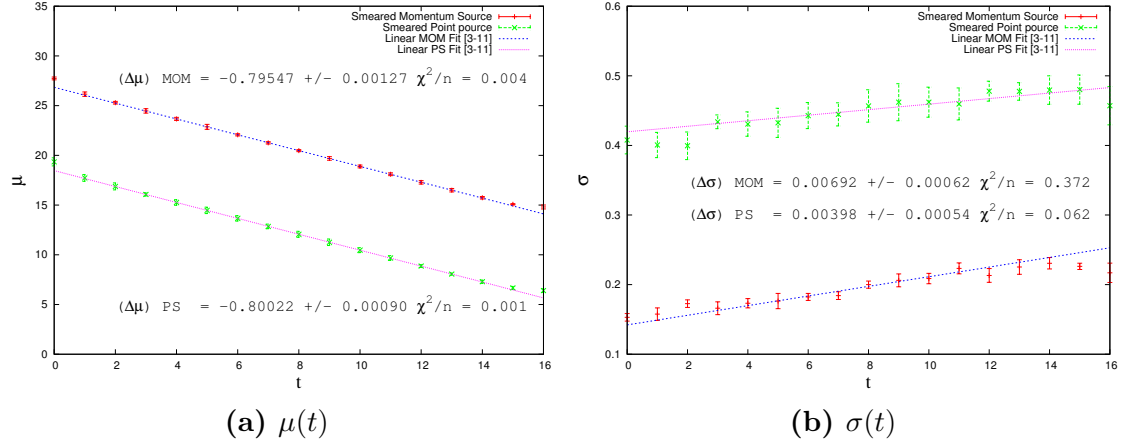


Figure 8.6: Evolution of μ (left) and σ (right) with t for smeared point and momentum sources for heavy mass pion from an $16^3 32$ quenched $\beta = 5.45$ ensemble.

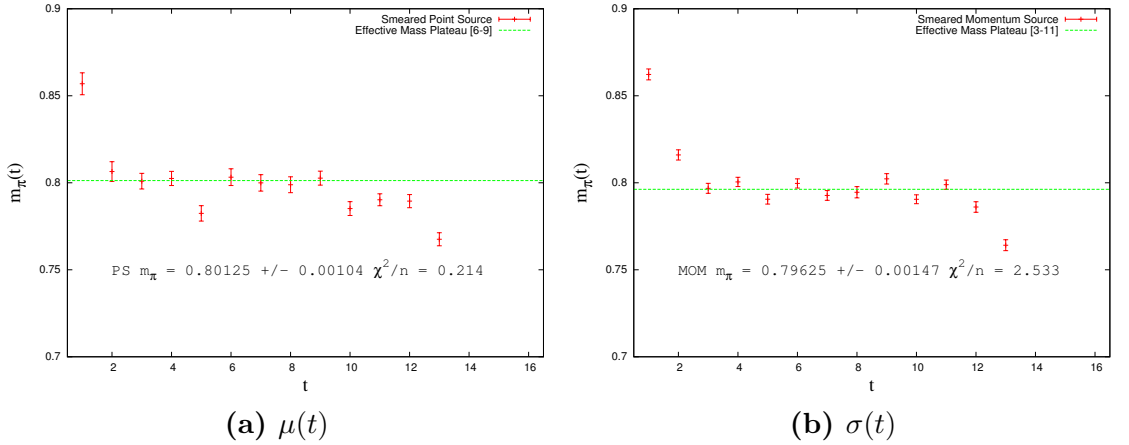


Figure 8.7: Effective mass plateaux for a heavy pion with from an $16^3 32$ quenched $\beta = 5.45$ ensemble.

when applying (8.3.5) to (8.3.7),

$$\begin{aligned}
 m_{eff}(t) &= - \left[\mu(t+1) + \frac{\sigma^2(t+1)}{2} \right] + \left[\mu(t) + \frac{\sigma^2(t)}{2} \right], \\
 &= - [\Delta_t \mu(t) + \sigma(t)(\Delta_t \sigma(t))].
 \end{aligned}
 \tag{8.3.8}$$

This explains why the bulk of the effective mass information is contained in $\mu(t)$ in these calculations as the $\sigma(t)(\Delta_t \sigma(t))$ term is very small by comparison.

8.4 Lattice and physical scales: the Sommer parameter

There are two fundamental scales involved in a lattice calculation; one is the number of spacetime points on the lattice (which is naturally dimensionless) and the other is the physical distance that the lattice spacing a represents. Knowledge of both of these scales allows us to match up the observables of a lattice calculation with the observables of QCD. We have already seen how measuring the exponential decay of a Euclidean correlation function allows us to measure the ground state energy E_0 of the system in question (6.1.14), but so far we have only been able to do so in dimensionless lattice units. In order to relate the lattice ground state to a physical ground state we must include the physical distance a ,

$$\begin{aligned} E_0\tau &= E_0aa^{-1}\tau = ma^{-1}\tau = mt \\ \Rightarrow \quad m &= aE_0. \end{aligned} \tag{8.4.1}$$

One such method for calculating a is by using the **Sommer parameter** r_0 (37). Consider the potential between two massive quarks separated by a distance r due to colour dynamics is known as the *static quark potential* $V(r)$,

$$V(r) = A + \frac{B}{r} + \sigma r. \tag{8.4.2}$$

The constant A is an irrelevant normalisation of the energy, B characterises the Coulomb part of the potential, and σ characterises the linearly rising part of the potential. One expects a value of around 900MeV/fm for σ (38). The form of $V(r)$ is justified by considering the effect of small gauge coupling g at short distance scales c.f. figure 2.1, where the gauge coupling becomes so small that non-commutative part of the field strength tensor is negligible. At these scales, the potential acts like a $U(1)$ abelian gauge theory and a Coulomb-like behaviour is expected. At larger distance scales, one calculates the expectation value of two temporally separated Wilson loops where one finds that the exponential decay is proportional to the area of the loop. One then concludes that in the strong coupling limit, the potential must be linear in r , hence string-like. The point of interest in such a situation is the physical distance at which the potential crosses from Coulomb-like, to string-

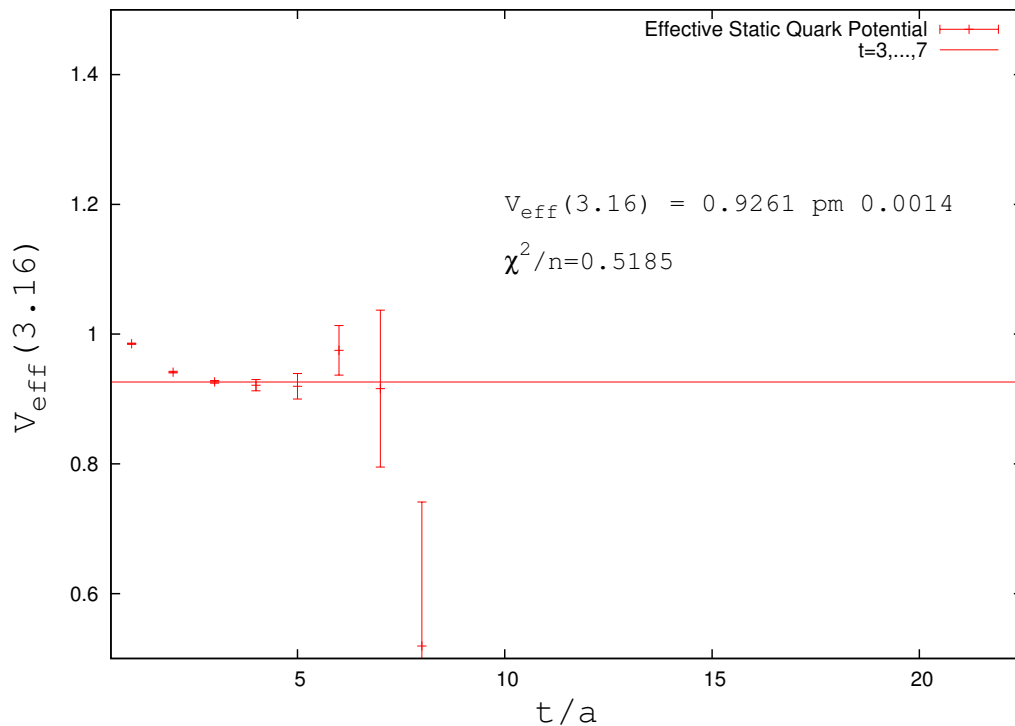


Figure 8.8: The static quark potential at $r = 3.16$ lattice units for $\beta = 5.80$ and $L = 14$ was calculated using 8.4.9 at late times to exclude excited states.

like. The physical value at which this happens is $r_0 \approx 0.5 \text{ fm}$, as can be deduced from experimental data in $\bar{b}b$ and $\bar{c}c$ spectra (37). With this information, one can perform calculations on the lattice to measure the static quark potential at a given value of the gauge coupling and measure the point at which the potential undergoes a transition. In order to identify this point, one must make a more rigorous definition of r_0 . Rather than being based on the potential $V(r)$, one defines the Sommer parameter in terms of the force between heavy quarks,

$$F(r) = \frac{\partial V(r)}{\partial r}, \quad (8.4.3)$$

where at the transition point $r_0 = 0.5 \text{ fm}$,

$$F(r_0)r_0^2 = 1.65. \quad (8.4.4)$$

Now, using 8.4.2, 8.4.3, and 8.4.4, we can derive an expression for r_0 in terms of lattice units and parameters B and σ ,

$$\begin{aligned} r^2 F(r) \Big|_{r_0} &= r^2 \frac{\partial V(r)}{\partial r} \Big|_{r_0} = -B + \sigma r_0^2 = 1.65 \\ \Rightarrow \frac{r_0}{a} &= \left(\frac{1.65 + B}{\sigma a^2} \right)^{\frac{1}{2}}. \end{aligned} \quad (8.4.5)$$

We must therefore extract from the lattice the static quark potential $V(r)$ and plot these data against r so that we can fit 8.4.2 and get values for B and σ . To do this, consider a rectangular Wilson loop starting and x and in the μ plane, going out to $x + n'\hat{\mu}$, the through the temporal direction by k' time slices, back to $x + k'\hat{4}$, then back to x ,

$$W_\mu(x, x + n'\hat{\mu}) = \prod_{n=0}^{n'} U_\mu(x + n\hat{\mu}) \prod_{k=0}^{k'} U_4(x + n'\hat{\mu} + k\hat{4}) \prod_{p=p'}^0 U_\mu^\dagger(x + k\hat{4} + p\hat{\mu}) \prod_{q=q'}^0 U_4^\dagger(x + q\hat{4}), \quad (8.4.6)$$

where in the first two products the index runs from $n = 0, 1, \dots, n'$; $k = 0, 1, \dots, k'$ and in the latter two $p = p', p'-1, \dots, 0$; $q = q', q'-1, \dots, 0$. The index '4' explicitly indicates the temporal direction. This product of gauge links is the operator associated with two, static quarks, spatially separated at x and $x + n\hat{\mu}$. The line connecting them is called a Wilson line and the lines connecting to respective points at $t = 0$ to $t = k'$ are the temporal transporters. This Wilson loop can be placed in the path integral as an operator to calculate the energy associated with the static quark system, and it will have a ground state and excited states. To do this, we must gauge transform to temporal gauge,

$$A_4 = 0, \quad (8.4.7)$$

which sends the temporal transporters to unity, but the expectation value of the gauge invariant Wilson will remain unchanged. Treating the Wilson lines as operators, the expectation value is,

$$\langle W_\mu(x, x + n'\hat{\mu}) \rangle = \left\langle \text{Tr} \left(\prod_{n=0}^{n'} U_\mu(x + n\hat{\mu}) \prod_{p=p'}^0 U_\mu^\dagger(x + k'\hat{4} + p\hat{\mu}) \right) \right\rangle, \quad (8.4.8)$$

into which we may insert a complete set of intermediate states comprising a ground state $E_0 = V(r)$ and excited states $E_s(r)$ where $r = x + n'\hat{\mu}$. Therefore, in precise analogy with the way in which we calculate the ground state of the $I = 0$ correlation function by identifying the effective mass plateau, we can identify the ground state potential $V(r)$ by taking the logarithm of successive, temporally separated correlation function values of the Wilson lines, or equivalently, expectation values of the wilson loop,

$$\begin{aligned} \langle W_\mu(x, r, t) \rangle &= \sum_s C_s \exp(-t(V(r) + E_s(r))), \\ \Rightarrow V(r) &= -\ln \left[\frac{\langle W_\mu(x, r, t+1) \rangle}{\langle W_\mu(x, r, t) \rangle} \right], \end{aligned} \quad (8.4.9)$$

and looking for the large time limit of $V(r)$. We then plot $V(r)$ Vs. r for many

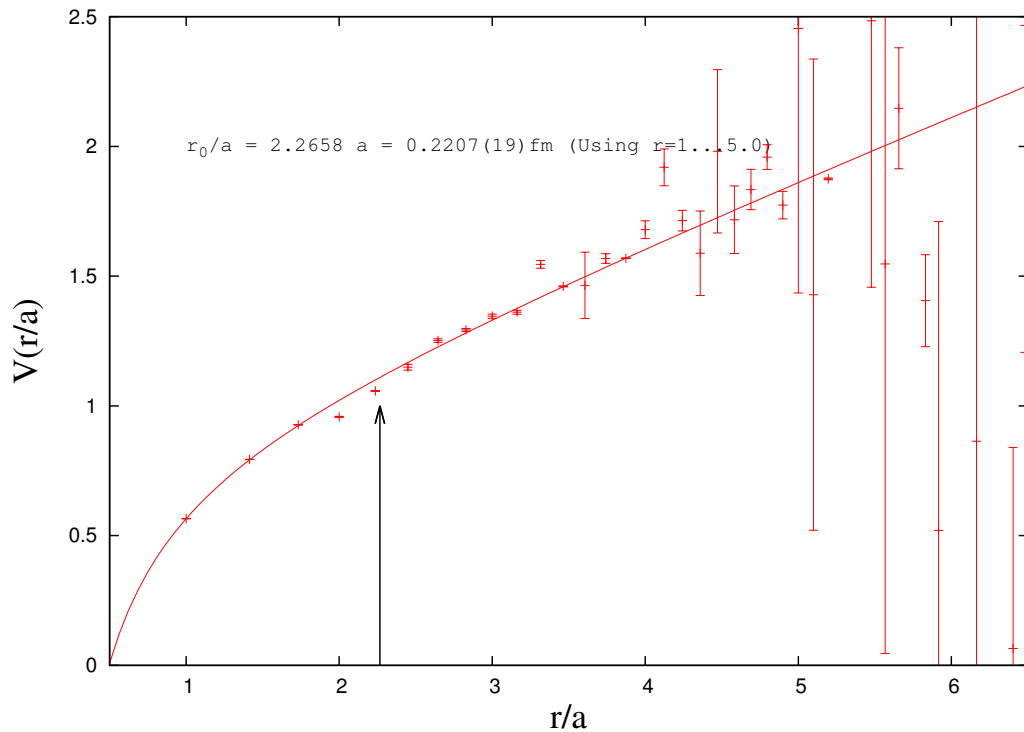


Figure 8.9: The static quark potential was calculated and the Sommer scale parameter $r_0 = 0.5\text{fm}$ is indicated with an arrow.

values of r as shown in figure 8.9. Although the description above explicitly places

r on some plane μ , one may in fact define any point on the same time slice as x , but one must use the Euclidean distance of these two points as the value of r when forming the plot. An example of the large time behaviour of the expectation value of the Wilson loop is given in figure 8.8 and the subsequent Sommer parameter plot in figure 8.9. In these calculations, the configurations were jack-knifed as explained in Appendix C.2. The error associated with the Sommer parameter is calculated in Appendix C.3.

8.5 Lüscher's Method

The ultimate goal of this study is to measure, if it exists, the scattering phase shift in the two pion flavour singlet channel. Its existence will be evidence that the $f_0(500)$ is indeed a resonance. The absence of a scattering phase shift would suggest that the peak in the 2 pion spectrum (fig 8.3 (a) and (c)). In order to measure this quantity we will use the method presented by Lüscher in a series of papers, (39), (40), (41), though only a schematic of the method will be given here.

The method uses the finite volume of the lattice to measure the change in energy levels of the 2 pion continuum spectrum due to finite volume effects, then relates these changes to the scattering phase shift. In order to measure the 2pion continuum energy levels (which are naturally quantised due to the discrete lattice) we create zero momentum pions at 0 and Z , and project the sinks at X , and Y to some desired momentum mode k using Fourier transformation. We then measure, using the effective mass plateau, the ground state energy for that momentum configuration and arrive at a value for the energy of that momentum level $\sqrt{E_k}$,

$$E_k = 2\sqrt{m_\pi^2 + k^2}. \quad (8.5.1)$$

Here of course we make the assumption that the lattice momentum in question satisfies ?? and we may use the continuum notation with impunity. Now, this energy level is related to the centre of mass momentum p^* through the relation,

$$E_k^2 = \mathbf{P}^2 + 4(p^{*2} + m_\pi^2) = \mathbf{P}^2 + s, \quad \text{where} \quad \mathbf{P} = \frac{2\pi k}{L} \quad \text{for} \quad k \in \mathbb{Z}^3. \quad (8.5.2)$$

Related to the quantity p^* is,

$$q = \frac{Lp^*}{2\pi}, \quad (8.5.3)$$

and Lüscher's Method instructs tell us that the scattering phase shift $\delta(s)$ can be obtained through,

$$\tan(\phi^k(q)) = \frac{\gamma q \pi^{\frac{3}{2}}}{Z_{00}^k(1; q^2)}, \quad (8.5.4)$$

where,

$$\delta(s) = -\phi^k(q) \pmod{\pi}, \quad (8.5.5)$$

$Z_{00}^k(1; q^2)$ is the generalised Reimann zeta function, and γ the relativistic gamma factor for the centre of mass momentum.

CHAPTER 9

Computational Setup

9.1 Software

A large selection of open source code libraries are available and we chose to use CPS (Columbia Physics System) which has a comprehensive range of functions for QCD, and QUDA, which utilises the proprietary CUDA libraries for the GPU code. In order to use the functionality of CPS on GPUs, we needed to rearrange the data that CPS produces, specifically, the layout of the clover matrix and the layout of the gauge fields. This is done with two custom written functions. The rearranged gauge field and clover matrix arrays are then passed to the GPUs via QUDA. We have written the code so that a only a single file in CPS needs to be changed, QUDA need not be modified. In general, three architecture types are available: a single CPU, known as scalar, BG/Q, and single GPU (Graphics Processing Unit.) The latter two are known as parallel as they can perform multiple floating point operations simultaneously. For the calculations performed, code was developed first on scalar architecture to ensure we had bona fide data. We then developed code on either the BG/Q or GPU as required and ensured that all data agreed with the data to the expected precision.

9.2 Hardware and Benchmarks

The calculations can be performed on three different types of architecture; scalar, multi-CPU, and GPU. The scalar machines we used had 32 AMD Opteron(TM) Processor 6272 processors and 80 Intel(R) Xeon(R) CPU E7- 4850 processors respectively. These machines did the bulk of the gauge fixing and miscellaneous analysis calculations. For local GPU code development we used two Tesla C2075 GPU cards connected to two quad core 2.40 GHz E5620 Intel Xeon processors as the host CPU. We also had access to 5 racks of BlueGene/Q installed at the Center for Computational Innovations which we use to generate dynamical gauge field configurations. We also have access the Kepler K20 GPU cards on both the TACC Stampede cluster

Table 9.1: Benchmarks for $12^3 \times 24, \beta = 5.60(a = 0.22fm)$ quenched lattices on Tesla K20

$12^3 \times 24$ Quenched Lattice			
Pion mass (MeV)	$m_\pi L$	12 Inversions (s)	smear, trace, FT (s)
440	6.024	32	3.7
418	5.724	34	3.7
397	5.436	37	3.7
374	5.124	39	3.7
348	4.764	42	3.7
314	4.308	45	3.7
271	3.708	47	3.7

Table 9.2: Benchmarks for $16^3 \times 32, \beta = 5.60(a = 0.22fm)$ quenched lattices on Tesla K20

$16^3 \times 32$ Quenched Lattice			
Pion mass (MeV)	$m_\pi L$	12 Inversions (s)	smear, trace, FT (s)
440	8.048	110	14.6
318	5.808	187	14.6
285	5.216	220	14.6
241	4.400	301	14.6

and the Fermilab Pi0g cluster. We reserve the allocations on these clusters to process the larger dynamical configurations. We give here timings data for two classes of calculations done on the Stampede allocation for $L = 12$ and $L = 16$. We also show data for some exploratory dynamical $L = 24$ lattices that we intend to use for full analysis once a large enough ensemble has been generated.

Table 9.3: Benchmarks for $24^3 \times 48$, $\beta = 5.30$ ($a = 0.16 fm$) dynamical lattices on Kepler C2075

$24^3 \times 48$ Dynamical Lattice

Pion mass (MeV)	$m_\pi L$	12 Inversions (s)
440	8.576	469
407	7.992	550
361	7.545	585

CHAPTER 10

Conclusions and Outlook

10.1 Preliminary Calculations

As a preliminary calculation, we use the quenched approximation on two lattices of size of $L^3T = 12^3 \times 24$ and $L^3T = 10^3 \times 20$. We used smeared, zero momentum sources as our operators, and performed the calculations in both Coulomb fixed, and unfixed gauges. The details are tabulated in 10.1.

Table 10.1: Data for preliminary simulations of two lattice sizes.

L^3T	β	Gauge	$a(\text{fm})$	$m_\sigma(\text{GeV})$
$10^3 \times 20$	5.45	unfixed	0.386	620 ± 80.0
$12^3 \times 24$	5.60	Coulomb	0.221	551 ± 40.7
$12^3 \times 24$	5.60	unfixed	0.221	532 ± 106

The lattice spacings of 0.221fm and 0.389fm are very coarse by modern standards but a large volume is needed when performing lattice calculations with multiple hadrons. In each case we determined the chiral limit of the pion mass and then calculated the correlation function 6.1.13 for several values of the pion mass. As can be seen from figures 10.1, the effective mass, which we label m_σ associated with 6.1.13 obeys $m_\pi < m_\sigma < 2m_\pi$ and $m_\sigma < m_\rho$, and extrapolates in the continuum limit to $m_\sigma = (551 \pm 40.7)\text{MeV}$. From 10.2 we see that a the effective mass m_σ exhibits a steep gradient with diminishing bare quark mass, but still extrapolates to $m_\sigma = (620 \pm 80.0)$, a value similar to the $L = 12$ lattice result. We also include data from a calculation using the $L = 12$ quenched ensemble where we omitted the gauge fixing steps to ascertain how much gauge fixing was helping with the signal to noise. The data are plotted in 10.3.

This encouraging result comes with the rather serious caveat, explained in 5.4, that we needed to remove exceptional gauge fields from the ensembles before taking

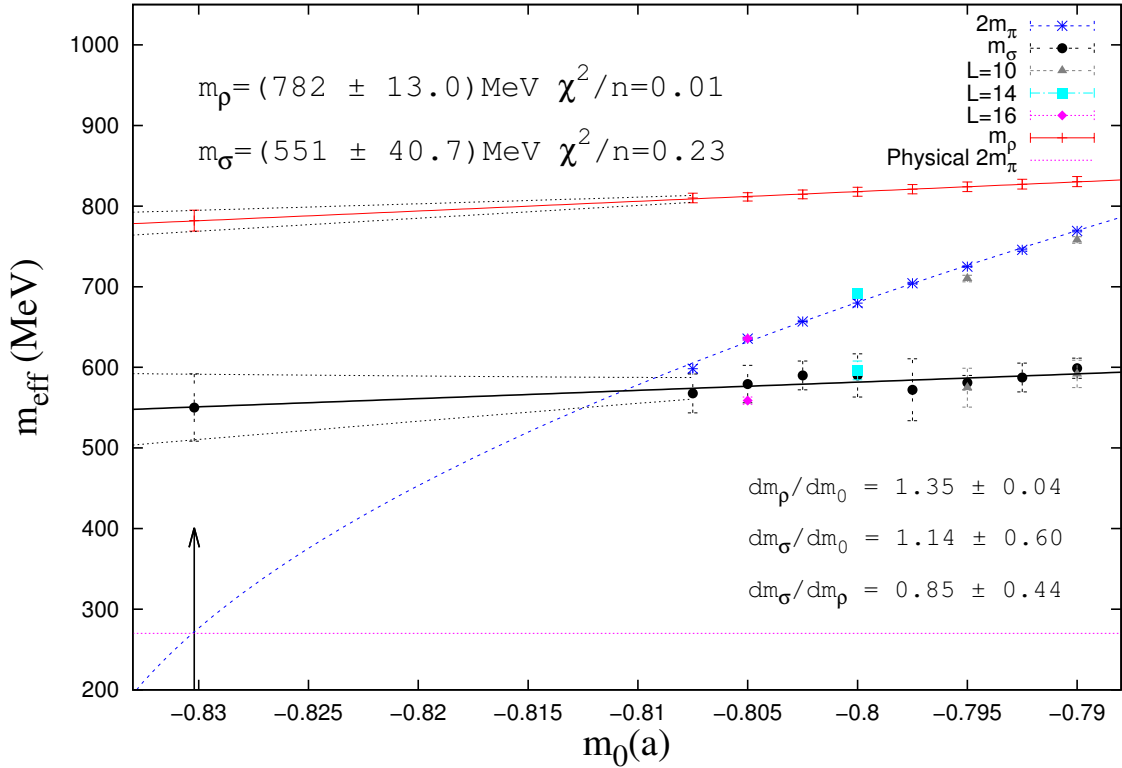


Figure 10.1: m_σ is extrapolated to the continuum. Also shown is m_ρ and $2m_\pi$ for comparison. The pions tend towards a massless state in the chiral limit, but the rho, and the sigma mass, remain approximately constant as expected. The extra m_σ data points labeled $L = 10, 14, 16$ agree with the $L = 12$ which shows that m_σ is a bound state.

the gauge average. Furthermore, we were forced to omit the $C_1(t)$ contribution from the correlation function as the noise from that digram completely drowned out all signal. It has been argued (42) that the most important diagram is the Box diagram, and that the Vacuum diagram can be neglected. Other studies (43, 44) have included the Vacuum diagram, and (44) report that the difference they see in the ground state energy in the $I = 0$ channel when the Vacuum graph is included is at the 1% level.

In both $L = 12$ plots there are data points from different lattice size calculations with the same β and pion masses. These checks were performed to ensure

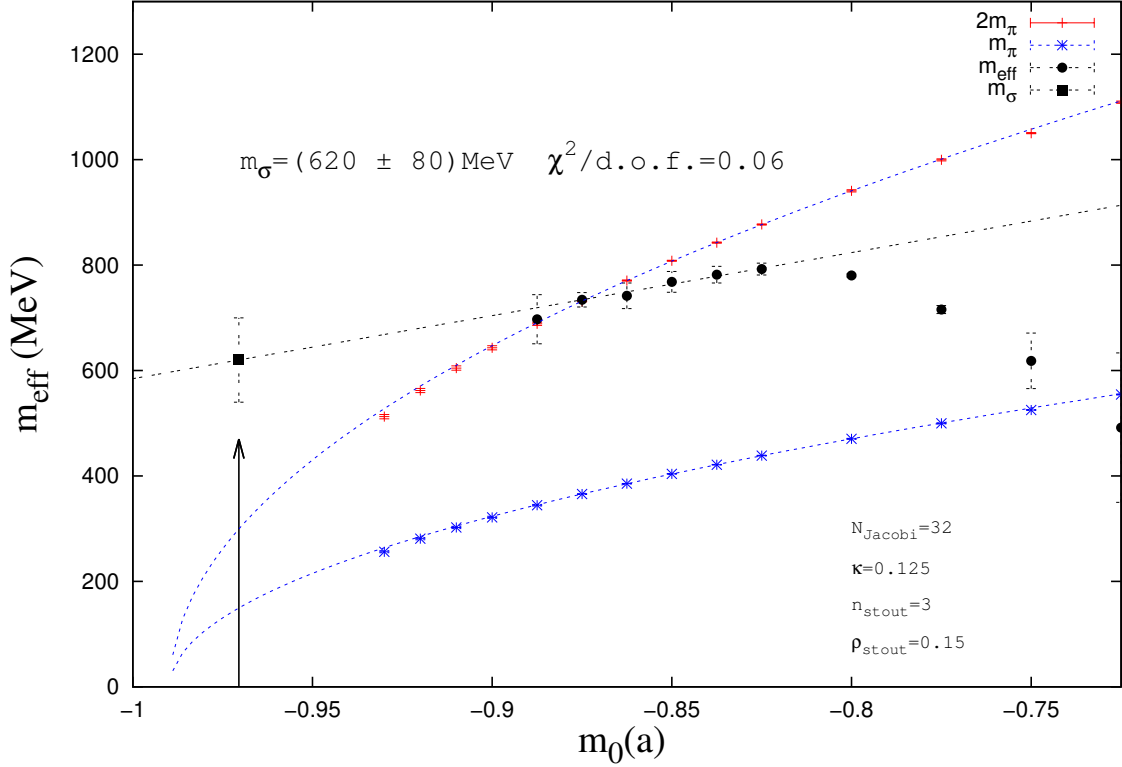


Figure 10.2: m_σ is extrapolated to the continuum. The unexpected gradient of m_σ with m_0 may be a result of discretisation error or over smearing.

that the effective mass plateau we observed was a genuine bound state and not a scattering state. By computing the correlation functions on different lattice sizes, we can compare the behavior of $\delta m_\sigma = 2m_\pi - m_\sigma$ as a function of L to the two forms:

$$\delta E = \frac{T_\alpha}{L^3} + \mathcal{O}\left(\frac{T_\alpha^2}{L^4}\right), \quad (10.1.1)$$

$$\delta E = C, \quad (10.1.2)$$

for some constant C . 10.1.1 would indicate a scattering state, where T_α is some element of a scattering matrix. The constant C is only strictly constant in the large L limit, but we can resolve to two scenarios even at these small lattice sizes due to

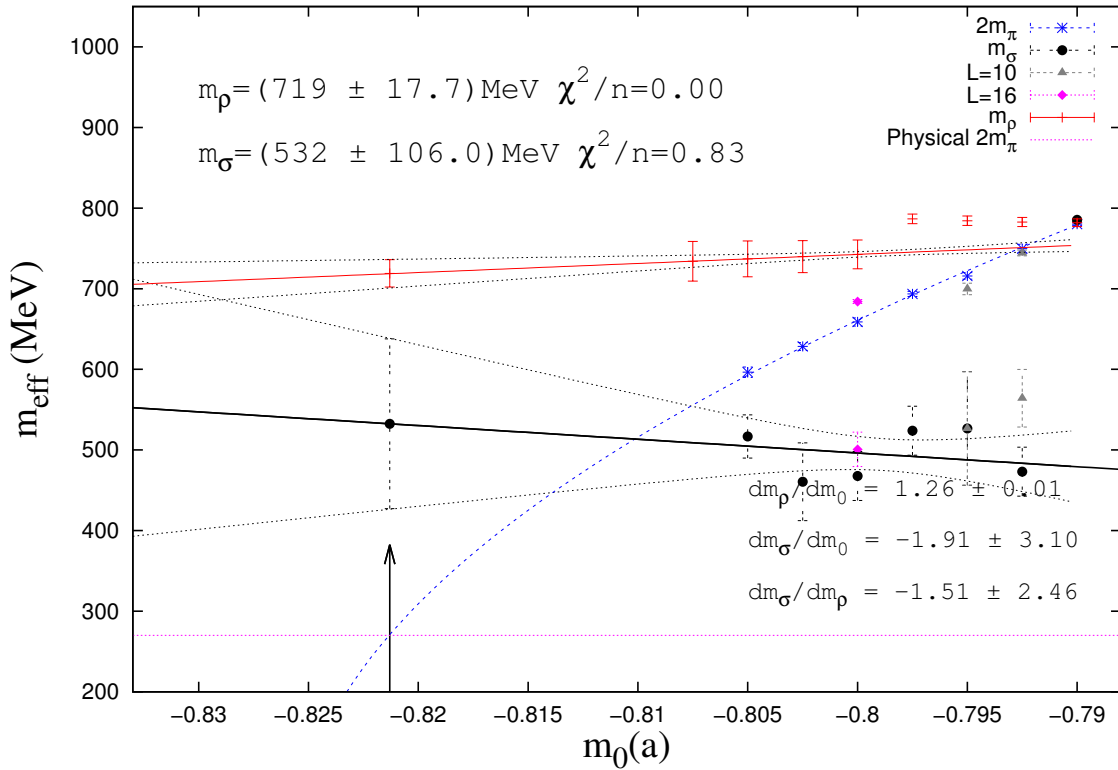


Figure 10.3: m_σ is extrapolated to the continuum. There are obvious differences between these data and 10.1, such as a different chiral limit for the pions, unphysical rho mass, and very large error on the m_σ extrapolation.

the coarse spacings a . We must therefore observe how far from the $L = 12$ sigma masses these other volume calculations deviate. Such an analysis is performed in C.5.

If we make some tentative assumptions about the how these data relate to the physical QCD scenario, we may assert that the sigma meson has strong overlap with the $\pi - \pi$ scattering state. Furthermore, the approximation we made by using quenched lattices means that sea quarks played no role on the sigma signal we detect, hinting that the sigma meson has strong overlap with the four quark $u\bar{u}d\bar{d}$ system, thus providing support for Jaffe's tetraquark model (45).

Shown in figure 10.4 is an effective mass extracted from a dynamical ensemble of $L^3T = 16^332$ with a pion mass of 445MeV. What we see are two plateaux: one in

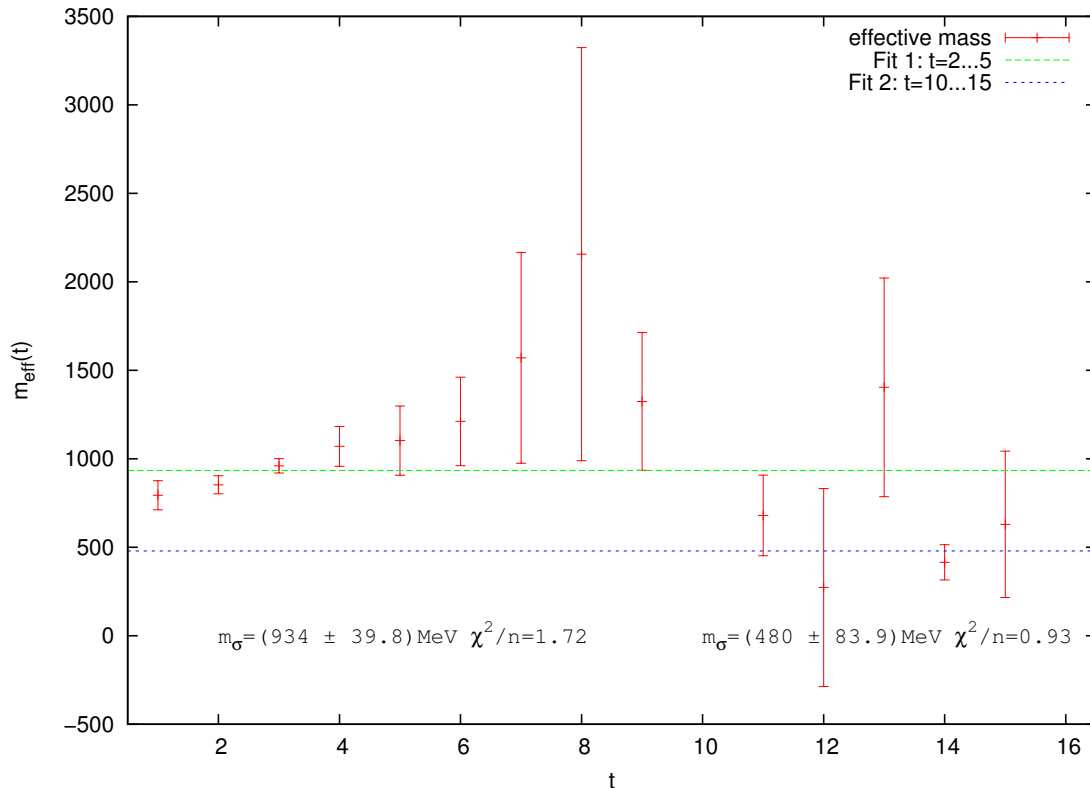


Figure 10.4: Two effective mass plateaux for dynamical $L = 16, \beta = 445\text{MeV}$ lattices. The tail end of the effective mass data could correspond to a sigma signal, but there is too much noise to be certain.

the early time slices at $\approx 934\text{MeV}$ and a less well defined plateau in the later timeslices at ≈ 480 . The former state could easily correspond to the 2 pion continuum of states, and the latter to the sigma meson, but the strange, monotonically rising value of the effective mass makes it unreliable as we ought to see a plateau. The latter state, though consistent with a sigma meson signal, is plagued with uncertainty. The data from this plot mirrors behaviour observed in the $L = 12$ calculations in that when the pion mass is half the rho mass, the ground state of the multi hadron correlation function is seen to lie at the 2 pion continuum value. It is only when $2m_\pi < m_\rho$ that we see a clear sigma signal in the early timeslices. Clearly, a pion mass of 445MeV places this calculation in the range where no sigma signal is seen (in quenched) which corroborates with the behaviour seen in this dynamical cal-

ulation. The reasonable thing to do is to generate dynamical configurations with pion masses in the same range as 10.1, but this requires a great deal of tuning and computational resources. Such dynamical configurations are being generated at the present time and the data from their analysis will be presented in the near future.

10.2 Future Work

This project has yielded some interesting results in the nature of Gribov copies in pure Euclidean $SU(3)$ Yang-Mills, the distribution of correlation functions from lattice QCD, the efficacy of using the smearing operator on momentum sources for gauge connection, and of course, some valuable insight into the quark content of the sigma meson. As was stressed in the previous section, performing this analysis on dynamical configurations is crucial to arriving at a lattice result that can be confidently compared to continuum QCD, but this is just a matter of time. When such ensembles are generated, many improvements can be made to the methods of calculation presented here that will enhance the signal to noise ratio. We have already discussed Fierz noise and isospin projection in 6.2, and we may also employ the moving wall source techniques in (43, 46).

Lastly, measurement of the scattering phase shift, loosely explained in section 8.5, will require using a bayesian analysis to extract the excited states of the 2 pion continuum in the regime where $2m_\pi < m_\sigma$ and measure the scattering phase shift via the interference due to the sigma state.

BIBLIOGRAPHY

- [1] M. Ablikim, et al., *Phys. Lett.* **B598**, 149 (2004).
- [2] K. A. Olive, et al., *Chin. Phys.* **C38**, 090001 (2014).
- [3] M. E. Peskin, D. V. Schroeder, *An Introduction to Quantum Field Theory* (Reading, USA: Addison-Wesley 1995), pp 141.
- [4] K. G. Wilson, *Phys. Rev.* **D10**, 2445 (1974).
- [5] B. Sheikholeslami, R. Wohlert, *Nucl. Phys.* **B259**, 572 (1985).
- [6] K. Symanzik, *Nucl. Phys.* **B226**, 187 (1983).
- [7] R. G. Edwards, B. Joo, H.-W. Lin, *Phys. Rev.* **D78**, 054501 (2008).
- [8] N. Metropolis, A. W. Rosenbluth, M. N. Rosenbluth, A. H. Teller, E. Teller, *J. Chem. Phys.* **21**, 1087 (1953).
- [9] M. Creutz, *Phys. Rev.* **D21**, 2308 (1980).
- [10] S. Gottlieb, W. Liu, D. Toussaint, R. L. Renken, R. L. Sugar, *Phys. Rev. D* **35**, 2531 (1987).
- [11] K. Fabricius, O. Haan, *Phys. Lett.* **B143**, 459 (1984).
- [12] S. P. Booth, et al., *Phys. Lett.* **B275**, 424 (1992).
- [13] C. Gatttringer, L. Ya. Glozman, C. B. Lang, D. Mohler, S. Prelovsek, *Phys. Rev.* **D78**, 034501 (2008).
- [14] J. Foley, et al., *Comput. Phys. Commun.* **172**, 145 (2005).
- [15] C. Eckart, G. Young, *Psychometrika* **1**, 211 (1936).
- [16] M. Albanese, et al., *Phys. Lett.* **B192**, 163 (1987).
- [17] C. Morningstar, M. J. Peardon, *Phys. Rev.* **D69**, 054501 (2004).
- [18] T. Kurth, et al., *PoS LATTICE2010*, 232 (2010).
- [19] V. N. Gribov, *Nucl. Phys.* **B139**, 1 (1978).
- [20] L. Giusti, M. L. Paciello, C. Parrinello, S. Petrarca, B. Taglienti, *Int. J. Mod. Phys.* **A16**, 3487 (2001).
- [21] M. L. Paciello, S. Petrarca, B. Taglienti, A. Vladikas, *Phys. Lett.* **B341**, 187 (1994).

- [22] C. Gatttringer, M. Gockeler, P. Huber, C. B. Lang, *Nucl. Phys.* **B694**, 170 (2004).
- [23] B. Holdom, *Phys. Rev.* **D79**, 085013 (2009).
- [24] P. Marenzoni, P. Rossi, *Phys. Lett.* **B311**, 219 (1993).
- [25] A. Cucchieri, *Nucl. Phys.* **B521**, 365 (1998).
- [26] M. L. Paciello, C. Parrinello, S. Petrarca, B. Taglienti, A. Vladikas, *Phys. Lett.* **B289**, 405 (1992).
- [27] Z. Fu, *JHEP* **01**, 017 (2012).
- [28] Z. Fu, *Commun. Theor. Phys.* **57**, 78 (2012).
- [29] L. V. Gribov, E. M. Levin, M. G. Ryskin, *Phys. Rept.* **100**, 1 (1983).
- [30] D. Zwanziger, *Nucl. Phys.* **B323**, 513 (1989).
- [31] F.-G. Cao, *Phys. Rev.* **D85**, 057501 (2012).
- [32] S. L. Olsen, *PoS BORMIO2012*, 021 (2012).
- [33] M. Ablikim, et al., *Phys. Lett.* **B607**, 243 (2005).
- [34] A. Abele, et al., *Phys. Lett.* **B415**, 280 (1997).
- [35] M. G. Endres, D. B. Kaplan, J.-W. Lee, A. N. Nicholson, *Phys.Rev.Lett.* **107**, 201601 (2011).
- [36] T. DeGrand, *Phys. Rev.* **D86**, 014512 (2012).
- [37] R. Sommer, *Nucl. Phys.* **B411**, 839 (1994).
- [38] E. Manousakis, J. Polonyi, *Phys. Rev. Lett.* **58**, 847 (1987).
- [39] M. Luscher, *Commun. Math. Phys.* **105**, 153 (1986).
- [40] M. Luscher, *Nucl. Phys.* **B354**, 531 (1991).
- [41] M. Luscher, *Nucl. Phys.* **B364**, 237 (1991).
- [42] F.-K. Guo, L. Liu, U.-G. Meissner, P. Wang, *Phys. Rev.* **D88**, 074506 (2013).
- [43] Z. Fu, *Phys. Rev.* **D87(7)**, 074501 (2013).
- [44] T. Blum, et al., *Phys. Rev.* **D84**, 114503 (2011).
- [45] R. L. Jaffe, *Phys. Rev.* **D15**, 267 (1977).
- [46] Z. Fu, *Phys. Rev.* **D85**, 074501 (2012).
- [47] F. A. Berezin, *Pure Appl. Phys.* **24**, 1 (1966).

APPENDIX A

Details on $SU(N)$

A.1 Generators and Algebra

Return to (3.2.23), (3.3.11)

The group elements of $SU(N)$ are infinitesimal transformations connected to the identity that are unitary and have determinant 1. Consider

$$U_{ij} = \delta_{ij} + i\epsilon^a M_{ij}^a \tag{A.1.1}$$

for some infinitesimal quantity ϵ^a , where i, j, \dots represent the dimension of the representation and a is used to label the distinct ‘directions’ of transformation. The factor of i is placed in the transformation for later convenience. Now, insist that this transformation be unitary, hence

$$\begin{aligned} U_{ij} U_{jk}^\dagger &= (\delta_{ij} + i\epsilon^a M_{ij}^a)(\delta_{jk} - i\epsilon^b M_{jk}^{b\dagger}) \\ &= \delta_{ik} + i\epsilon^a (M_{ik} - M_{ik}^\dagger)^a + \mathcal{O}(\epsilon^2) \\ \Rightarrow M_{ik}^a &= M_{ik}^{a\dagger} \end{aligned} \tag{A.1.2}$$

This imposes the condition of hermiticity on M . Also, this is why an i is placed in (A.1.1), as without it one would have to impose an *anti*-hermitian condition. Now,

consider the determinant of (A.1.1),

$$\begin{aligned}
\det U_{ij} &= \det(\delta_{ij} + i\epsilon^a M_{ij}^a) \\
&= \begin{vmatrix} 1 + i\epsilon^a M_{11}^a & \cdots & i\epsilon^a M_{1N}^a \\ \vdots & \ddots & \vdots \\ i\epsilon^a M_{N1}^a & \cdots & 1 + i\epsilon^a M_{NN}^a \end{vmatrix} \\
&= [(1 + i\epsilon^a M_{11}^a)(1 + i\epsilon^b M_{22}^b) \dots (1 + i\epsilon^c M_{NN}^c)] + \mathcal{O}(\epsilon^2) \\
&= 1 + i\epsilon^a (M_{11} + M_{22} + \dots + M_{NN})^a + \mathcal{O}(\epsilon^2). \tag{A.1.3}
\end{aligned}$$

From this condition, one can see that the matrices M must be traceless. For an $N \times N$ complex matrix M , this means that there are $N^2 - 1$ independent real numbers that parameterise M . Consequently, there must exist a set of $N^2 - 1$ linearly independent matrices that form a basis for the vector space on which M resides. These matrices are known as *generators*. The colour gauge group of QCD is $SU(3)$ and all possible gauge transformations can be expressed as linear combinations of the $3^2 - 1 = 8$ generators. The set of generators most commonly used are the Gell-Mann matrices,

$$\begin{aligned}
\lambda^1 &= \begin{pmatrix} 0 & 1 & 0 \\ 1 & 0 & 0 \\ 0 & 0 & 0 \end{pmatrix}, \quad \lambda^2 = \begin{pmatrix} 0 & -i & 0 \\ i & 0 & 0 \\ 0 & 0 & 0 \end{pmatrix}, \quad \lambda^3 = \begin{pmatrix} 1 & 0 & 0 \\ 0 & -1 & 0 \\ 0 & 0 & 0 \end{pmatrix}, \\
\lambda^4 &= \begin{pmatrix} 0 & 0 & 1 \\ 0 & 0 & 0 \\ 1 & 0 & 0 \end{pmatrix}, \quad \lambda^5 = \begin{pmatrix} 0 & 0 & -i \\ 0 & 0 & 0 \\ i & 0 & 0 \end{pmatrix}, \quad \lambda^6 = \begin{pmatrix} 0 & 0 & 0 \\ 0 & 0 & 1 \\ 0 & 1 & 0 \end{pmatrix}, \\
\lambda^7 &= \begin{pmatrix} 0 & 0 & 0 \\ 0 & 0 & -i \\ 0 & i & 0 \end{pmatrix}, \quad \lambda^8 = \frac{1}{\sqrt{3}} \begin{pmatrix} 1 & 0 & 0 \\ 0 & 1 & 0 \\ 0 & 0 & -2 \end{pmatrix}. \tag{A.1.4}
\end{aligned}$$

Notice how the Pauli matrices,

$$\sigma^1 = \begin{pmatrix} 0 & 1 \\ 1 & 0 \end{pmatrix} \quad \sigma^2 = \begin{pmatrix} 0 & -i \\ i & 0 \end{pmatrix} \quad \sigma^3 = \begin{pmatrix} 1 & 0 \\ 0 & -1 \end{pmatrix} \quad (\text{A.1.5})$$

appear in the upper-left of the λ^1, λ^2 , and λ^3 generators. This is because the Gell-Mann representation was first used to describe the approximate $SU(3)$ flavour symmetry of u , d , and s quarks, and the u and d quarks respect an approximate $SU(2)$ flavour symmetry known as *isospin*. Regardless of the original motivation for their construction, the Gell-Mann representation of the $SU(3)$ algebra has been adopted as the standard representation for the colour gauge group of QCD.

The generators of an $SU(N)$ group obey particular commutation properties. Consider two elements of $SU(N)$ in an exponential representation. The product of two such elements should produce a third element, as prescribed by the group axioms,

$$e^{i\alpha^a \lambda^a} e^{i\beta^b \lambda^b} = e^{i\gamma^a \lambda^a}. \quad (\text{A.1.6})$$

for $a, b, \dots = 1, 2, \dots, N^2 - 1$. Expanding both sides of (A.1.6) will reveal an ambivalence in the order in which individual terms are multiplied, which must be resolved.

$$\begin{aligned} (1 + i\alpha^a \lambda^a - \frac{1}{2}\alpha^a \alpha^b \lambda^a \lambda^b)(1 + i\beta^a \lambda^a - \frac{1}{2}\beta^a \beta^b \lambda^a \lambda^b) &= (1 + i\gamma^a \lambda^a - \frac{1}{2}\gamma^a \gamma^b \lambda^a \lambda^b) \\ (1 + i(\alpha^a + \beta^a)\lambda^a - \frac{1}{2}(\alpha^a \alpha^b + \beta^a \beta^b + 2\alpha^a \beta^b)\lambda^a \lambda^b) &= (1 + i\gamma^a \lambda^a \\ &\quad - \frac{1}{2}(\alpha^a + \beta^a)(\alpha^b + \beta^b)\lambda^a \lambda^b) \\ i(\alpha^a + \beta^a - \gamma^a)\lambda^a - \frac{1}{2}(2\alpha^a \beta^b - \alpha^a \beta^b - \beta^a \alpha^a)\lambda^a \lambda^b &= 0 \\ i(\alpha^a + \beta^a - \gamma^a)\lambda^a - \frac{1}{2}\alpha^a \beta^b (\lambda^a \lambda^b - \lambda^b \lambda^a) &= 0 \\ i(\alpha^a + \beta^a - \gamma^a)\lambda^a - \frac{1}{2}\alpha^a \beta^b [\lambda^a, \lambda^b] &= 0 \\ \Rightarrow \gamma^a \lambda^a &= i(\alpha^a + \beta^a)\lambda^a - \frac{1}{2}\alpha^a \beta^b [\lambda^a, \lambda^b]. \end{aligned} \quad (\text{A.1.7})$$

From this result, it is clear that the only way a solution for γ can be achieved is if

the following property of the generators holds,

$$[\lambda^a, \lambda^b] = if^{abc}\lambda^c, \tag{A.1.8}$$

where f^{abc} are the structure constants of the $SU(N)$ group. The generators of the group, along with this commutation relation, form the *Lie algebra* of the $SU(N)$ Lie group. The algebra is denoted using a gothic script $\mathfrak{su}(N)$ to distinguish it from the group.

APPENDIX B

Fermionic Path Integrals

Consider two fermion fields with quantum numbers for position, spin, colour, and flavour, x, α, a , and f respectively. The product of these two fields (or the order in which the field operators act) must undergo a sign change when the quantum numbers of the two fields are exchanged,

$$\psi_a^{\alpha f}(x)\psi_{a'}^{\alpha' f'}(x') = -\psi_{a'}^{\alpha' f'}(x')\psi_a^{\alpha f}(x). \quad (\text{B.0.1})$$

Exactly the same rule applies for both $\psi\bar{\psi}$ and $\bar{\psi}\psi$ products. The fermion fields are therefore Grassmann valued and obey an a **Grassmann Algebra**. Calculus over such Grassmann valued variables is known as **Berezin Calculus** and both are necessary to evaluate the fermionic path integral.

B.1 Grassmann Algebra

The Grassmann Algebra G_N or Λ_N ¹⁹ is defined over the complex field \mathbb{C} and is generated by $2n$ anti-commuting generators θ_i and $\bar{\theta}_i$ for $i = 1 \dots N$. We can multiply the generators by complex numbers, which commute with the generators, and we can define a product between generators,

$$\theta_i\theta_j = -\theta_j\theta_i \quad \Rightarrow \quad \theta_i\theta_i = -\theta_i\theta_i = \theta_i^2 = 0. \quad (\text{B.1.1})$$

The same rules apply for products $\theta\bar{\theta}$ and $\bar{\theta}\theta$, though the product $\theta_i\bar{\theta}_i$ is not nilpotent. We can define a general element g of the algebra G_N as the sum of all possible combinations of generators,

$$g = c + d_i\theta_i + e_i\bar{\theta}_i + f_{ij}\theta_i\bar{\theta}_j + \dots + h_{\{i\}\{j\}}\theta_{i_1} \dots \theta_{i_k}\bar{\theta}_{j_1} \dots \bar{\theta}_{j_l}. \quad (\text{B.1.2})$$

¹⁹ Λ is often used by mathematicians as the Grassmann algebra is the same algebra as the exterior product (wedge \wedge) algebra in geometry

The latin coefficients are all elements of \mathbb{C} and braces around the latin subscript denote a sum over distinct sets $h_{\{i\}} = h_{i_1}h_{i_2}\dots h_{i_N}$. This series truncates at the $(2N+1)$ th term as any repeated generator in any term will evaluate to zero by B.1.1. Furthermore, we can always place the barred generators to the right of the unbarred generators by the same rule and collect similar terms. The rules of addition $g_1 + g_2$ of this algebra are trivial; one simply adds the complex coefficients of g_1 and g_2 . For multiplication $g_1 \times g_2$, one multiplies each term in g_1 by each term in g_2 and then use B.1.1 to eliminate terms that evaluate to zero and rearrange into $\theta \dots \theta \bar{\theta} \dots \bar{\theta}$ order. In general, the elements of the algebra neither commute nor anti-commute.

One can decompose G_N into even and odd terms, where the even terms contain an even number of generators, and the odd terms have an odd number of generators,

$$G_N = (G_N)_{\text{even}} \oplus (G_N)_{\text{odd}}. \quad (\text{B.1.3})$$

One can see intuitively that (using primes to distinguish between elements)

$$\begin{aligned} g_{\text{even}} \times g'_{\text{even}} &= g''_{\text{even}} \in (G_N)_{\text{even}} \\ g_{\text{even}} \times g'_{\text{odd}} &= g'_{\text{odd}} \in (G_N)_{\text{odd}} \\ g_{\text{odd}} \times g_{\text{even}} &= g'_{\text{odd}} \in (G_N)_{\text{odd}} \\ g_{\text{odd}} \times g'_{\text{odd}} &= g_{\text{even}} \in (G_N)_{\text{even}}. \end{aligned}$$

In this sense, the Grassmann algebra is a \mathbb{Z}_2 graded (super)algebra, as the even and odd decompositions follow the group properties of \mathbb{Z}_2 .

We can define a conjugation operation on the Grassmann elements $g \rightarrow g^*$ by defining the conjugation of the generators and products. The complex coefficients take on the natural form of conjugation $z \rightarrow \bar{z}$ and the generators similarly $\theta \rightarrow \bar{\theta}$. Using this, one can easily write down g^* for any general element g . The consequence of this definition is that the conjugate of the product $g_1 g_2$ takes the form,

$$(g_1 g_2)^* = g_2^* g_1^*, \quad (\text{B.1.4})$$

which is reminiscent of the conjugation of products of matrices, $(AB)^\dagger = B^\dagger A^\dagger$.

B.2 Berezin Calculus

The calculus of Grassmann numbers was devised by Felix Berezin (47). When performing calculus on functions of Grassmann variables, it is sufficient to consider the rules of the calculus with respect to the generators only, as all elements of the algebra (and therefore all functions of elements) can be expressed as a sum of products of the generators θ and $\bar{\theta}$. The rules of derivation with respect to θ_i and $\bar{\theta}_i$ are defined in the natural way,

$$\frac{\partial}{\partial \theta_i} c = 0, \quad \frac{\partial}{\partial \theta_i} \theta_j = \delta_{ij} \quad \frac{\partial}{\partial \theta_i} \bar{\theta}_j = 0, \quad (\text{B.2.1})$$

and,

$$\frac{\partial}{\partial \bar{\theta}_i} c = 0, \quad \frac{\partial}{\partial \bar{\theta}_i} \bar{\theta}_j = \delta_{ij} \quad \frac{\partial}{\partial \bar{\theta}_i} \theta_j = 0. \quad (\text{B.2.2})$$

Now, when considering derivatives of terms with more than one generator,

$$\frac{\partial}{\partial \theta_i} \theta_1 \theta_2 \dots \theta_i \dots \theta_n, \quad (\text{B.2.3})$$

one simply uses B.1.1 to move the θ_i element to the left, and apply differentiation by parts,

$$\frac{\partial}{\partial \theta_i} \theta_1 \theta_2 \dots \theta_i \dots \theta_n = (-1)^{i-1} \theta_1 \theta_2 \dots \theta_{i-1} \theta_{i+1} \dots \theta_n. \quad (\text{B.2.4})$$

The rule for $\frac{\partial}{\partial \bar{\theta}_i}$ is exactly the same. As an example, for $N = 1$, the derivate of g with respect to θ is,

$$\begin{aligned} \frac{\partial}{\partial \theta} g &= \frac{\partial}{\partial \theta} (c + d\theta + e\bar{\theta} + f\theta\bar{\theta}) \\ &= d + f\bar{\theta}. \end{aligned} \quad (\text{B.2.5})$$

Furthermore, one can use this rule to show that derivatives anti-commute,

$$\left\{ \frac{\partial}{\partial \theta_i}, \frac{\partial}{\partial \theta_j} \right\} = 0. \quad (\text{B.2.6})$$

Integration of Grassmann variables takes on a curious form. The two definitions,

$$\int d\theta_i = 0 \quad \int d\theta_i \theta_i = 1, \quad (\text{B.2.7})$$

can be used to show that,

$$\int d\theta_i \frac{\partial}{\partial \theta_i} g = 0, \quad (\text{B.2.8})$$

simply by expanding g as a sum of generators and applying the rules of differentiation and B.2.7. This rather incredible result is schematically attributed to the notion that the boundary terms of g ought to vanish. One is then left with the even more incredible property,

$$\int d\theta_i \equiv \frac{\partial}{\partial \theta_i}. \quad (\text{B.2.9})$$

B.3 Gaussian Integration of Fermion Fields

The results of the previous section can now be employed to the path integral formalism to compute the functional integrals of fermion fields. Consider some element e of G_N defined to be the exponential of some other element $-g = -\bar{\theta}_{ij} A_{ij} \theta_j$ for some complex valued self-adjoint matrix $A = A^\dagger$,

$$e = \exp(-\bar{\theta}_{ij} A_{ij} \theta_j). \quad (\text{B.3.1})$$

Now, exponentiation of the element g gives rise to an expansion,

$$e = \exp(-g) = 1 - g + \frac{1}{2!} g^2 + \cdots + (-1)^N \frac{1}{N!} g^N. \quad (\text{B.3.2})$$

This expansion necessarily terminates after the N th power because the element e is in the Grassmann algebra and therefore has a term with a maximal number of generators, which is $2N$. Another way to see this is that if one were to raise g to some power greater than N , one would include some product of generators with more than $2N$ generators which would necessarily contain a repetition of some generator(s) and therefore evaluate to zero. Further, the element e is a member of the the sub-algebra $(G_N)_{\text{even}}$. Using an example of an $N = 2$ Grassmann algebra, we can see a useful property of the integral emerge. The exponentiation of a general

$g = \bar{\theta}_i A_{ij} \theta_j$ for $i, j = 1, 2$ is,

$$\begin{aligned} \exp(-g) &= 1 - g + \frac{1}{2!} g^2 \\ &= 1 - (\bar{\theta}_i A_{ij} \theta_j) + \frac{1}{2} (\bar{\theta}_i A_{ij} \theta_j) (\bar{\theta}_k A_{kl} \theta_l) \\ &= 1 - (\bar{\theta}_i A_{ij} \theta_j) + \frac{1}{2} \left[\begin{pmatrix} \bar{\theta}_1 & \bar{\theta}_2 \end{pmatrix} \begin{pmatrix} A_{11} & A_{12} \\ A_{21} & A_{22} \end{pmatrix} \begin{pmatrix} \theta_1 \\ \theta_2 \end{pmatrix} \right]^2 \end{aligned} \quad (\text{B.3.3})$$

$$= 1 + \dots + (A_{12}A_{21} - A_{11}A_{22})(\theta_1\theta_2\bar{\theta}_1\bar{\theta}_2). \quad (\text{B.3.4})$$

The only term of interest is the term with the maximal number of generators, which was constructed using matrix multiplication and the Grassmann algebra anti-commutation rules B.1.1. The factorial in the denominator will always cancel with the combinatorial coefficient of the maximal term. Now, the order of the measures of a Grassmann integral are important and follow,

$$\int \prod_{i=1}^N d\bar{\theta}_i d\theta_i = \int d\bar{\theta}_1 d\theta_1 d\bar{\theta}_2 d\theta_2 \dots d\bar{\theta}_N d\theta_N. \quad (\text{B.3.5})$$

Working from the rightmost measure and commuting the generators of the integrand to the left and using B.2.7, we see that any term in the integrand that does not contain exactly one instance of each generator will evaluate to zero and we are left with only the last term. Commuting the variables will give an overall minus sign and the integral over each Grassmann generator evaluates to one. This allows us to evaluate the integral of the exponential of a Grassmann variable,

$$\begin{aligned} \int \prod_{i=1}^N d\bar{\theta}_i d\theta_i \exp(-g) &= -(A_{12}A_{21} - A_{11}A_{22}) \int d\bar{\theta}_1 \bar{\theta}_1 \int d\theta_1 \theta_1 \int d\bar{\theta}_2 \bar{\theta}_2 \int d\theta_2 \theta_2 \\ &= \det[A]. \end{aligned} \quad (\text{B.3.6})$$

This result for $N = 2$ holds for all $N \in \mathbb{Z}^+$. We can now extend this result to calculate the expectation value of some element of G_N with respect to the exponential,

$$\langle g \rangle = \frac{\int \prod_{k=1}^N \bar{\theta}_k \theta_k \exp(-\bar{\theta}_i A_{ij} \theta_j) g}{\int \prod_{k=1}^N \bar{\theta}_k \theta_k \exp(-\bar{\theta}_i A_{ij} \theta_j)}. \quad (\text{B.3.7})$$

We can immediately deduce that the expectation value of an *odd* number of generators will evaluate to zero, as the measure contains an even number of generators and the exponential, when expanded, will always contain even elements. Let us therefore concentrate on a simple example where we calculate the expectation value $\langle \theta \bar{\theta} \rangle$ for an $N = 1$ Grassmann algebra. The result is very simple,

$$\langle \theta \bar{\theta} \rangle = \frac{\int \bar{\theta} \theta (1 + A \bar{\theta} \theta) \theta \bar{\theta}}{\int \bar{\theta} \theta (1 + A \bar{\theta} \theta)} = \frac{1}{A}, \quad (\text{B.3.8})$$

and highly suggestive of the result for higher dimensional Grassmann algebras. We shall now explicitly calculate the result $N = 2$,

$$\langle \theta_i \bar{\theta}_j \rangle = \frac{\int \bar{\theta}_1 \theta_1 \bar{\theta}_2 \theta_2 \left[1 - (\bar{\theta}_1 \ \bar{\theta}_2) \begin{pmatrix} A_{11} & A_{12} \\ A_{21} & A_{22} \end{pmatrix} \begin{pmatrix} \theta_1 \\ \theta_2 \end{pmatrix} + \frac{1}{2} (\bar{\theta}_i A_{ij} \theta_j)^2 \right] (\theta_i \bar{\theta}_j)}{\det[A]}. \quad (\text{B.3.9})$$

We can immediately evaluate the denominator via B.3.6. We also see that the relevant term in the exponential in the denominator is not the maximal N th term, but the $(N - 1)$ th term, as all other terms will evaluate to zero. One finds, after expanding the $(N - 1)$ th term and applying the rules B.2.7 and anti-commuting the generators,

$$\langle \theta_i \bar{\theta}_j \rangle = \frac{(-1)^{i+j} \text{minor}[A_{ij}]}{\det[A]} = \frac{1}{\det[A]} C_{ij}^\top = A_{ij}^{-1}, \quad (\text{B.3.10})$$

where C_{ij} is the matrix of cofactors of A_{ij} . This result holds for all $N \in \mathbb{Z}^+$. Furthermore, because we know from the Grassmann algebra that θ and $\bar{\theta}$ anti-

commute, we can immediately write down the result for the expectation value $\langle \bar{\theta}_j \theta_i \rangle$,

$$\langle \bar{\theta}_j \theta_i \rangle = -\langle \theta_i \bar{\theta}_j \rangle = -A_{ij}^{-1}. \quad (\text{B.3.11})$$

This result leads us to deduce how Wick's theorem applies to Grassmann valued expectation values. Consider some Grassmann algebra G_N and some expectation value of $n\theta$ and $n\bar{\theta}$ Grassmann generators. In the following, all latin indices run from 1 to N and subscripts on those indices run from 1 to n . Products and sums over these indices are included for clarity,

$$\langle \theta_{i_1} \bar{\theta}_{j_1} \dots \theta_{i_n} \bar{\theta}_{j_n} \rangle = \frac{1}{\det[A]} \int \prod_{k=1}^N d\bar{\theta}_k d\theta_k \exp \left(\sum_{i,j=1}^N -\bar{\theta}_i A_{ij} \theta_j \right) \theta_{i_1} \bar{\theta}_{j_1} \dots \theta_{i_n} \bar{\theta}_{j_n} \quad (\text{B.3.12})$$

We can evaluate this integral more easily by introducing source terms $\eta_i, \bar{\eta}_i$ and forming a generating functional $W[\eta_i \bar{\eta}_i]$. Like in all generating functionals, the source terms will be set to zero at the end of the calculation,

$$W[\eta_i \bar{\eta}_i] = \int \prod_{k=1}^N d\bar{\theta}_k d\theta_k \exp \left(\sum_{i,j=1}^N -\bar{\theta}_i A_{ij} \theta_j - \sum_{i=1}^N \bar{\eta}_i \theta_i - \sum_{i=1}^N \bar{\theta}_i \eta_i \right). \quad (\text{B.3.13})$$

We can 'complete the square' in the exponent by rewriting it as,

$$- (\bar{\theta}_i + \bar{\eta}_j A_{ji}^{-1}) A_{ik} (\theta_k + A_{kl}^{-1} \eta_l) + \bar{\eta}_m A_{mn}^{-1} \eta_n, \quad (\text{B.3.14})$$

and then we perform a transformation on the $\theta, \bar{\theta}$ fields,

$$\theta'_k = \theta_k + A_{kl}^{-1} \eta_l, \quad \bar{\theta}'_i = \bar{\theta}_i + \bar{\eta}_j A_{ji}^{-1}. \quad (\text{B.3.15})$$

The measure of such a transformation remains invariant due to the rules of Grassmann algebra and Berezin calculus B.1.1, B.2.7. We can now evaluate the integral

over the $\theta, \bar{\theta}$ fields,

$$\begin{aligned} W[\eta_i, \bar{\eta}_i] &= \exp\left(\sum_{m,n=1}^N \bar{\eta}_m A_{mn}^{-1} \eta_n\right) \int \prod_{i=1}^N d\bar{\theta}'_i d\theta'_i \exp\left(-\sum_{jk} \bar{\theta}'_j A_{jk} \theta'_k\right) \\ &= \det[A] \exp\left(\sum_{m,n=1}^N \bar{\eta}_m A_{mn}^{-1} \eta_n\right) \end{aligned} \quad (\text{B.3.16})$$

Now, the $2n$ point correlation function B.3.12 may be expressed as the differential of the generating functional with respect to η_i and $\bar{\eta}_i$,

$$\begin{aligned} \langle \theta_{i_1} \bar{\theta}_{j_1} \dots \theta_{i_n} \bar{\theta}_{j_n} \rangle &= \frac{1}{\det[A]} \frac{\partial}{\partial \bar{\eta}_{i_1}} \frac{\partial}{\partial \eta_{j_1}} \dots \frac{\partial}{\partial \bar{\eta}_{i_n}} \frac{\partial}{\partial \eta_{j_n}} W[\eta_i, \bar{\eta}_i] \Bigg|_{\eta_i, \bar{\eta}_j=0}, \\ &= \sum_{P(1\dots n)} \text{sign}(P) A_{i_1 j_{P_1}}^{-1} A_{i_2 j_{P_2}}^{-1} \dots A_{i_n j_{P_n}}^{-1}. \end{aligned} \quad (\text{B.3.17})$$

The function P is all possible permutations of $(1, 2, \dots, n)$, which is the same as all the possible Wick contractions between the θ and $\bar{\theta}$ and $\text{sign}(P)$ evaluates to $+1$ or -1 if there are an even or odd number (respectively) of contractions. This rather cumbersome notation belies a very simple structure. Let us consider a four-point ($n = 2$) Grassmann valued correlation function over G_N to see how it unpacks,

$$\begin{aligned} \langle \theta_{i_1} \bar{\theta}_{j_1} \theta_{i_2} \bar{\theta}_{j_2} \rangle &= \frac{1}{\det[A]} \int \prod_{k=1}^N d\bar{\theta}_k d\theta_k \exp\left(\sum_{i,j=1}^N -\bar{\theta}_i A_{ij} \theta_j\right) \theta_{i_1} \bar{\theta}_{j_1} \theta_{i_2} \bar{\theta}_{j_2} \\ &= \sum_{P=1,2} \text{sign}(P) A_{i_1 j_{P_1}}^{-1} A_{i_2 j_{P_2}}^{-1} \\ &= A_{i_1 j_1}^{-1} A_{i_2 j_2}^{-1} - A_{i_1 j_2}^{-1} A_{i_2 j_1}^{-1} \end{aligned} \quad (\text{B.3.18})$$

This result is used in section 6.1 when evaluating the eight-point function of the $\pi_+ \pi_- \rightarrow \pi_+ \pi_-$ system.

APPENDIX C

Error Calculations

C.1 Error on correlation functions

The main source of error in this calculation comes from gauge noise because we must approximate the path integral over the gauge fields 5.1.2. From the central limit theorem, we expect that the distribution of correlation function values around the gauge average to follow a Gaussian profile and, provided we average over sufficient gauge field configurations, the error on these correlation function values can be quoted using the standard error,

$$\langle O \rangle_{true} = \langle O \rangle_G \pm \frac{\sigma}{\sqrt{N}}, \quad (\text{C.1.1})$$

where $\langle O \rangle_G$ denotes the measured average over the gauge field, σ is the standard deviation, and N is the number of gauge field configurations. We are not usually interested in correlation function values, and in this study we are concentrating on the exponential decay properties of correlation functions. We therefore use standard regression and reduced χ^2 analysis to measure the ground state and associated error.

C.2 Autocorrelation and Jack-Knife Error Estimates

Although we assume that the gauge field configurations we generate are sampled randomly from their parent distribution, this is in practice impossible and successive gauge field configurations in the Markov chain will exhibit correlations that will affect any measurement. Indeed, this autocorrelation can extend beyond single, successive steps in the Markov chain and therefore one must skip some number of configurations between sampling to minimise this effect. It is, in fact, possible to measure the *autocorrelation time* of the Markov chain (or, the number of updates one must discard in order to have satisfactorily uncorrelated data) but that can prove expensive computationally, especially for QCD.

There exist other options for dealing with autocorrelation, namely Blocking,

Bootstrap, and Jackknife. Blocking is a simple technique that blocks the full set of calculated observables N into subsets of size K and calculates the mean of each block. These block means X_i for $i = \dots (N/K)$ are then treated as independent variables. The variance of these blocks ought to decrease as $1/K$ as the block size is varied. As soon as this $1/K$ behaviour is observed, one may treat the blocked means as independent variables.

The Jackknife method takes the original N set of observables and calculates the mean \bar{X} . One then removes a subset of entries of size K and recalculates the mean, denoted X_K . One then calculates the variance of these X_K via,

$$\sigma_{\bar{X}}^2 = \frac{N-1}{N} \sum_{n=1}^{N-K+1} (X_K - \bar{X})^2. \quad (\text{C.2.1})$$

One then quotes the error on \bar{X} as,

$$\langle X \rangle = \bar{X} \pm \sigma_{X_K}. \quad (\text{C.2.2})$$

C.3 Error on the Sommer parameter

In order to quote an error on the lattice spacing some elementary error propagation calculation must be performed. Using the formulas,

$$V(r) = A + \frac{B}{r} + Cr, \quad (\text{C.3.1})$$

and,

$$\frac{r_0}{a} = \left(\frac{1.65 + B}{C} \right)^{\frac{1}{2}} \Rightarrow a(B, C) = r_0 \gamma^{-\frac{1}{2}} \quad | \quad \gamma = \left(\frac{1.65 + B}{C} \right), \quad (\text{C.3.2})$$

then the error on $a(B, C)$ is given by,

$$\begin{aligned}
\sigma_a^2 &\approx \left| \frac{\partial a}{\partial B} \right|^2 \sigma_B^2 + \left| \frac{\partial a}{\partial C} \right|^2 \sigma_C^2 + 2 \frac{\partial a}{\partial B} \frac{\partial a}{\partial C} \sigma_{BC}, \\
&\approx \left(-r_0 \frac{1}{2} \frac{1}{C} \gamma^{-\frac{3}{2}} \right)^2 \sigma_B^2 + \left(-r_0 \frac{1}{2} (-\gamma) \frac{1}{C} \gamma^{-\frac{3}{2}} \right)^2 \sigma_C^2, \\
&\approx \frac{1}{4C^2} r_0^2 \gamma^{-3} (\sigma_B^2 + \gamma^2 \sigma_C^2), \\
\sigma_a &\approx \sqrt{\frac{1}{4C^2} r_0^2 \gamma^{-3} (\sigma_B^2 + \gamma^2 \sigma_C^2)}. \tag{C.3.3}
\end{aligned}$$

The error on the Sommer parameter itself can be calculated from,

$$\begin{aligned}
\frac{r_0}{a} &= \left(\frac{1.65 + B}{C} \right)^{\frac{1}{2}}, \\
\Rightarrow \sigma_{\frac{r_0}{a}}^2 &\approx \left| \frac{\partial(r_0/a)}{\partial B} \right|^2 \sigma_B^2 + \left| \frac{\partial(r_0/a)}{\partial C} \right|^2 \sigma_C^2, \\
&\approx \frac{1}{4} (\gamma - B)^2 \gamma^{-1} \sigma_B^2 + \frac{1}{4C} \gamma \sigma_C^2, \\
\sigma_{\frac{r_0}{a}} &\approx \frac{1}{2} \sqrt{(\gamma - B)^2 \gamma^{-1} \sigma_B^2 + \frac{1}{C} \gamma \sigma_C^2}. \tag{C.3.4}
\end{aligned}$$

The standard deviations of B and C were calculated using the GNU PLOT package.

C.4 Error on effective mass extrapolation

From the book *Statistics: A Guide to the Use of Statistical Methods in the Physical Sciences* by R. J. Barlow, Eq 6.15b, p 103, the variance of an extrapolated value Y at a given X is,

$$\text{Var}(Y) = \frac{\sigma_y^2 (X - \bar{x})^2}{N(\bar{x}^2 - \bar{x}^2)} + \frac{\sigma_y^2}{N} \tag{C.4.1}$$

where σ_y is the (constant) error associated with each y_i and N is the number of points in the fit. Here I make the assumption that the errors on y_i are indeed constant, but take the average of the respective errors giving $\sigma_y = 17.6\text{MeV}$. The standard error on this estimate is 2.56MeV which makes it fairly reasonable to make this assumption. The final number comes out to be $\text{Var}(Y) = 2250\text{MeV}^2$ so

$\sigma_Y = 47.4\text{MeV}$, which is around 10% of our calculated value.

C.5 Error on $\Delta E(L_1)/\Delta E(L_2)$

Using the formula,

$$\delta \equiv \Delta E(L_1)/\Delta E(L_2) = \frac{2m_\pi - m_\sigma(L_1)}{2m_\pi - m_\sigma(L_2)} \quad (\text{C.5.1})$$

and making the assumption that the error on $m_\pi \approx 0$ given that these errors are around 0.25% for each pion mass, error propagation gives

$$\sigma_{\delta(m_\sigma(L_1), m_\sigma(L_2))}^2 \approx \left(\frac{-1}{2m_\pi - m_\sigma(L_2)} \right)^2 \sigma_{m_\sigma(L_1)}^2 + \left(\frac{2m_\pi - m_\sigma(L_1)}{(2m_\pi - m_\sigma(L_2))^2} \right)^2 \sigma_{m_\sigma(L_2)}^2. \quad (\text{C.5.2})$$

Using the values in they data file, I find that for $L = 10$ and $m_0 = -0.790$, $\sigma_\delta = 0.097$; for $m_0 = -0.795$, $\sigma_\delta = 0.25$. Lastly, for the $L = 14$ data point, $\sigma_\delta = 0.25$ also. This gives:

$$\Delta E(10)/\Delta E(12) = 1.00 \pm 0.097 \text{ for } m_0 = -0.790$$

$$\Delta E(10)/\Delta E(12) = 0.92 \pm 0.25 \text{ for } m_0 = -0.795$$

$$\Delta E(12)/\Delta E(14) = 1.04 \pm 0.25 \text{ for } m_0 = -0.800$$

These numbers with errors are consistent with the bound state as $(10/12)^3 = 0.58$ and $(12/14)^3 = 0.63$ are outside the ranges given for all δ .

ACKNOWLEDGMENT

Part II: The Human Condition

In the gray-washed hue of the quantum state,
There is no coercion with love or with hate.
Half go to B and half go to C,
Reality reduces to probability,
And we must accept what Nature dictates:
There is no control over quantum fates,
We are merely spectators in Her game of chance,
Even if we take a Bohmian stance.
But this conclusion should give you pause,
For you are the event and the cause.
Would you please indulge my curious mood,
And partake in a game I just construed.
Hold out your arms as wide as you can,
I beg you, for science, go along with my plan,
And lose your fear and hold your breath,
And imagine yourself on the verge of death,
Forced to choose between left and right.
Make the choice now.

I trust you see what has just occurred:
The quantum rules have become absurd.
The synapse fired and your mind was made,
Was your choice chance? Did free will fade?
Some of you played and some read on,
But there is no escape. That choice relied on
Some electron, deep in your gray-dappled dome,

Shuffled into place by your genome,
Superimposed, and ready to say,
Whether you'll pass or whether you'll play.
The essence of life, choice itself,
Is shown to be random and not of yourself!
This, I assure you, takes time to sink in,
And most of you rightly refuse to give in.
Your soul, your self, the thing that is you,
Is all locked up in a fictitious hue,
And all we can say of what you'll become,
Is the likelihood of some measured outcome.

So nothing has changed in the game of life,
Quantum enlightenment gives no extra strife,
To the every day toll that reality takes,
Scientist or not we all play the same stakes.
Each of us trapped at the same forked road,
And even if waiting for all stories told,
Until we make our final decision,
The path that we take is not purely our vision.
The billions of roads that have forked hitherto,
Some walked by others and some walked by you,
Encodes the shuffling synaptic source,
Of your personal choice and your future course.
So just be human and embrace your condition,
And let your life flow without inhibition.
Sure, reason and logic will give you an edge,
Stop you from falling into a thorned hedge,
But often you'll find that you already know,
Whom you wish to be and where you must go,
And the longer you waste with the reason machine,

The less time you have to enjoy the scene.

It does you no good to fight this one out,
But go right ahead if you think you've a shout!
And please, come crying to me when you fail,
Because I made the tracks you'll see on the trail,
And I felt hope on the steep hill's brow,
And I cried by the rusted and busted old plough,
And I walked the bend that goes on for miles,
With walls either side, and mirrors for tiles,
That creep ever higher and shut out the sky,
No forks in this road, one way till you die,
And I stopped and looked and saw all my fates.
And I thought of the chances I'd missed, all the gates,
The stiles I'd passed on my route here,
The fence of mistakes and regret to the rear,
The dust of trust that lay on the road,
The litter and rubbish of friends gone cold,
And waiting for me in the way up ahead,
Is a narrowing lane of echoing dread,
Paved with the ice of lover's dead hearts,
Furnished with signs of one-way white darts.

A choice was made and a chance was taken,
It was not fate. Do not be mistaken.
Your life is not fixed and you are not bound.
But you have to choose to turn it around.
To those in front, my thanks, you are owed,
The burden you carried has lightened my load,
And for payment of that which has been borrowed,
I leave for you, reader, this note in the road.